# ESTIMATE OF PROMPT NEUTRINO PRODUCTION IN THE BEBC BEAM DUMP EXPERIMENT

by

SEYED MEHRZAD TALEBZADEH

A dissertation submitted to the University of London in partial fulfilment of the requirements of the degree of Doctor of Philosophy

April 1987

Imperial College of Science and Technology,
London

## ABSTRACT

Results are presented from a BEBC beam dump experiment carried out at CERN in 1982. The 400 GeV protons from the super proton synchrotron were buried in a massive dense target which absorbed them almost entirely. By minimising the decay path of the secondaries, the neutrino fluxes from long lived particles such as pions and kaons were strongly suppressed, however for particles with lifetimes less than $10^{-11}$ s, the decay length was of the order of or less than the interaction length and most of these particles had time to decay giving rise to the so called prompt neutrinos.

The characteristics of the prompt neutrinos have been studied and their flux estimated. The ratio of the prompt electron neutrino flux to prompt muon neutrino flux is estimated. A comparison is made with the previous reported values of this ratio. The ratio obtained in this experiment is compatible with the value of unity, expected from electron-muon universality. Attempts are made to look for interactions induced by tau neutrinos using several different kinematical methods. An estimate of the Neutral Current (NC) to Charged Current (CC) ratio is made for events with hadronic energies above 10 GeV. The observed ratio is compatible with the values observed in normal neutrino experiments.

The hadronic background for events with hadronic energies below 10 GeV is estimated and the NC to CC ratio is obtained at these energies. Contrary to previous reports no evidence for excess of NC events below hadronic energy 10 GeV is observed. No clear evidence for tau neutrino interaction is observed and an upper limit is set for the fraction of the observed events due to tau neutrino interactions. Assuming the prompt neutrino production to be due to charmed particle decays, an estimate of the charm production cross-section in hadron-hadron collisions is made.

## ACKNOWLEGEMENTS

Without the work and help of a very large number of people it would have been impossible to produce this thesis. First thanks must go to my parents for their constant love and support, and for the sacrifices they have made over the years to further my education. I dedicate this work to them as a small token of my thanks.

I would like to express my deep gratitude to my supervisor, Dr Donald B. Miller for his constant advice, encouragement and his friendship throughout the years we worked together.

I wish to express my appreciation to all my colleagues in the Imperial College High Energy Physics Group, who contibuted to the stimulating and friendly atmosphere. From the staff, I would like to thank Professor Ian Butterworth for providing me with the opportunity to study in Imperial College, and Drs Keith Barnham and Edward Clayton for their help and advice with many problems.

I very much like to thank Drs Wilbur Venus and Jon Guy of Rutherford Laboratory who devoted a large amount of their time to my problems. Without their help and advice my thesis would never have been finished. My deepest gratitude to them for

friendship and humour during my time as research associate in Rutherford Laboratory.

I have enjoyed working with the WA66 collaboration and thank everyone for their work in building and running the experiment. In particular I must thank Drs Per-Olof Hulth, Horst Wachsmuth, Gerald Myatt, Peter Schmid and Klas Hultqvist for their dedicated work with the WA66 data and for many stimulating meetings and lively discussions.

My thanks to Paul Baker and Mike Waters, the systems managers in Imperial College and Rutherford Laboratory respectively, for helping me with various computer related problems.

Finally I would like to acknowledge financial support from the Committee of Principals and Vice Chancellors of the Universities of the United Kingdom.

CONTENTS

ABSTRACT . . . . . ii

ACKNOWLEGEMENTS . . . . . iv

Chapter

page

I. INTRODUCTION . . . . . 1

Previous beam dump experiments . . . . . 2
The features of beam dump experiments . . . . . 5
The scheme of this thesis . . . . . 5

II. EXPERIMENTAL SETUP . . . . . 9

Beam line . . . . . 9
The target . . . . . 11
The muon detectors . . . . . 13
The neutrino detector . . . . . 15
The external muon identifier . . . . . 16
Arrangement of the EMI . . . . . 17
Muon identification . . . . . 20
The internal picket fence . . . . . 20

III. EXPERIMENTAL PROCEDURE . . . . . 22

Exposure and acceptance . . . . . 22
Scanning . . . . . 23
Scanning for neutrino events . . . . . 23
Scanning for electron tracks . . . . . 26
Scanning of through-going muons . . . . . 27
Events visible on the high resolution camera . . 28
Measuring . . . . . 29
Measurements of through-going muons . . . . . 30
The labelling scheme . . . . . 30
Measurements procedure . . . . . 32
Measurements checking . . . . . 34
Production of the data summary tape (DST) . . . 36

IV. EXPERIMENTAL CORRECTIONS . . . . . 39

Scanning efficiency . . . . . 39
Corrections for electrons . . . . . 40
Corrections for muons . . . . . 41

Estimate of the electronic efficieny of the EMI . 42
Edge effect . . . . . 46
Electron tracks . . . . . 48
Comparison with other estimates . . . . . 50
Estimate of geometrical efficiency of the EMI . . 50
Estimate of the total muon loss . . . . . 51
Estimate of the effective interaction length. . 53
Track following in the bubble chamber . . . 56
Results . . . . . 58
Correction for lepton momentum cut . . . . . 60
Energy corrections . . . . . 61
Association of neutron stars . . . . . 62

V. EVENT SELECTION AND CORRECTED CHARGED CURRENT RATES . . . . . 70

Track selection . . . . . 70
Event selection . . . . . 73
Event classification . . . . . 74
The x and y distribution of cc events . . . . . 75
Corrected event rates . . . . . 79

VI. THE PROMPT CHARGED CURRENT SAMPLE . . . . . 86

The source of conventional neutrinos . . . . . 87
Observed events and the expected conventional background . . . . . 89
The muon neutrino and antineutrino samples . . 89
The electron neutrino and antineutrino samples 90
Estimate of the prompt rates . . . . . 96
The prompt rates from the subtraction method . 96
The prompt rates from the extrapolation method 97
The through-going muons . . . . . 100
Fitting prompt rates . . . . . 102
The source of prompt neutrinos . . . . . 104
Electron-muon universality . . . . . 110
Discussion of the prompt rates . . . . . 112
Comparison with other experiments . . . . . 114
Comparison with 1979 rates from CERN beam dump experiments . . . . . 114
Rates from the present CERN beam dump experiments . . . . . 115
Comaprison of the prompt rates . . . . . 117
Prompt $\nu_e$-$\nu_\mu$ asymmetry . . . . . 119
Prompt neutrino-antineutrino asymmetry . . 120

VII. THE NEUTRAL CURRENT SAMPLE . . . . . 122

Estimate of hadronic background in the NC sample 124
Method . . . . . 125
Correction for misidentified charged current events 138
The Neutral current to Charged current ratios . . 138

NC to CC ratio for electron neutrinos . . . . . 153
Comparison with conventional neutrino experiments . . . . . 154
Excess of low energy NC events . . . . . 154

VIII. SEARCH FOR TAU NEUTRINO INTERACTIONS . . . . 156

Possible sources of tau neutrinos . . . . . 157
Simulation of the expected tau neutrino flux . . . 159
The decay of $\tau^- \rightarrow e^- \nu_e \nu_\tau$ . . . . . 161
The decay of $\tau^- \rightarrow \mu^- \nu_\mu \nu_\tau$ . . . . . 161
The decay of $\tau^- \rightarrow \pi^- \nu_\tau$ . . . . . 162
The decay of $\tau^- \rightarrow \rho^- \nu_\tau$ . . . . . 163
Multipion final states . . . . . 164
The energy distribution of tau neutrino flux . . 164
The tau neutrino charged current cross-section suppression . . . . . 167
Simulation of $\nu_\tau$ interactions in BEBC . . . . . 171
Simulation of the tau decay products . . . . . 172
Simulation of the expected background distributions . . . . . 176
Search for a tau neutrino signal . . . . . 177
Experimental distributions . . . . . 185
Results . . . . . 186
Comparison with other methods . . . . . 191
Estimate of the $D_s$ meson production cross-section 196

IX. CONCLUSIONS . . . . . 199

REFERENCES . . . . . 202

# Chapter I

## INTRODUCTION

This thesis is about a neutrino beam dump experiment carried out at CERN in 1982 using The Big European Bubble Chamber (BEBC) as the detector [1]. The beam dump experiments have been a suitable way to search for new phenomena in hadron-hadron collisions. The term 'beam dump' refers to the fact that the incident beam particles are buried in a massive dense target which absorbs them almost entirely. The most likely penetrating particles, unhindered by the target, will be the neutrinos coming from the decay of secondaries. By minimising the decay path of these secondaries, the neutrino fluxes from long lived particles such as pions and kaons are strongly suppressed, however for particles with lifetimes less than $10^{-11}$ s the decay path length is of the order of or less than interaction length and most of these particles have time to decay before being absorbed.

Both charged and neutral leptons are produced in the purely leptonic and semileptonic decay modes of the short lived particles. The leptons from the decay of these short lived particles are refered to as **prompt** while the ones from the decay of longlived parents are called **conventional.** The prompt neutrinos produced can be detected and give information about very short

lived particles produced in hadron-hadron collisions. New processes with very small cross-sections will in this way have a chance to show up above the background. New types of neutrinos produced from the decay of heavy mesons or from the decay of heavy leptons can be detected. In addition search can be done for new unexpected effects, axions, supersymmetric particles, etc.

## 1.1 PREVIOUS BEAM DUMP EXPERIMENTS

Beam dump experiments were first suggested by Pontecorvo as a method of searching for alternative neutrino sources [2]. The first CERN beam dump experiment was carried out in 1971 using the 26 GeV PS proton beam and the Gargamelle bubble chamber as the detector [3]. This experiment set limits on the production of heavy neutral leptons, without observing any prompt signal. It was followed in 1977 by three CERN beam dump experiments making use of the 400 GeV proton beam from the SPS [4-6]. The detectors used were the two bubble chambers BEBC and Gargamelle and the CDHS counter set-up. These experiments established the existence of a prompt electron neutrino signal which was assumed to originate from decays of charmed particles, produced with a cross-section at least one order of magnitude larger than previous limits.

In 1979 three beam dump experiments were performed at CERN using BEBC and the CHARM and CDHS detectors [7-9]. The main reasons for these experiments were:

1. To allow longer run periods, thus estimate of prompt rates with better statistical accuracy;
2. To investigate the previous rate discrepencies and obtain the prompt rates by extrapolation using 2 dump densities;
3. To disprove $K^0$'s as source of $\nu_e$ source;
4. To measure the conventional flux.

These experiments confirmed the prompt electron neutrino flux, and a $\nu_\mu$ signal was also found. The $\bar{\nu}_\mu$ signal, on the other hand was seen by BEBC and CHARM only, in spite of the larger statistics of the CDHS group [9], and therefore needed confirmation. On the other hand CHARM [8] reported an unexpected excess of low energy ($< 20$ GeV) events without final state charged leptons. If real, this effect would be a clear indication of some new process. The question most obviously in need of clarification, however, was the observed ratio of prompt electron to muon neutrino interactions. Table 1 shows the value of this ratio for the three experiments and for the two different background subtraction methods. Decays of charmed particles would give a unit ratio as a consequence of e-μ universality. If taken at face value, the results indicate a ratio less than unity. It is possible, however, that there is some common systematic error, since the three detectors were in the same beam-line.

To settle the questions raised by the CERN 1979 results four different groups performed beam dump experiments at CERN and in Fermilab in 1981-1982. The major improvements for CERN experiments over previous setups were:

TABLE 1

Prompt e/μ ratios from the CERN 1979 beam dump experiments

| Experiment | BEBC | CDHS | CHARM |
|---|---|---|---|
| e/μ (extrap.) | - | 0.78±0.20±0.24, | 0.49±0.21 |
| e/μ (subtr.) | $0.59^{+0.35}_{-0.21}$, | 0.56±0.07±0.19, | 0.48±0.12±0.10 |

i) Protons were transported through the vacuum all the way to the shielding and the dumps were installed there. As a result the source of prompt neutrinos was closer to detectors resulting in a solid angle acceptance about four times as large;

ii) There was more systematic monitoring of proton interactions upstream of the dump by means of increasing the number of beam loss monitors from 8 to 24;

iii) Better knowledge of conventional flux from particle production measurements in proton-copper collisions in spectrometer experiments.

In addition to improvements in the general layout, the following improvements were made to BEBC:

a) BEBC was equipped with a picket fence allowing better muon detection efficiency and association of neutral hadron induced events to neutrino interactions outside BEBC, thus reducing the background in the NC sample;

b) The installation of a high resolution camera allowed detailed vertex studies in a subsample of events.

## 1.2 THE FEATURES OF BEAM DUMP EXPERIMENTS

Given the small production cross-section for the very short lived particles, and their leptonic and semileptonic branching ratios of few percent we expect:

1. A low event rate;
2. A substantial fraction of electron neutrino induced events;
3. A finite chance to see tau neutrino interactions;
4. A chance to observe or put an upper limit on the production of axions, susy particles and heavy neutrino decays.

Given the above facts, one can finally add that compared to the normal neutrino experiments the beam dump experiments have a different feature in that they look at the neutrino production and qualities of the neutrinos themselves, rather than using them as probes only.

## 1.3 THE SCHEME OF THIS THESIS

This thesis is organised in the following way: Chapter 2 describes the whole experimental setup with emphasis on the beam line, the targets, the muon flux monitors, the bubble chamber and the electronic detectors associated with charged track and muon identification. The content of this chapter is based upon

my experience of attending data taking runs together with information available in various forms about the individual detectors. Where applicable, relevant references are given in the text for the interested reader.

Chapter 3 deals with the task of scanning and measuring the raw data. The rules governing the scanning and measuring were set by the collaboration and were applied in the individual laboratories. Again I actively took part in scanning and checking the quality of measurements in close collaboration with my other colleagues and the scanning and measuring staff in Imperial College.

Chapter 4 deals with corrections required to the data because of various inefficiencies associated with the detectors. The content of this chapter is largely based upon my own work, although where applicable appropriate references are made and other independent estimates quoted.

Chapter 5 discusses the criteria used in selecting tracks and events for physics analysis. These selection criteria were adopted by the whole collaboration and chosen as standard cuts applied to the data. This chapter also considers the usual kinematical parameters associated with CC events and gives their corrected rates using estimated efficiencies from chapter 4.

Chapter 6 deals with the prompt charged current event rates. Because of importance of this topic many people contributed to various estimates and the final results. The conventional background estimate for the subtraction method was done by Rutherford and CERN groups. The prompt rates from the subtraction and extrapolation methods were also estimated by other members of collaboration namely CERN, Stockholm, Bonn and Oxford groups. The rates for through-going muons were estimated by Rutherford, CERN and Bonn groups and are quoted here. The generalised least squares fits to prompt rates using all information including those from through-going muons were obtained by Stockholm group and are quoted in this chapter.

Chapter 7 covers the NC sample. It gives an estimate of the hadronic background in the observed NC sample for various hadron energy cuts. It also discusses various corrections needed in order to estimate the number of misidentified CC events in the observed NC sample and compares the results with values obtained for the NC to CC ratio using kinematical methods. Similar estimates were also made by Stockholm and Oxford groups. This chapter also discusses the implication of the NC to CC ratio obtained and compares the results from this experiment with similar results from conventional neutrino experiments. It also discusses the excess of so called low energy NC events reported by CHARM beam dump collaboration.

Chapter 8 deals with an important aspect of beam dump experiments which is search for tau neutrino interactions. It considers the possible sources of $\nu_\tau$ and discusses the kinematics of $\nu_\tau$ interactions in the bubble chamber. This chapter presents a new and efficient method used to estimate the number of $\nu_\tau$ charged current interactions in the bubble chamber. It compares the results obtained from this method with other methods used to estimate the number of $\nu_\tau$ interactions. It also puts limits on the $D_s/D$ cross-sections ratio. The results from this chapter have since been published. The method used was developed in close collaboration with Wilbur Venus and Jon Guy at Rutherford laboratory with contributions from Stockholm and CERN groups.

Finally chapter 9 concludes on the results of previous chapters and considers the importance of the results obtained.

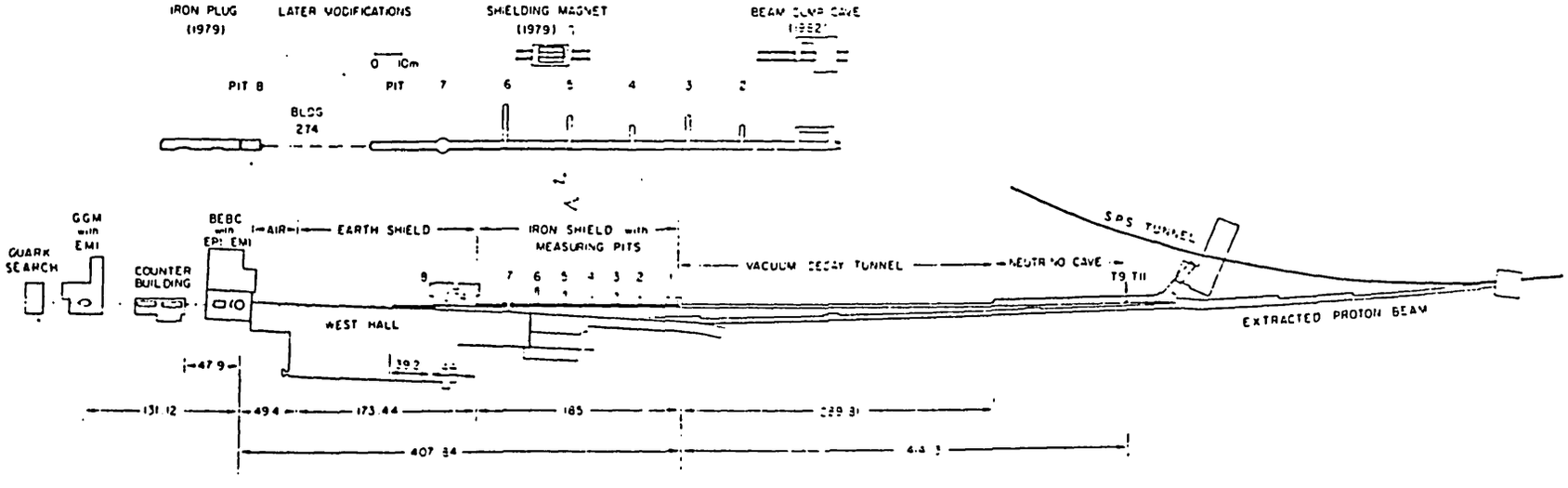
## Chapter II

## EXPERIMENTAL SETUP

### 2.1 BEAM LINE

The beam in this experiment was the 400 GeV Proton beam which was ejected from the CERN Super Proton Synchrotron (SPS). Figure 1 shows the the neutrino beam line set up. After a 25.5 milliradian bend, the protons entered the beam line. The protons were delivered pulse by pulse in spills of 23 microseconds, corresponding to one revolution of the SPS internal proton beam along the 6.9km circumference. About $10^{13}$ protons were extracted in a single pulse. The proton beam extracted from the SPS was transported through the standard wide band magnetic system into the neutrino decay tunnel.

The proton transport beam pipe was equipped with 24 ionisation chambers which measured the ionisation coming from possible interaction of the protons with the beam pipe (the so called beam scraping). These ionisation chambers (scraping monitors) were calibrated by placing Aluminium foils of 70 micrometres thickness into the beam and simulating beam losses of $10^{-5}$ - $10^{-3}$ at different positions. The beam intensity was measured by three independent Beam Current Transformers (BCT) at different positions along the beam line. The beam position immediately before




Scale drawing of the West Area Neutrino Facility WANF. The region of the iron shield with flux measurement pits is also shown enlarged. Indicated are modifications in 1979, when a magnet just after pit 5 and additional shielding behind building 274 were installed, and in 1982, when a cave for the proton beam dump was built.

Figure 1: The Beam Line set up

the target was monitored by two position sensitive counters just in front of the target. The signals from all the monitors were recorded for each beam spill and were used later in the data analysis stage in order to exclude bad events and reduce the background of fake prompt events from possible beam-pipe interactions.

## 2.2 THE TARGET

In the beam dump three interchangeable targets of different densities were used. These are shown in figure 2. The full density target was a 3m long solid copper block of density 9.0 gm/$cm^3$. The half and one third density targets were obtained by spacing copper disks of 2.5cm thickness with 2.5cm and 5.0cm of air respectively. In this way effective densities of 4.5 gm/$cm^3$ and 3.0 gm/$cm^3$ were achieved. Behind the dump a 3m long water cooled solid copper block (catcher) was installed to absorb any hadrons coming through the target.

Unlike the previous beam dump experiments at CERN, in this experiment the target and the catcher were placed just in front of iron shielding. This meant that the proton beam was transported through the vacuum all the way to the iron shielding resulting in a larger solid angle for the detector. The front of the dump was 405.9m from the centre of the BEBC compared to a distance of 821.2m in the prevoius BEBC beam dump experiments resulting in gain in solid angle of 4.08.

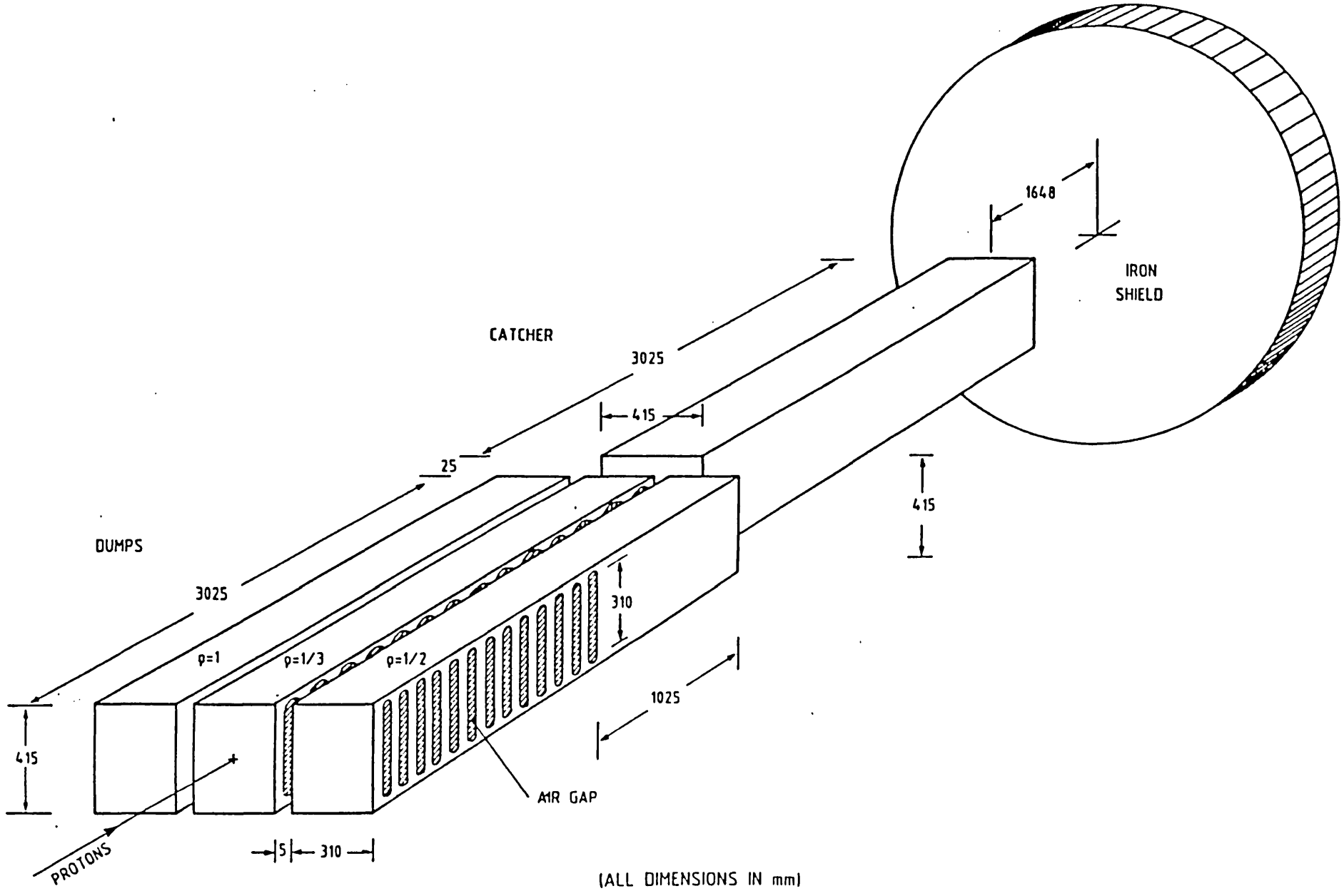



Figure 2: Dumps used in this experiment

## 2.3 THE MUON DETECTORS

Inside the iron shielding there were six gaps housing a system of solid state detectors which measured the muon flux.

For our purpose, only the first four gaps were used. The standard geometry of detector positions in one gap is shown in figure 3. As can be seen from this figure, the detector box allows full detector circles at radii of 150mm, 300mm, 450mm, 600mm and 750mm. Only the first three circles were used. Refering to figure 3,the positions are numbered 'nm' where n is the angle in units of $\pi/4$ and m is the radius in units of 150mm.

There were two main problems with these detectors:

1. Their pulse heights were not proportional to the charge passing through.
2. It was not possible to manufacture them in such a way that under equal conditions, different detectors gave identical signals.

So each detector had to be calibrated individually. This was done during wide band running prior to the beam dump experiment. The error on the calibration was estimated to be 6% [10]. The absolute calibration of these detectors was done by comparison of their output pulse heights with the number of muon tracks found in nuclear emulsion, which was placed immediately upstream of the counters for a few beam pulses.

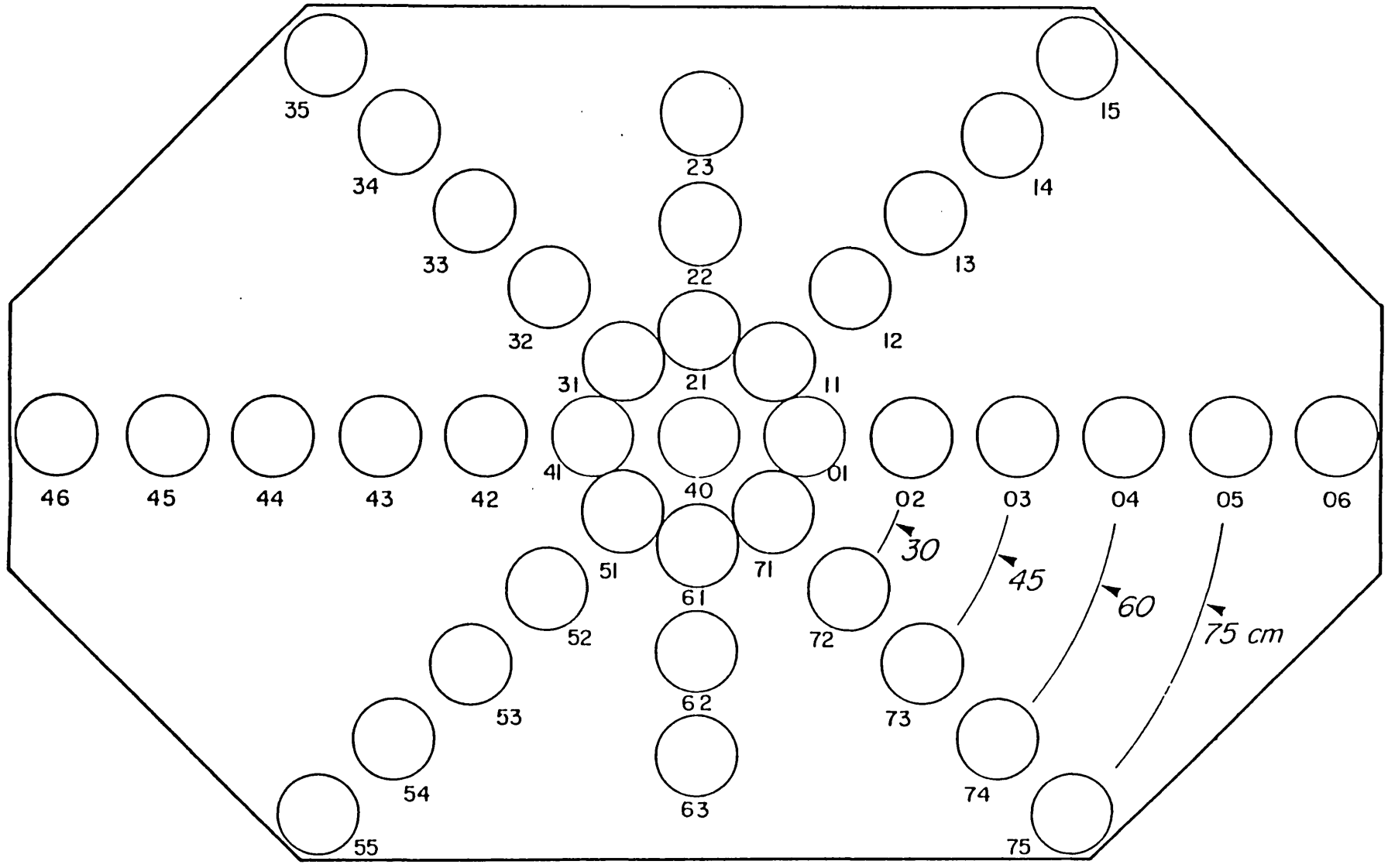



Figure 3: The standard geometry of a detector

## 2.4 THE NEUTRINO DETECTOR

BEBC has been described in many publications, so its description will be brief and main attention will be paid to the condition under which it was operating at the time. A sketch of the detector is shown in figure 4. As can be seen from this figure, BEBC is a stainless steel cylinder, 3.7m in diameter and 4.0m in height with a hemispherical cap. The chamber volume is approximately $32m^3$.

BEBC was filled with a neon/hydrogen mixture of 74 mol-% neon with a mean density of 0.69 $gm/cm^3$ and radiation length of 43cm. The bubble chamber was surrounded by two superconducting coils producing a magnetic field of 35 KG which allowed determination of the sign of the charge and the momentum of each individual track. In the hemispherical cap, there were 5 points, arranged in a regular pentagon, which housed the wide angle lenses, fish eye optics and flash bulbs. For our purpose BEBC was equipped with four standard cameras and one with "high resolution" of about 200 micrometres. The field of the high resolution camera was small and as a result only 10% of the observed events were within the range of this camera. Since the cameras were not able to give accurate pictures of the whole inside of the chamber, a fiducial volume of $16.6m^3$ was chosen such that the event rate and the measurability of the tracks was optimised. This fiducial volume corresponded to a target mass of 11.5 tonnes.

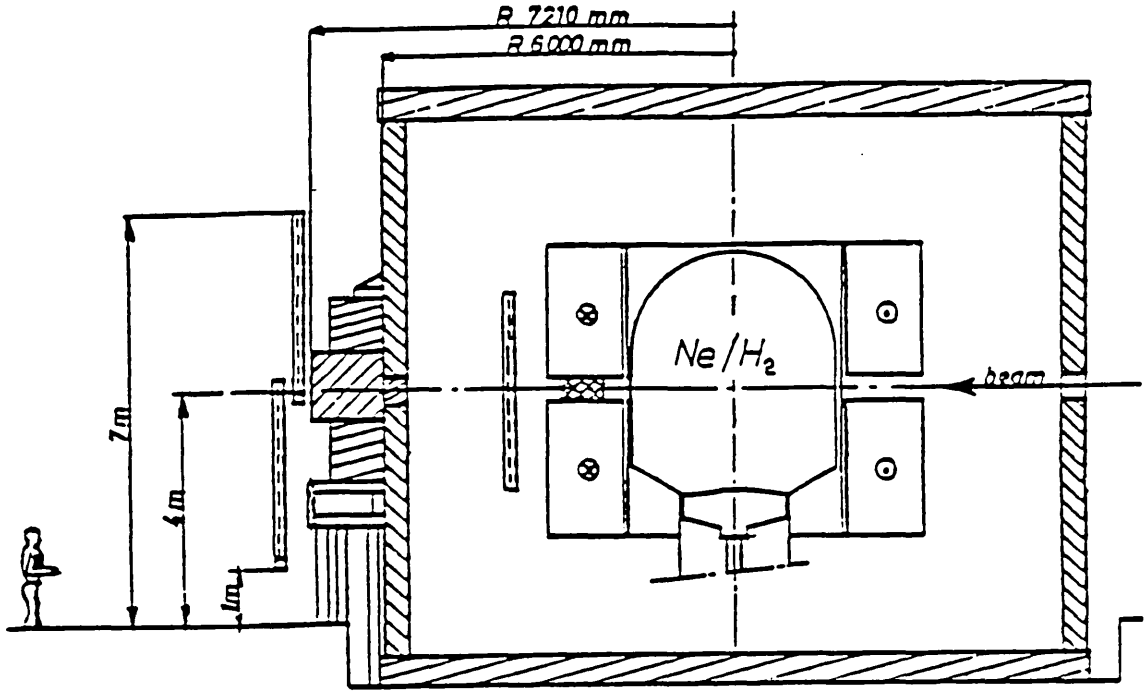



Figure 4: The Big European Bubble Chamber

## 2.5 THE EXTERNAL MUON IDENTIFIER

In neutrino physics it is important to know whether or not a muon is produced in an interaction in order to classify the event as a muon charged current event.

Since from the bubble density fast muons can not be identified an alternative detection method must be employed. In figure (5) the arrangement of the External Muon Identifier (EMI) and BEBC is shown as it existed in this experiment. A detailed

description of EMI can be found in reference [11], a short description is given below.

### 2.5.1 Arrangement of the EMI

Muons may be identified by means of their penetration of matter. A block of lead with a thickness of 0.5m just behind the BEBC plus the iron shielding enlarged with some 150 tonnes of additional iron absorbed hadrons but were transparent for muons with sufficient momentum. The shape of the iron shielding was asymmetric; in the forward direction of the beam where the most energetic hadrons were expected the thickness was 1.7m, at the corners of the shielding the thickness was 0.5m.

Muons were identified by two planes of multiwire proportional chambers (MWPC) set up downstream of the BEBC. The inner plane was situated at about 4m from the centre of BEBC and in this experiment consisted of 8 modules covering an area of $24m^2$ and subtending a solid angle of $-34^\circ$ to $+64^\circ$ horizontally and $-18^\circ$ to $+18^\circ$ vertically. The outer plane at about 7.6m from the BEBC centre had two rows of 45 modules covering an area of $138m^2$ from $-66^\circ$ to $+84^\circ$ horizontally and from $-20^\circ$ to $+20^\circ$ vertically. The sensitive area of each of the wire chambers measured roughly 3x1m. Two independent wire planes were provided at $\pm 30^\circ$ with respect to the short side. In addition, two cathode strip planes were formed at $90^\circ$ and $0^\circ$ with respect to the 1m side. Each module provided three hit coordinates. Two came

from independent sense wire planes. To resolve ambiguities from multiple hits, information from one cathod (strips at $90^{o}$ with respect to the short side) was read out too.

The spatial resolution was determined by the grouping of several wires into single electronic channels. The inner plane had a spatial resolution of 32mm (8 wires per channel). The spatial resolution of the outer plane was made to vary from 8 mm (2 wires per channel) in the central region where the highest concentration of background hits occurs, to 32mm (8 wires per channel) at large angles.

The system of the array of multiwire proportional chambers and the iron shielding is called the External Muon Identifier

A veto plane consisting of 6 low resolution EMI chambers was installed in front of the BEBC. These chambers were used in coincidence with the two EMI planes to overcome the background problems in the EMI due to the beam associated muons or muons coming from the neutrino interactions upstream of the BEBC. Hits from these muons in the two downstream planes of the EMI could be vetoed by this plane.

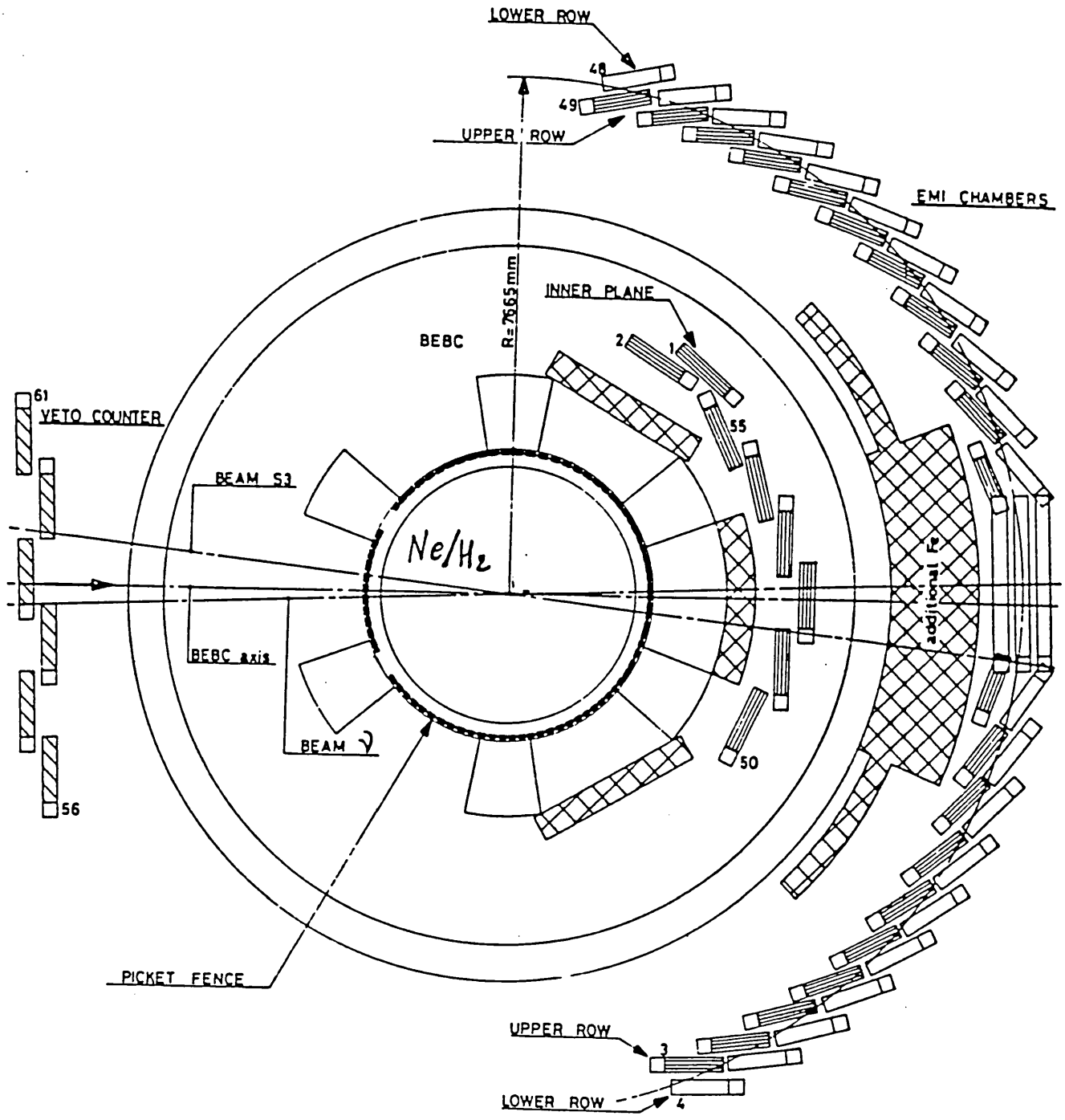



Figure 5: The arrangement of the BEBC with the EMI

### 2.5.2 Muon identification

For muon identification, each leaving track from a neutrino event in the chamber is extrapolated towards the EMI chambers. The uncertainty in the determination of the interception point of the extrapolated track and the EMI chamber is dependent on the momentum of the particle, the multiple scattering and bremsstrahlung on the path followed by the particle in the shielding. A chisquare is calculated for the correlation between the coordinates of the interception point and the recorded hits at that plane. A second chisquare is determined for the correlation between the hit in the inner plane and in the outer plane. If hits are found in both EMI planes within a time resolution of ~ 300 ns (i.e. within the same time slot) which coincide with the extrapolated track, the muon mass is assigned to the track.

## 2.6 THE INTERNAL PICKET FENCE

The Internal Picket Fence (IPF) [12a] is a proportional tube counter system mounted in the BEBC vaccum tank close to the liquid. The IPF is a device giving a timing signal for all events where a charged particle leaves the chamber. The addition of IPF to BEBC was justified by physics arguments, and provided valuable information in the following areas [12b]:

a) association of reinteracting neutrals (which would not be recognised otherwise);

b) vetoing of incident neutral hadrons (generated by neutrino interactions in the magnet coils or other material upstream);

c) use as an off-line trigger;

d) improvement of the EMI efficiency for muons of low momenta.

The time resolution of the pickets was 230 ns full width, which fitted well to the resolution of the EMI electronics.

For this experiment, however, because of unavailability of the necessary software and PAM files, the IPF was mainly used for improving the identification of low energy muons and as an off-line event trigger in conjunction with the EMI [1].

# Chapter III

# EXPERIMENTAL PROCEDURE

## 3.1 EXPOSURE AND ACCEPTANCE

In this experiment a total of 300,000 pictures were taken corresponding to $3 \times 10^{18}$ protons extracted from the SPS.

For a photo to be accepted, the following main criteria had to be satisfied:

a) the last four scraping monitors situated just in front of the decay tunnel were required to have a reading of less than 150mV (this corresponded to a beam loss of less than $10^{-5}$);

b) the vacuum in the decay tunnel required to be below $3 \times 10^{-2}$ torr.

As a result of these and other conditions [13], a part of the data had to be rejected and the number of protons (9% of the total ) corresponding to this data had to be excluded from the integrated sum of the protons.

## 3.2 SCANNING

### 3.2.1 Scanning for neutrino events

The film was scanned twice, using views 2 and 4 for the first and views 3 and 5 for the second scan respectively. On the first scan all the frame numbers were recorded including the very first and the very last frame on the film. All missing, dark or damaged frames on either of the views were also recorded.

A neutrino event candidate was defined by the following criteria :

a) it should have at least one minimum ionising track in the forward direction with a radius of curvature greater than 15cm on the low magnification view corresponding to a minimum momentum of 500 MeV/c in the chamber;

or

have a $V^0$ or an electron pair in the forward direction where the sum of the momenta of both tracks was at least 500 MeV/c;

b) the event originated in the chamber (i.e. it was not due to a charged track entering the chamber and interacting).

In addition to the neutrino candidates the following background events were also recorded:

i) type X : These were interactions due to an incoming track where the track was signed to be incoming because it had a delta-ray showing its direction;

ii) type Y : These were events thought to be due to an incoming charged track but there was no clear indication as to whether the track was leaving or entering the chamber. In order to be classified as a 'Y' type, the event had to have a track with a radius of curvature greater than 30cm, and backwards from the event vertex;

iii) type W (Wallon) : These were events where the event vertex was not in the bubble chamber liquid but in or just before the wall of the chamber. The event consisted of at least 3 tracks entering the chamber within a distance of a scotchlite panel (34cm) horizontally and vertically. At least one of these tracks had to be an identified hadron (i.e. interact, stop or decay);

iv) type Z : When all tracks failed the criteria for a neutrino event, the event was classified as Z-type;

v) associated events : All neutrino candidates were checked if they were possibly neutral stars ( $n^*$ ), due to neutral hadrons coming from an upstream interaction of any sort. The following possibilities were considered:

a) Events which could be associated with a neutrino interaction or an interaction of a track from a neutrino interaction;

b) Events which could be associated with a wallon or a secondary interaction of one of the tracks of the wallon;

c) events associated with the interaction of an incoming track (i.e. type X and Y), or the interaction of a track produced in such an interaction.

Using the results of the two scans an event check list consisting of the frame number of all the possible neutrino and the ambiguous background events observed in either scan was prepared. From the event check list, each frame with an identified interaction was checked again with the aid of a physicist. At this stage those events which had relatively simple topologies (i.e. events with no complicated close secondary interactions or electromagnetic showers) were drawn and the vertices and the tracks were labelled on a X18 magnification table. More complicated events were left to be drawn at the measuring stage on a X50 magnification table. It should be noted here than the scanning and measuring was done for a part of the data at Imperial College. The other participating laboratories [1] were also involved in scanning and measuring of the data and generally followed a procedure not necessarily the same but similar to the scheme adopted by Imperial College which was described above.

### 3.2.2 Scanning for electron tracks

In scanning for the neutrino events all tracks originating from the vertex were specially checked for the "electron" signals.

This was important since in this experiment we were looking for electron charged current events. The use of heavy liquid with a radiation length of 43cm allowed us to identify the potential electron tracks by means of their radiation loss in the liquid.

Since the electron is about 200 times lighter than the next heavier known particle, according to the "Bethe Heitler" formula, its radiation loss due to collision with nuclei in the chamber is by a factor

$$( m_\mu / m_e )^2 \approx 42500 \qquad (3.1)$$

larger than for the muon, and even larger when compared with hadrons. Thus an electron could be identified by its rapid loss of energy.

To be accepted as an electron the track required to have at least two of the following identifiers:

1. Change of curvature without a visible kink (non-converted bremsstrahlung);
2. an $e^+e^-$ pair pointing tangentially to the track (converted bremsstrahlung);
3. an $e^+e^-$ pair lying on the track and carrying more than 10% of the track energy;

4. a delta-ray taking at least 25% of the primary energy.

An identified pair of electrons $e^+e^-$ from the main vertex ("Dalitz pair") was not accepted as a signal for $\nu_e$ events.

### 3.2.3 Scanning of through-going muons

In front of the fiducial volume of BEBC there was about 50 tons of material in the form of the upstream part of the superconducting magnet, the support structure and the magnetic shielding. The muons produced in the neutrino interactions in this material could be detected as "through-going muons" inside BEBC.

Using the "EMI-IPF" System as an offline trigger it was possible to find muons which came from interaction points between the EMI veto plane and the IPF upstream plane.

For this reason a special list was provided for those photos for which the EMI and the IPF signalled a leaving track. The list was used in scanning for through-going muons.

In addition to scanning for through-going muons the list was also used as a cross check for those muon charged current events where the muon was identified by the EMI-IPF system. This helped to identify those muon CC events which were missed in the scanning stage.

A through-going muon was defined by the following criteria:

1. a minimum ionizing track with a radius of curvature greater than 15cm in the forward direction on the low magnification view corresponding to a minimum momentum of 500 MeV/c in the chamber;

2. the track had to be incoming by having its entry point on the upstream wall of the chamber and not originating in the liquid (this was further checked by means of delta-rays on the track identifying its direction of entry into the chamber);
3. the entry and exit points of the track had to be visible on at least two views.

In order to facilitate the identification of the through-going muons each scanning table was provided with a drawing which identified the region of the bubble chamber walls corresponding to each IPF chamber. This enabled scanners to find the track between the correlated hits in the IPF chambers.

### 3.2.4 Events visible on the high resolution camera

As mentioned earlier (see 2.4) the BEBC was equipped with a special "High Resolution Camera" (HRC) of resolution about 200 micrometres. The purpose of this scan was primarily to look for "tau" decays or kinks very close to the primary vertex.

In order to predict those neutrino events with their primary vertices within the view of HRC a special routine was provided which took the co-ordinates of the event vertex and returned a one bit flag which indicated whether or not the vertex was expected to be visible on the HRC.

Using the special HRC list all events were scanned on the HRC view and normal BEBC views. The primary vertices were

recorded if they were visible and well focused on the HRC view. All tracks appeared to be originating from the primary vertex with a length less than 2cm on the low magnification view were recorded. In addition all tracks were followed from the end to see whether they extrapolated back to the primary vertex. All $V^0$'s within 2cm of the primary vertex were also recorded. The events were drawn and a photo was taken on the HRC view and on the best normal view if :

1. they had charged decays or interactions visible on the HRC view;
2. a track appeared to miss the primary vertex but could not be matched or paired with other tracks by eye.

## 3.3 MEASURING

At measuring stage all the events had to satisfy the following criteria :

1. events were measured fully if the event vertex was within the fiducial volume. This volume was defined in the "X-Y" plane by a semicircle of radius 180cm in the upstream direction, and a semicircle of the same radius, but with its centre displaced 50cm upstream, in the downstream direction. In the Z direction the region was defined by a cut at Z = ±125cm. If the event was out of the fiducial volume then the corresponding primary vertex was recorded and no further measurements was made;

2. if the selected frame contained a W, X or Y type event, then the corresponding neutrino event was not measured.

The events passing the above criteria were measured on the "best" three views. For all accepted events, the following neutral secondaries were also measured:

i) all $V^0$'s;

ii) $n^*$'s; downstream of the primary vertex (those with stopping protons were measured if the sum of the length of the tracks exceeded 2cm);

iii) evaporation protons from the primary vertex.

### 3.3.1 Measurements of through-going muons

The through-going muons were measured in a similar fashion to one prong neutrino events.

### 3.3.2 The labelling scheme

In order to simplify and facilitate the measuring of events, a comprehensive vertex/track labelling scheme was employed in the drawing stage. The use of labelling scheme allows the identification of different events for frames with more than one event on them, and for the association of gammas and $V^0$'s to vertices. It also helps the measurer in communication with the measuring control program, specially in sorting out the complicated events.

The track end-type labels are useful for the "Geometry" program for matching of tracks from secondary scatters. The track

labels are also used to reduce the number of mass hypothesis attempted (eg no muon hypothesis is attempted on an interacting track). Finally since the track end-type labels are produced on the final data summary tape (DST), they can be used for eventual physics analysis (for example in searching for all interacting tracks etc).

The labelling scheme for the vertices in this experiment was as follows :

1. Primary vertices : All the main vertices of potential neutrino events. All associated events (see 3.2.1) were also included in this category;
2. Secondary vertices : All interaction points, kink points, stopping points and decays;
3. $V^0$ vertices : Charged decays of $V^0$'s;
4. Gamma vertices : Vertices of $e^+$ or $e^-$ or $e^+e^-$ pairs.

The track end-type labels used were:

i) Leaving (L) : Non interacting tracks which left the chamber (i.e. intersected the chamber wall);

ii) Interacting (I) : A non stopping track which interacted and;

a) produced more than 1-prong, or

b) disappeared in flight (usually a negative), or

c) produced 1-prong with a clear ionization and/or momentum change.

iii) Stopping (S) : Any stopping track whose charge could be determined by curvature and which was very heavy at the end. For these tracks all mass hypotheses were tried and the fit was rejected if there was a momentum-range incompatibility;

iv) Proton (P) : A heavy ionizing short stopping track;

v) Decay (D) : Decay at rest of $\pi$-$\mu$-e or $\mu$-e;

vi) Kink (K) : A one prong interaction where the outgoing track scattered through a small angle;

vii) Electron (E) : Definite electron for which only the electron mass hypotheses was tried (eg at a gamma vertex);

viii) Possible electron (PE) : A possible electron from a primary vertex or a kink for which other mass hypotheses were also attempted.

### 3.3.3 Measurements procedure

Using the above vertex/track labelling scheme, the events were measured on a X25 and a X50 magnification measuring machines. The X50 machine was particularly useful for measuring complicated events with heavy gamma showers or poor track visibility near the vertex.

The measuring machines were connected via a PDP 8L minicomputer to a VAX 11/780. Each machine was monitored by a measurement control program on the VAX.

The measurement control program enabled:

1. Steering of the measuring tables, positioning of the film, measurements of fiducial marks, automatic track following, test of electronics etc.
2. Communication between the operator on the measuring machine and the software on the main computer.

The events were measured by entering the roll and the frame number followed by a measurement of fiducial marks. The vertices and the corresponding tracks were measured on three views in turn with their appropriate label/end-type code supplied. At the completion of the measurement of any item, the control program called for the "On-line Geometry" which in turn reconstructed the vertices and the tracks using helix fits. If the measurement was diagnosed bad (normally large chisquare or residuals), it was reported back to the measurer by the control program requesting a remeasurement of the item. For badly measured tracks the program allowed for the measurement to be repeated three times. If at the end of the third measurement no satisfactory result was obtained the last measurement was accepted.

Once all or a good fraction of the events were measured they were processed by the Hydra "Off-line Geometry" program. The "Off-line Geometry " program transforms all the measurements on each view to a reference system defined by the expected positions of a set of fiducial marks in a plane parallel to the film.

Knowing the camera positions in a common reference frame, the spatial coordinates of a given point were determined from the measurement of its image on 3 views.

From a knowledge of the magnetic field map and the range-momentum relation of the chamber liquid, the track parameters were determined by fitting of the track measurements to the expressions for the trajectory of the particle in a magnetic field taking into account the multiple scattering etc.

The "Off-line Geometry" program then attempted various mass hypotheses and performed kinematical reconstruction of measured $V^0$'s and gammas and attempted to associate them to the upstream primary and secondary vertices.

### 3.3.4 Measurements checking

The output from the "Off-line Geometry" program was processed by a checking program called "Quack". The "Quack" program attempted to identify badly diagnosed events, vertices or tracks.

The outputs from the "off-line Geometry" and the "Quack" programs were then used by physicists in conjunction with the original drawings of events (mainly to identify the individual vertices and tracks by their labelling/end-type codes), to check the event measurement quality at the scan table.

In checking the measured events the following procedure was normally carried out:

1. the vertices and tracks of an event were checked if they were labelled properly and had the right end-type code. If the "Quack" signalled an ambiguity due to an event; not completely measured or more than one primary vertex was associated with the event or the tracks carried wrong end-type codes, then the appropriate action was taken and the corresponding vertex or track was identified and labelled properly. The redundant vertices or tracks were subsequently dropped from the geometry. The incomplete events were required to be remeasured completely.
2. all primary charged (non electron) tracks were required to have a momentum error $\Delta P/P \leq 30\%$. They also required to have residuals of less than 20micron.
3. in the case of primary tracks being too short to give an accurate momentum estimate, the secondaries from such primaries were required to be measured, in order to allow a minimum momentum estimate to be made for the primary track. In addition, if the measured track length was cut by the measurement program, (i.e. part of the track was rejected), then the reason was investigated and the track was carefully checked for kinks, brems etc.
4. all events were checked for associated $V^0$'s and gammas in order to make sure that as much as possible of the primary neutral energy was measured. The ambiguous $V^0$/gamma vertices and the tracks from such vertices were

also checked in order to identify them positively and reduce the number of $V^0$'s ambiguous with gammas.

On the basis of these checks, the correct action was taken for diagnosed events and the procedure was repeated until satisfactory measurement results were obtained for each event.

## 3.4 PRODUCTION OF THE DATA SUMMARY TAPE (DST)

Once satisfactory measurements for all events were obtained the measurements were sent to CERN where, together with the rest of measurements from other labs they were processed by a series of analysis programs.

The basic function of these programs were as follows :

1. to merge the external detectors information with the geometry/kinematics data. The output from the geometry program together with the raw EMI data were used as input for the EMI analysis program. Leaving tracks were followed through the fringe field to the various detector planes encountered and the muon candidates were identified (see 2.5.2) [14];
2. to use the Neutrino Flux Monitor (NFM) data, in order to create a special beam dump bank with the relevant NFM information on it [15];
3. to make final decisions on muon candidates, and in cases where the muon momentum was badly determined, an attempt was made to improve the error by comparing the

position of the extrapolated points to the EMI hit positions (program DCID);

4. to flag the identified "electron" tracks and the corresponding brems appropriately, and store different electron track measurements and relevant information including the leakage corrections [1] in the banks;
5. to select the best origins for the association of $n^*$'s, gammas and $V^0$'s, and synthesise neutral track connections for $n^*$'s and $V^0$'s (program SYNTH). The criteria at CERN for linking neutron stars was found not to be satisfactory, therefore a method had to be devised to identify the potential unlinked $n^*$'s (see chapter 4). In the case of $V^0$'s and gammas the best origins were determined from the results of 3c fits to each vertex;
6. to select the best mass fit for each particle using the routine BESTMF . If kinematics fits were available, then the one with the best kinematics hypothesis was chosen (i.e. the one with highest number of degrees of freedom and highest fit probability), otherwise the geometry/feed results were used to select the best mass fit. If mass identification was not possible the pion mass was assigned to the track.

Finally the program DSTOUT was used to generate for each primary vertex a physics bank from the PF/TF/MF banks (with mass selection specified in routine BESTMF). This program also

stored the complete Hydra-structure in a magnetic tape. The created data tape was used as the basis for physics analysis.

# Chapter IV

# EXPERIMENTAL CORRECTIONS

## 4.1 SCANNING EFFICIENCY

The film was scanned twice, using views 2 and 4 for the first, and views 3 and 5 for the second scan respectively. The estimated combined efficiency of these two scans is given by :

$$P(1U2) = (N_{12}(N_{12}+N_1+N_2)) \;/\; (N_{12}+N_1)(N_{12}+N_2) \qquad (4.1)$$

Where:

$N_{12} + N_1$ = number of events found in the first scan

$N_{12} + N_2$ = number of events found in the second scan

$N_{12}$ = events found in both scans

In applying the above formula, one assumes that all the events have the same probability of being detected. Such an assumption is not strictly true, since the probability of finding a multiprong event is higher than one or two prong events and as a result of this the above formula was used to obtain the scanning efficiency for different topologies with the following results:

TABLE 2

scanning efficiency for different topologies

| Topology | Scanning efficiency |
|---|---|
| 1 prong | 69 % |
| 2 prong | 87 % |
| 3 prong | 91 % |
| 4 prong | 97 % |
| 5 prong | 98 % |
| > 5 prong | 100 % |

The overall systematic uncertainty in the scan efficiency was estimated to be 3% [13].

## 4.2 CORRECTIONS FOR ELECTRONS

The electron tracks were identified by at least two signatures as described in 3.2.2.

The most significant sources of background which simulated genuine electrons from the vertex were:

i) asymmetric Dalitz pairs or Compton electrons or asymmetric electron pairs appearing to be attached to the primary vertex because the presence of other tracks created a "confusion" region.

ii) delta-rays emitted within the confusion region by energetic primary particles.

In order to reduce the above backgrounds a momentum cut of 0.8 GeV/c was applied to all electron candidates. The detection efficiency for electrons was determined twice, by a Monte Carlo study and by an attempt to evaluate the probability of finding electrons with two or more identifiers experimentally [1]. The results of both method agreed well, yielding an electron detection efficiency of (96+2-1)%. The probability of an electron track not being identified due to "confusion" near the vertex, caused by hadron tracks or an electromagnetic shower was estimated to be of order of 1%. The probability to have a primary electron faked by an asymmetric Dalitz pair, a Compton or a delta-electron near to the vertex was estimated to be less than 0.5% of the electron candidates and thus could be neglected. In summary, these probabilities yielded a total probability of finding an electron in an electron event of (95+2-1)% [1].

## 4.3 CORRECTIONS FOR MUONS

As mentioned earlier, the muons in this experiment were identified by the External Muon Identifier. Given the limited geometry of the EMI and the so called electronic inefficiency associated with this type of detector, possible losses of muons were due to:

1. dead wires in the EMI planes.
2. the EMI chambers down for period of time.

3. chambers taken out of trigger.

4. muons scattering in the shielding.

5. loss of muons due to limited geometry of the EMI.

Taking the above points and other considerations, two types of efficiencies are generally associated with the EMI:

a) the 'electronic efficiency' of the EMI;

b) the 'geometrical efficiency' of the EMI.

Losses 1 to 3 are attributed to the electronic inefficiency of the EMI, whereas points 4 and 5 are dealt under the overall geometrical acceptance for muons.

### 4.3.1 Estimate of the electronic efficiency of the EMI

Good muons are lost due to the electronic inefficiency of the EMI. The most important contribution to this inefficiency is the point 1 mentioned above; the so called dead wires. This arises if any anode wire in any EMI chambers is electronically dead so no signal could be obtained from that particular wire. As mentined earlier (see 2.5.2), the chamber will write out if hits are found in both anode 1 (A1) and anode 2 (A2) in coincidence. The cathode 1 reading is also recorded. If for some reason either A1 or A2 is inactive, then no hit is recorded and the muon will be lost. The lost muon will then be identified as a leaving hadron and will contaminate the hadron shower.

In principle one can rely on the different characteristic behaviour of muons compared to hadrons in order to estimate the

contamination of hadron shower by unidentified muons in events with no observed muon or primary electron, the so called Neutral Current candidates. The misidentified muons will be labelled as leaving hadrons and will be extrapolated through the fringe field to the EMI planes by the EMI analysis programs EMI/DCID (see 3.4) if they have sufficient momentum. The extrapolated hit coordinates will then be recorded in the appropriate banks and kept in the Hydra structure for future reference. Note that the extrapolated track is only identified as muon if actual hits are found in the EMI planes, in the same time slot, within a few multiple scattering distances of the extrapolated hit points. If no actual hit points are recorded for electronic reasons, then no muon will be reconstructed and the track will be labelled as leaving hadron on the DST. These misidentified leaving hadrons will have kinematical characteristics identical to the EMI identified muons and can be identified by these characteristics.

In order to estimate the electronic efficiency of the EMI a kinematical method was used. The analysis relied on the different transverse momentum behaviour of leptons and hadrons as explained below.

In neutrino-nucleon scattering, the momenta transverse to the neutrino direction of both the outgoing lepton and the outgoing observed hadronic system are in general large and in opposite direction. In addition, because of the limited transverse momentum of hadrons relative to the direction of the hadronic shower,

the transverse momentum of individual hadrons is much smaller than that of the total hadronic system, and consequently, the $P_T$ spectrum of leptons will be different from that of hadrons.

For this analysis three samples of tracks were defined as follows:

1. Muons : EMI identified with momentum above 3 GeV.
2. Hadrons ($\bar{c}c$) : Leaving charged hadrons with momentum above 3 GeV, from the muon charged current sample. The tracks were required to extrapolate to both planes of the EMI.
3. Hadrons ($\bar{N}c$) : Leaving charged tracks with momentum above 3 GeV, from events which did not have EMI identified muon or identified primary electron. The tracks were required to extrapolate as in sample 2.

For this analysis only accepted events with visible energy above 10 GeV for which the EMI was functioning properly were used. In addition the standard cuts were also applied.

The transverse momentum of the tracks with respect to the beam '$P_T$ 'of samples 1, 2, and 3 are shown in figure 6. As can be observed, sample 3 (fig. 6a) shows a harder distribution than sample 2 (fig. 6b) suggesting some contamination from sample 1 (fig. 6c).

Assuming sample 3 is a linear superposition of 2 and 1, one can perform linear fits of the form :

$$\text{sample 3} = \alpha\ (\text{Sample 2}) + \beta\ (\text{Sample 1}) \qquad (4.2)$$

giving an efficiency for correct classification:

$$\varepsilon = 1/(1+\beta) \qquad (4.3)$$

Using the three spectra one obtains:

$$\varepsilon = (97\pm4)\% \qquad (4.4)$$

Of course in applying the fit we assumed that the $P_T$ distribution of genuine hadrons in the NC sample was the same as those from CC events.

In order to check further the validity of this method, another kinematical variable, namely the transverse momentum of the track with respect to the final state hadron vector '$P^t$' was used. This used the fact that the distribution of the $P^t$ of one hadron calculated with respect to the vector sum of all hadron momenta is limited. In contrast, the lepton has a large transverse momentum relative to the beam direction and, by conservation of transverse momentum, has an even larger transverse momentum, relative to the total hadron momentum, as shown in figure 7.

In order to be consistent in defining the resultant hadron vector for the 3 samples of tracks as defined immediately above, the following procedure was carried out:

1. Sample 1 : The hadron direction was found by excluding the track with the largest $P_T$ (whether it was

muon or hadron), and summing the momenta of all remaining charged hadrons.

2. Sample 2 : The hadron direction was taken to be the sum of all charged tracks excluding the muon and the hadron with the largest $P_T$.
3. Sample 3 : The hadron track was taken to be the sum of all charged tracks excluding the track with the largest $P_T$ with respect to the beam.

The $P^t$ distribution for these samples is shown in figure 6. As can be seen from this figure, sample 3 (fig. 6d) has a harder spectrum than sample 2 (fig. 6e), suggesting some contamination from sample 1 (fig. 6f). Using the same fit as before we get:

$$\varepsilon = (97.8 \pm 2.9)\% \qquad (4.5)$$

Generally one needs to consider:

a) the so called "edge effect"

b) the contamination of sample 3 by electrons

#### 4.3.1.1 Edge effect

Muons which are genuinely outside the acceptance may, by error, be extrapolated to inside giving contribution to sample 3. One needs to take away this contribution from the 'electronic inefficiency' because it is geometrical.

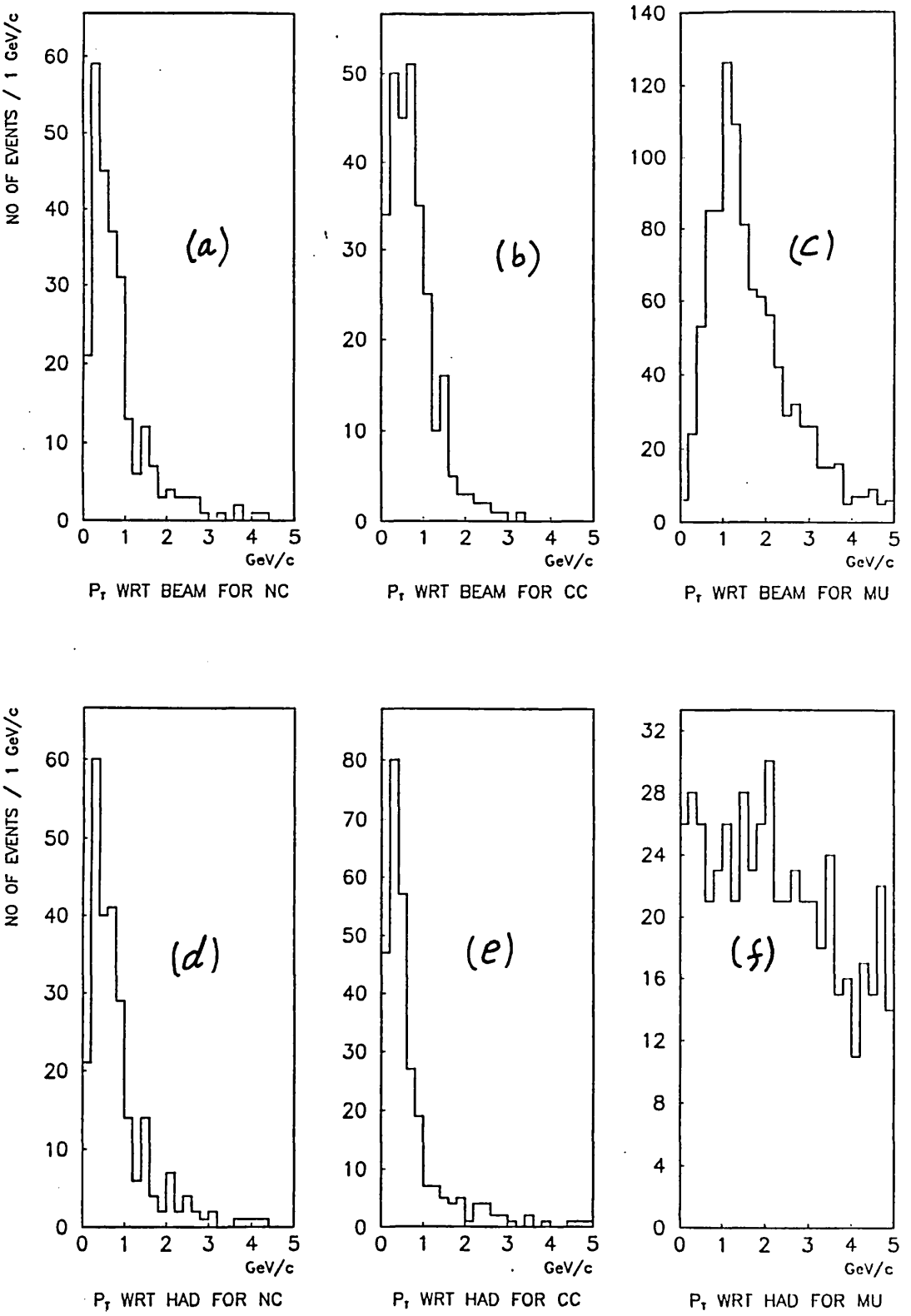



Figure 6: Transverse momentum wrt the beam for leaving hadrons from NC (a), CC (b) and the transverse momentum of the muon wrt the beam (c). Transverse momentum wrt the final state hadron vector of leaving hadrons in NC (d), CC (e) and the muon in the CC sample (f).

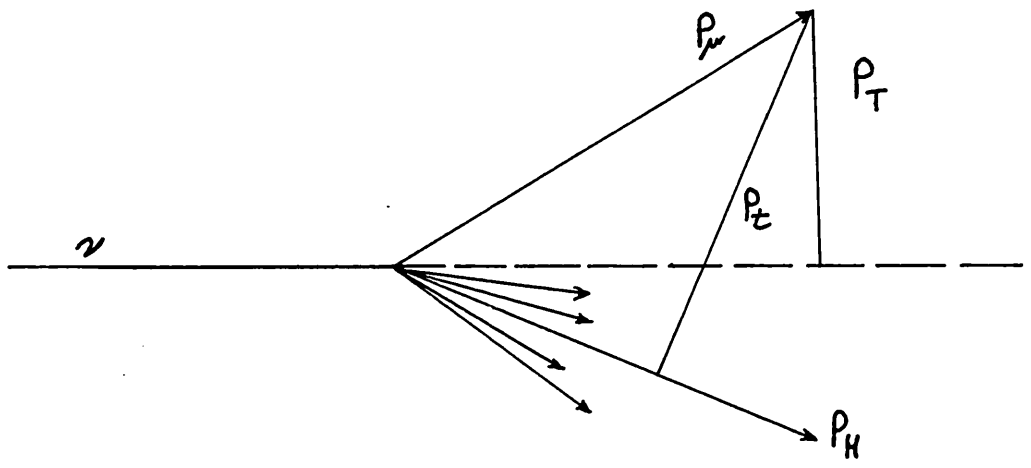



Figure 7: Definition of $P^t$ and $P_T$

Figure 8 shows the predicted 'W' coordinates versus the associated 'W' coordinates at the inner plane. From studies of 'extrapolated W' coordinates, it was observed that only 1.3% of the 'extrapolated' tracks extrapolate within 20cm of the chamber edges and no track was associated within 5cm from the chamber edges. This distance implies errors much smaller than those from measurements. So the edge effect was found to be negligible.

#### 4.3.1.2 Electron tracks

Although all flagged electron events were excluded from the analysis, the misidentified electron tracks could contaminate sample 3 particularly at large $P_T$, forcing the fit to add more muons

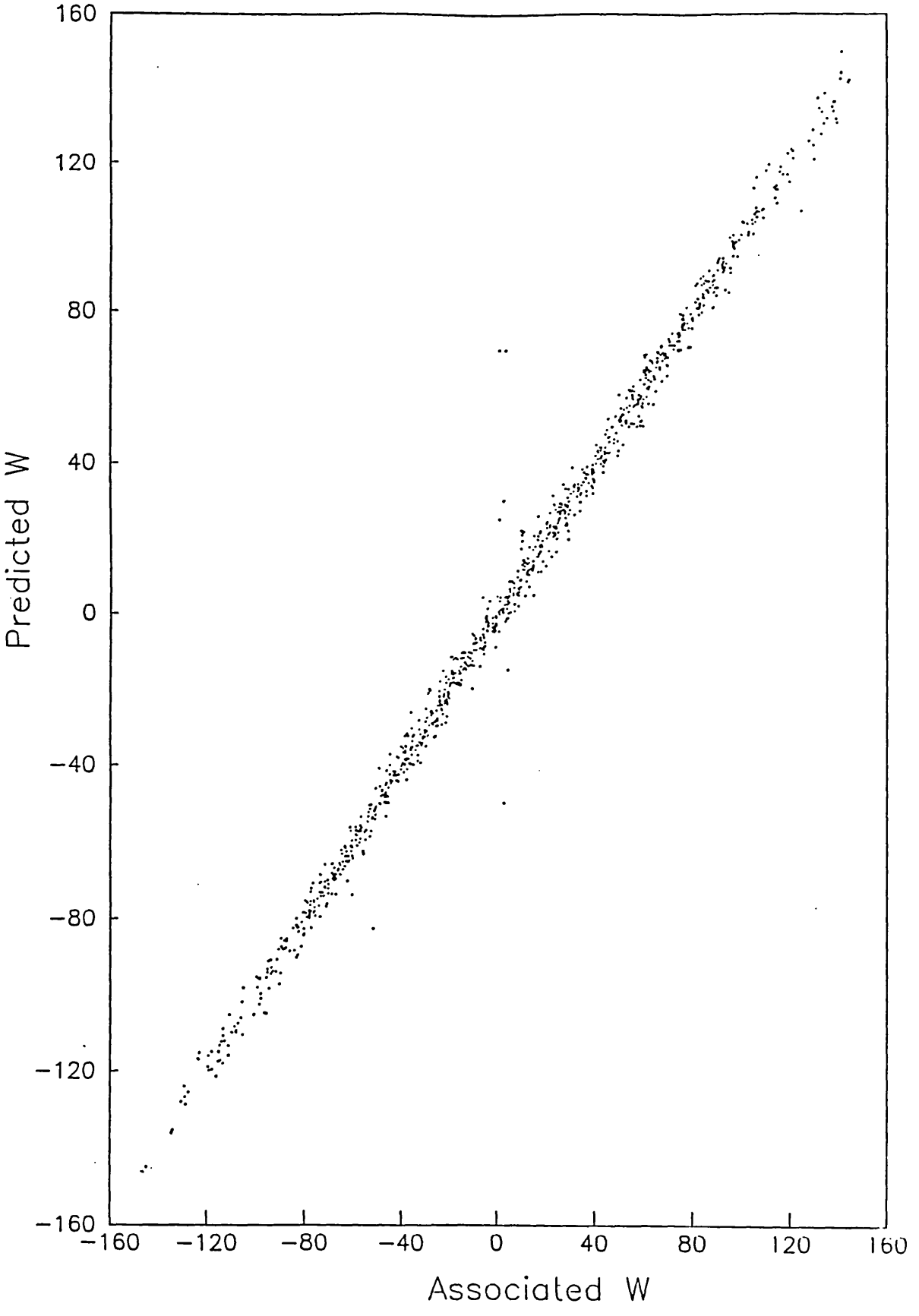



Figure 8: The predicted W coordinates versus the associated W coordinates at the inner plane.

from sample 1. Although the electron detection efficiency was estimated to be (95+2-1)%, it was generally assumed that this background was negligible, since the probability of an electron track hitting both planes of the EMI was very low.

If 'f' were the fraction of electron neutrino events in the NC sample, the efficiency 'ε' would be replaced by

$$\varepsilon = \varepsilon/(1-f) \qquad (4.6)$$

#### 4.3.1.3 Comparison with other estimates

Another estimate of the EMI electronic efficiency was made using through-going muons [16]. This method estimated the efficiency to be (97±2)%, in good agreement with the above values.

### 4.3.2 Estimate of geometrical efficiency of the EMI

The geometrical efficiency of the EMI was estimated by H.Kreutzmann [16].

Table 3 gives the global estimates for the geometrical acceptance of the EMI for neutrino energies above 10 GeV and the muon momentum above 3 GeV/c, for both type of muons. A more accurate estimate required corrections, on an event by event basis, taking into account the momentum, and the transverse momentum of the muon, with respect to the beam direction. This correction was carried out using tables from [16].

TABLE 3

Geometrical acceptance for BEBC ($E_\nu$ > 10 GeV)

| | $\mu^+$ | $\mu^-$ |
|---|---|---|
| $P_\mu$ > 5 GeV/c | 99.9% | 99.1% |
| $P_\mu$ > 4 GeV/c | 99.8% | 98.6% |
| $P_\mu$ > 3 GeV/c | 99.7% | 97.8% |

### 4.3.3 Estimate of the total muon loss

For muons with momentum above 3 GeV/c there are losses due to electronic and geometrical inefficiencies of the EMI. To determine this loss a method using interacting tracks from actual events was used. The lost muons will give an excess of leaving tracks in the NC sample. The NC sample will give an apparent $(\ell/i)^+$ ratio which will be higher than the same ratio for hadrons in the CC sample. By determining the true number of leaving hadron tracks in the NC sample, the number of excess tracks will give the number of lost muons.

The true number of leaving hadrons above the momentum cut was obtained by weighting each of the interacting tracks, by the probability that they should have left the chamber without inter-

---

$^+\ell/i$ is the ratio of leaving hadrons to the interacting ones.

acting.

The probability density function for interacting hadrons is given by:

$$f(\ell) = [\ \exp(\ -\ell/L\ )\ ]\ /\ L \qquad (4.7)$$

Using the above formulae, the probability of interaction for a hadron of length '$\ell$' will be:

$$P(\ell) = 1/L[\ \int_{\ell_{min}}^{\ell} f(\ell)\ d\ell\ ] \qquad (4.8)$$

$$P(\ell) = 1/L\ [\exp(\ -\ell_{min}/L\ )\ -\ (\exp(\ -\ell/L\ )\ ] \qquad (4.9)$$

where:

i) L = Effective interaction length for hadrons in the liquid.

ii) $\ell_{min}$ = The minimum interaction length. It takes into account the confusion near the vertex. In this analysis it was set to 1cm.

iii) $\ell$ = The track length, defined from the primary vertex, to the point where the track left the chamber.

In order to estimate the effective interaction length 'L', one needs the spectrum of interacting tracks. For this purpose the data from a wide band neutrino experiment[+] carried out in BEBC under very similar conditions (see below) was used.

---

[+]mainly because of better statistics

4.3.3.1 Estimate of the effective interaction length.

The effective interaction length for hadrons was estimated using the interacting hadrons from the CC events observed in the WA59 wide band neutrino experiment [17], where an almost identical target was used and the bubble chamber was operating in a very similar condition. The choice of this data allowed the determination of the effective interaction length with a better statistical accuracy.

From equation (4.8) one can obtain the differential spectrum for the interacting hadrons given by:

$$dN(\ell)/d\ell = N_0 \exp( -\ell/L ) \qquad (4.10)$$

In order to observe this spectrum, CC events with visible energy above 10 GeV and muon momentum above 3 GeV/c were selected. In addition, the interacting tracks were required to have momentum errors below 30%. The distribution of track length for interacting hadrons is shown in figure 9. As can be observed from this figure the differential spectrum has an approximately exponential shape as expected from equation (4.10).

Since the probability of interaction was sensitive to the value of L, then it was important to obtain the most realistic value for this factor. Further, one could check the validity of the effective interaction length obtained by estimating the true number of leaving hadrons in the CC sample. Knowing the number of muons and the number of interacting and leaving hadrons in the

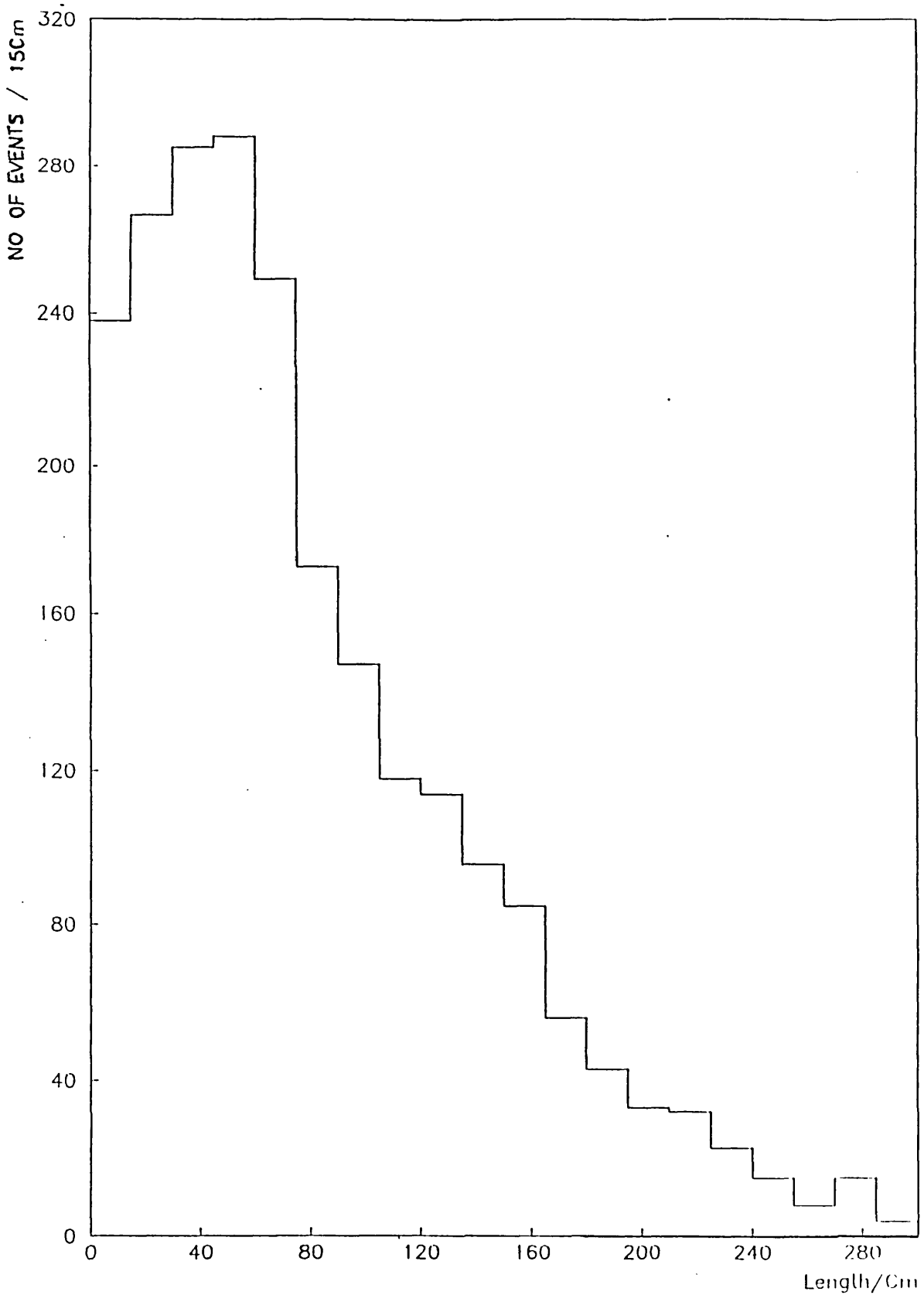



Figure 9: Interaction length for hadrons with momentum > 3 Gev/c

CC sample, then one could use this as a further constraint to obtain L. For every interacting hadron, the number of leaving ones will be given by:

$$N_{leav} = 1/P(\ell) - 1 \tag{4.11}$$

We define the $x^2$:

$$x^2 = \sum_{i=1}^{N_{bins}} \{ [ (N(\ell_i) - N_0 \exp( -\ell_i/L ) ] / \sqrt{N(\ell_i)} \}^2 \tag{4.12}$$

subject to

$$N_L - F_L = 0 \tag{4.13}$$

where

$$F_L = \sum_{j=1}^{N_1} ( 1/P_j - 1) \tag{4.14}$$

One can define a least squares function:

$$M(N_0, L, \lambda) = \sum_{i=1}^{N_{bins}} \{ [ N(\ell_i) - N_0 \exp( -\ell_i/L ) ] / \sqrt{N(\ell_i)} \}^2 + \chi [ N_L - F_L ] \tag{4.15}$$

Where:

$\ell_i$ = The track length from figure 9 for interacting hadrons.

$N_{bins}$ =The total number of bins in figure 9.

$N(\ell_i)$ = Number of entries for $\ell_i$.

$N_0$ = Scaling coefficient

$N_L$ = The total number of leaving hadrons in the CC sample.

$N_I$ = The total number of interacting hadrons in the CC sample.

$F_L$ = The estimated number of leaving hadrons in the CC sample.

$P_j$ = The probability of interaction for the hadron j in the CC sample.

Using equation (4.15), we carry out a least squares minimisation of

$$|\partial M/\partial N_0| + |\partial M/\partial L| + |\partial M/\partial x| \qquad (4.16)$$

in the Minuit [18] and reconstruct every interacting hadron in the CC sample. Using this method (see below), the effective interaction length 'L' in the target was estimated to be 164cm†, taking into account the small correction required for the density differences between the beam dump and the wide band experiment.

#### 4.3.3.2 Track following in the bubble chamber

The total number of hadrons was obtained by estimating the probability of interaction for every interacting hadron. The probability of interaction was obtained by following the track in the liquid until it left the chamber and estimating its total length. The interaction cross-section was assumed to be inde-

---

†This value was used for the whole data, although the liquid density varied slightly for different runs

pendent of of the energy of the track. This was supported by the fact that only tracks with momentum above 3 GeV/c were considered and at the energies above this cut the interaction cross-section of hadrons (i.e. pions,protons and kaons) with the nucleon remained fairly constant independent of the hadron energy (for example see reference 19 plots of cross-sections and related quantities, p86.).

In order to reconstruct the charged interacting hadron tracks and estimate the total track length in the bubble chamber, the tracks were followed in the liquid by making steps of adjustable size, taking into account the density and the field configuration. The momentum loss and multiple scattering were taken into account.

In order to check the validity of the method in estimating the total track length, the identified muons were used. The muons were particularly suitable, because the majority of the muon tracks were measured up to the end point, and as a result one could reconstruct the muon track and compare the estimated ( reconstructed ) total track length with the measured length. Figure (10) shows the estimated muon track length versus the measured track length. As can be seen from this figure, a very strong correlation exists between the corresponding lengths, and the procedure is satisfactory in estimating the track length of hadrons in the bubble chamber.

#### 4.3.3.3 Results

Only accepted events with total visible energy above 10 GeV were used in the analysis. Table 4 summarises different types of hadrons observed in the NC sample.

TABLE 4

Hadron results obtained in the NC sample

| | |
|---|---|
| Obseved number of interacting hadrons | = 434±20.83 |
| Estimated number of leaving hadrons | = 241.25±13.20 |
| Total number of leaving tracks | = 306±17.49 |
| Estimated number of leptons lost | = 64.8±21.9 |

Table 5 shows the number of leptons observed in the muon and electron CC samples. As can be seen from this table a total of 1216 leptons were observed giving the number of leptons lost as a percentage of total leptons observed to be (5.3±1.8)%.

TABLE 5

Lepton tracks observed in the CC sample

| | |
|---|---|
| Total number of muons observed | = 1013 ± 31.83 |
| Total number of electrons observed | = 203 ± 14.25 |

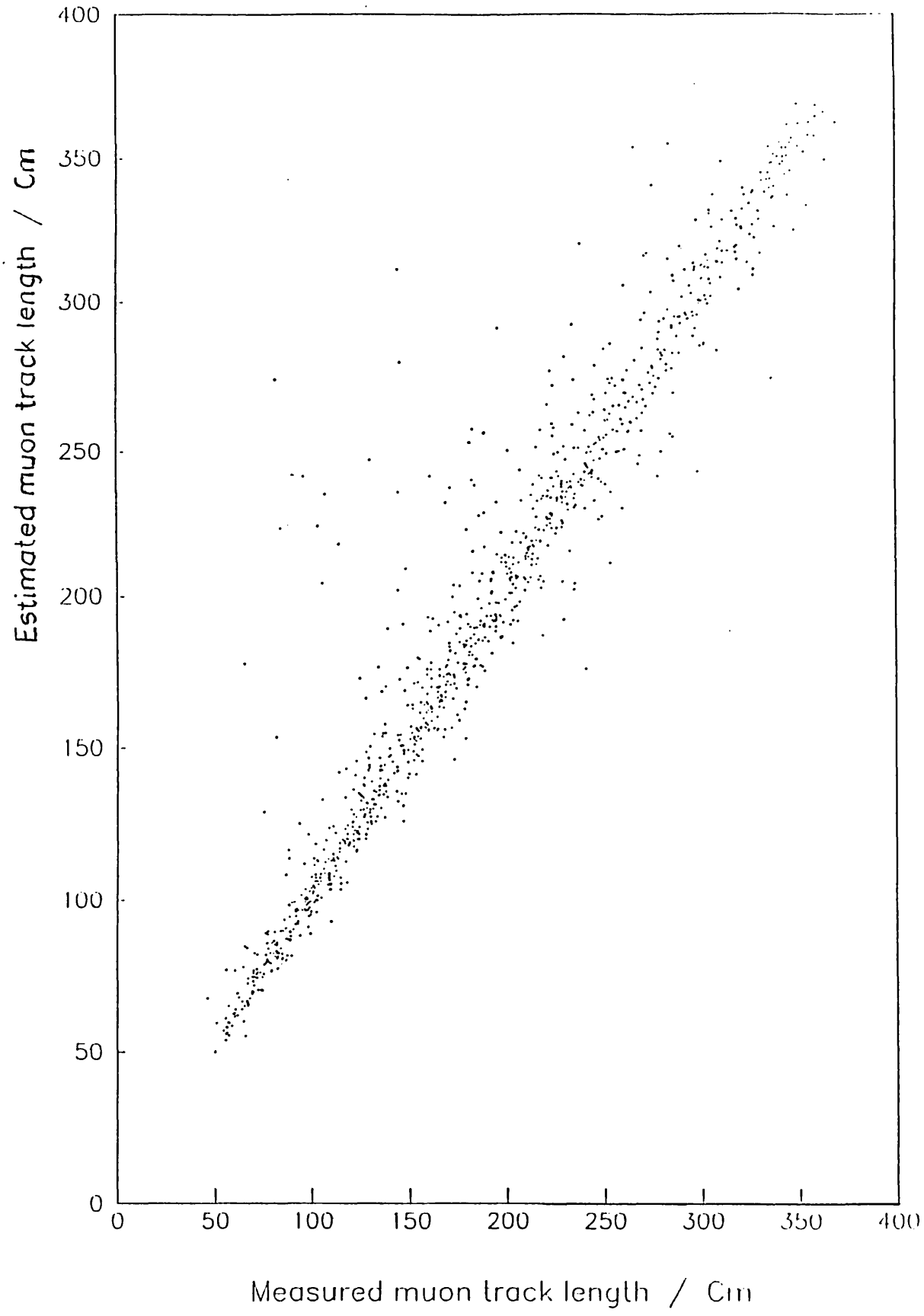



Figure 10: The estimated muon length versus the measured length

## 4.4 CORRECTION FOR LEPTON MOMENTUM CUT

Corrections are required for the 3 GeV/c and 0.8 GeV/c cuts on muon and electron momenta respectively. The differential cross-section for neutrino interaction in the scaling region is given by [19]:

$$d^2\sigma^\nu/dxdy = (G^2ME_\nu/\pi)[\ (1 - y - Mxy/2E_\nu)F_2(x) + (\tfrac{1}{2}y^2)2xF_1(x) + (y - \tfrac{1}{2}y^2)xF_3(x)\ ] \qquad (4.17)$$

where G is the Fermi coupling constant, M is the nucleon mass, $E_\nu$ is the neutrino energy and $F_i(x)$ are the neutrino production structure functions. Using the Callan-Gross relation [19]:

$$F_2(x) = 2xF_1(x) \qquad (4.18)$$

and ignoring the term Mxy/2E in (4.17), the above equation reduces to:

$$d^2\sigma^\nu/dxdy = (G^2ME_\nu/2\pi)\{\ [F_2(x)+xF_3(x)] + [F_2(x)-xF_3(x)](1-y)^2\ \} \qquad (4.19)$$

Integrating (4.19) over x gives

$$d\sigma/dy = (G^2ME_\nu/2\pi)\{\int_0^1[F_2(x)+xF_3(x)]dx + (1-y)^2\int_0^1[F_2(x)-xF_3(x)]dx\ \}.$$

Using

$$\beta = \int_0^1 xF_3(x)dx \Big/ \int_0^1 F_2(x)dx \qquad (4.20)$$

one obtains:

$$d\sigma/dy = (G^2 M E_\nu/2\pi)\{\int_0^1 F_2(x)dx[(1+\beta) + (1-y)^2(1-\beta)]\}. \quad (4.21)$$

Changing the cross-sectional dependence from y to $E_\ell$ we obtain:

$$d\sigma/dE_\ell = (G^2 M/2\pi)\{\int_0^1 F_2(x)dx[(1+\beta) + (E_\ell / E_\nu)^2(1-\beta)]. \quad (4.22)$$

Requiring $E_\ell > E_{cut}$ and integrating over the energy spectrum we obtain the ratio of the number of events lost due to lepton momentum cut to total number of events as:

$$R = N_{lost}/N_{total} = [(1+\beta)E_{cut} + ((1-\beta)/3) \times (E^3_{cut}/E^2_\nu)] / E_\nu[(1+\beta) + (1-\beta)/3] \quad (4.23)$$

The β value used was 0.8, obtained from the best fit to the Gargamelle data on the y distribution [20]. For antineutrinos the β value should be replaced by -β.

## 4.5 ENERGY CORRECTIONS

The estimation of the hadronic energies by measurement of the tracks observed in the bubble chamber only represents a lower limit on the true hadronic energy. This is because of neutral energy losses through unconverted gammas and undetected neutrals, and due to incompletely measured, complicated electromagnetic showers and secondary scatters. In order to account for

such energy losses, a global energy correction was applied. The hadronic energy was scaled up by 20% to account for unseen neutrals. This correction was based on the results obtained in a narrow band neutrino experiment [21] with BEBC running under very similar conditions, where the correction relied on the balance of the transverse momentum of the muon relative to the neutrino direction in a CC event, with the transverse momentum of the sum of obseved hadrons multiplied by the correction factor to be determined. The value of the correction factor was observed to be independent of hadronic energy and a mean value of 1.20 was obtained for the correction factor.

## 4.6 ASSOCIATION OF NEUTRON STARS

As mentioned earlier (see section 3.4), at the production stage of the Data Summary Tape, attempts were made to select the best origin for the association of $n^*$'s.

Using the program SYNTH, the best vertex for the association of the $n^*$ was selected as the one which gave the minimum angle between the line of flight, obtained from the vertex under test, and the $n^*$ vertex; and the sum of the momenta of the outgoing tracks from the $n^*$ vertex, (i.e. the so called final state hadron vector). If the transverse momentum of the final state hadron vector relative to the line of flight was greater than 5 GeV/c the vertex was rejected altogether otherwise the $n^*$ was associated to that vertex.

Although the above procedure was used in linking $n^*$'s, in the data analysis stage many frames were noted to have more than one event, with the downstream vertex having no identified lepton associated to the event and appearing as a NC candidate. These so called unlinked $n^*$'s were a background to the low energy NC events and could distort the shape of NC spectrum.

In order to identify and associate the potential $n^*$'s events, all frames with more than one event on the frame were checked. To determine whether two vertices were associated the following kinematical parameters were used:

$|AB|$: the distance between two vertices;

$\theta$: the angle between the beam direction and AB;

$P^t_B$: The transverse momentum of the final state hadron vector of the downstream vertex B relative to AB;

$P^t_{BA}$: The transverse momentum of the component of the final state hadron vector of vertex B along AB, relative to the final state hadron vector of vertex A.

The definition of these parameters is given in figure (11).

In order to study the association of vertices on frames with more than one event, the observed vertices on frames with more than one event were catagorized as shown in table 6
Column 3 of this table gives the sets of vertices observed in each category. As can be seen from this table, the observed

TABLE 6

Association of vertices

| Vertex A | Vertex B | Total |
|---|---|---|
| CC | CC | 4 |
| NC | CC | 3 |
| CC | NC | 67 |
| NC | NC | 78 |

number of random CC-CC and NC-CC sequences is almost the same whereas the observed sequences of CC-NC and NC-NC vertices is very high indicating the existence of unlinked associated events.

In order to identify the most effective parameter(s) in eliminating the hadronic background, the following plots were made:

i) $\theta$ versus $|AB|$;

ii) $\theta$ versus $P^t_B$;

iii) $|AB|$ versus $P^t_B$;

iv) $P^t_{BA}$ versus $P^t_B$,

for both the CC-CC and NC-CC sequences (assuming these were genuine neutrino events), and CC-NC and NC-NC sequences. All plots were checked and efforts were made to choose the best cuts on the kinematical parameters in order to eliminate the ha-

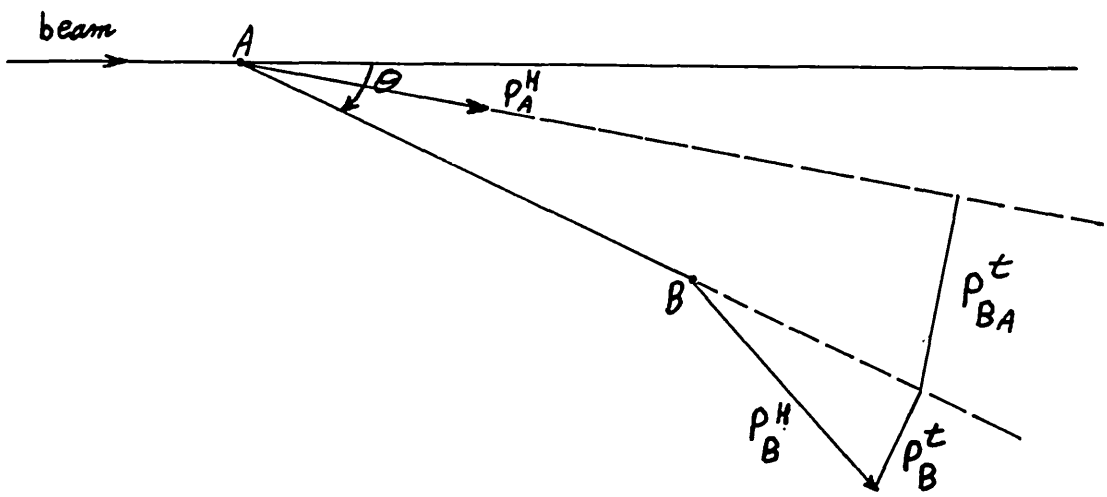
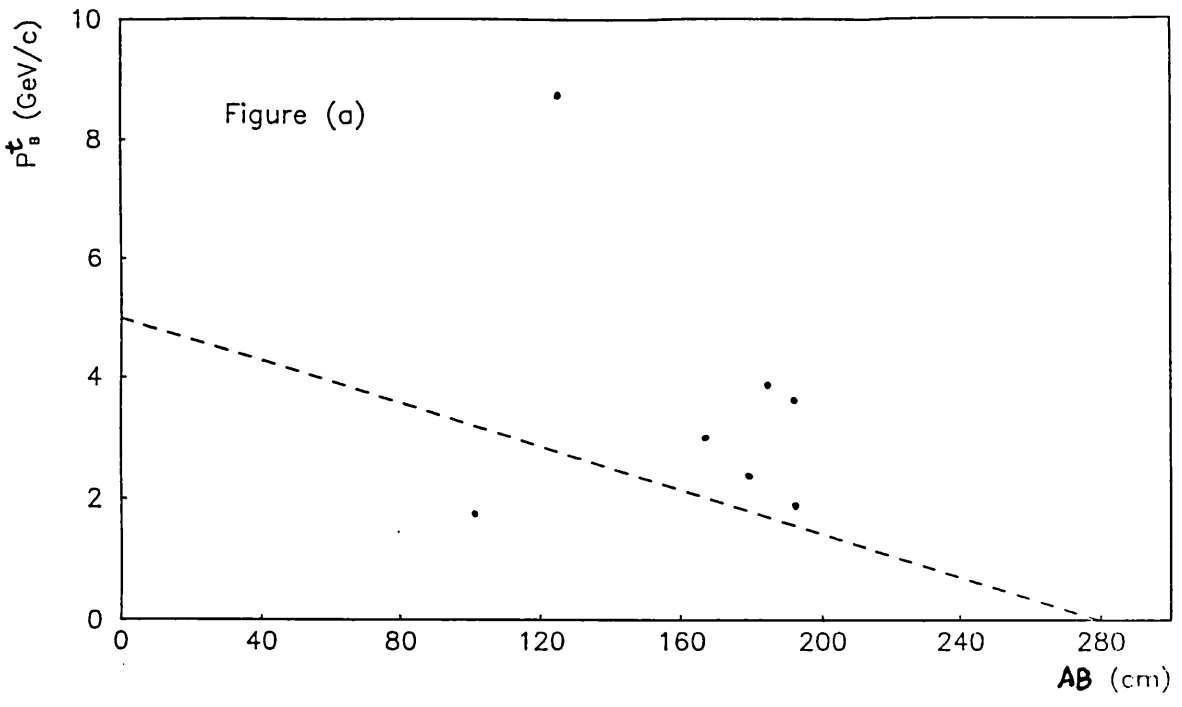


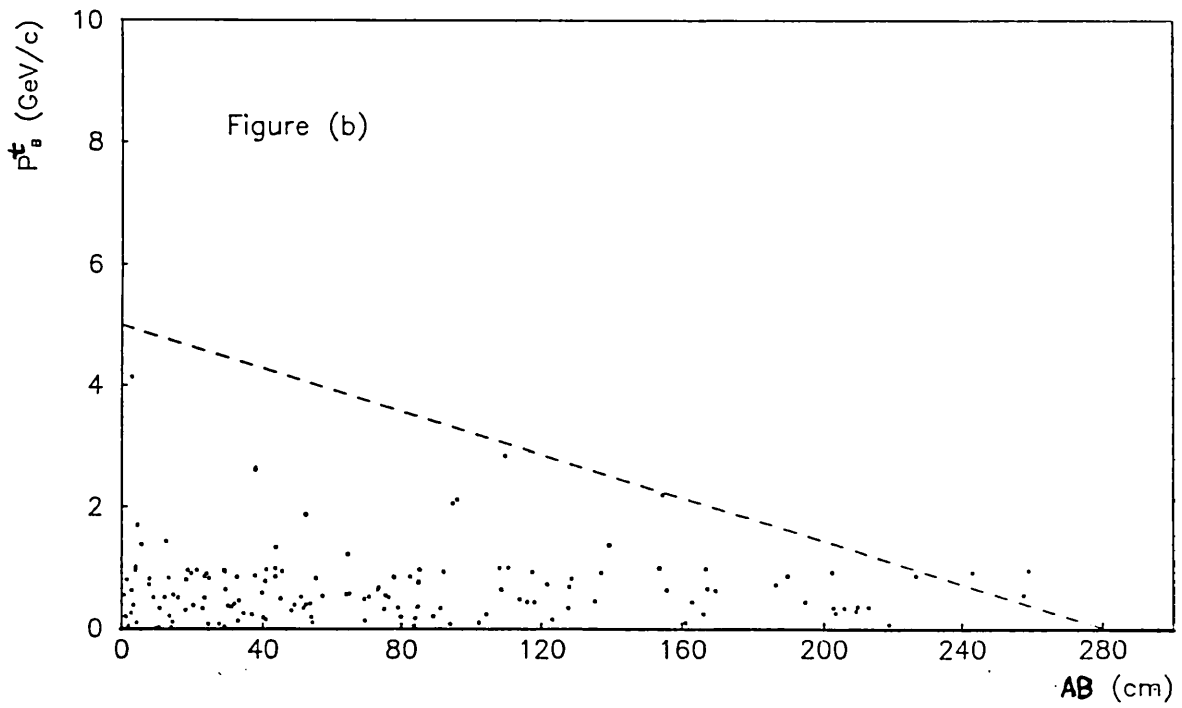

Figure 11: The definition of the kinematical parameters.

dronic background. Figure 12 shows plots of |AB| versus $P^t_B$ for the neutrino (figure 12a) and the contaminated samples (figure 12b). As can be seen from figure 12b, the majority of the events in the contaminated sample are concentrated at low |AB| and $P^t_B$, whereas the neutrino events appear to have large |AB| and $P^t_B$ values.

Taking |AB| and $P^t_B$ as the best kinematical parameters, the following linear cuts were made in this plane:




IABI versus $p_B^t$ for neutrino events




IABI versus $p_B^t$ for mixed sample

Figure 12: AB vs $P^t_B$ for neutrino (a) and mixed sample (b).

from $|AB| = 0$, $P^t_B = 5$ GeV/c To $|AB| = 280$cm, $P^t_B = 0$

giving a linear cut for neutrino events:

$$\text{Cut} = P^t_B + |AB|/56 - 5 > 0.$$

As a result of this cut all but one of CC-CC and NC-CC events remained whereas 134 apparent NC events were identified as $n^*$ and subsequently dropped from CC-NC and NC-NC sample.

The energy spectrum of the associated $n^*$ is shown in figure 13. Only two of the identified $n^*$'s have hadron energies above 5 GeV, the remaining ones have very low energies.

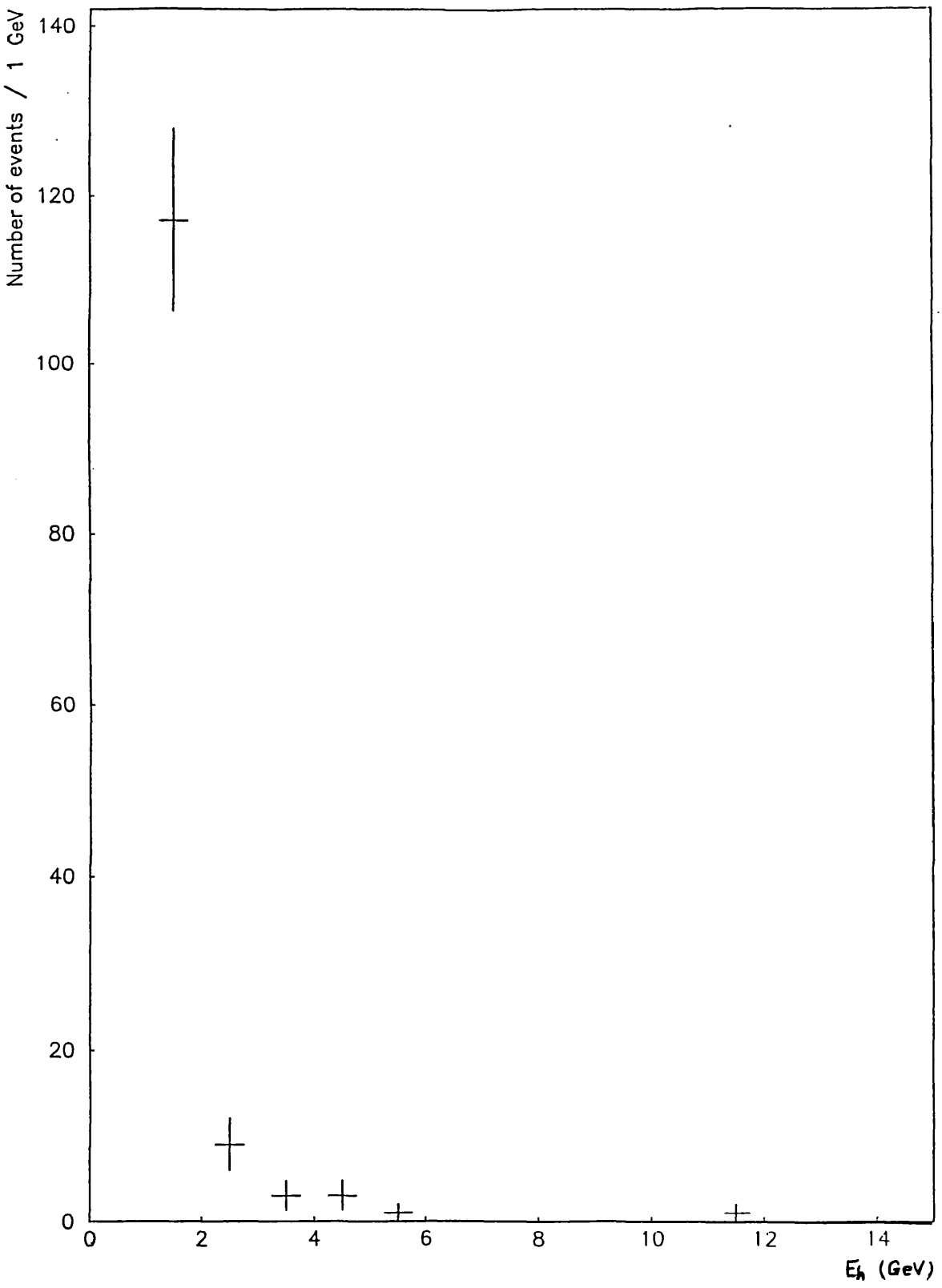



Figure 13: The energy distribution of associated events

# Chapter V

# EVENT SELECTION AND CORRECTED CHARGED CURRENT RATES

The physics analysis was carried out using the Data Summary Tape which contained the full measurement information of all neutrino interactions, all relevant information such as the status of the beam, the external detectors and the relevant bits corresponding to the location of identified primary electrons (the CC electron tracks ). These enabled the user to check the status of the events, apply different cuts to individual tracks or events and manipulate the data as required by the physics analysis under consideration.

## 5.1 TRACK SELECTION

All tracks corresponding to an event were checked for quality of their measurements. The main problem came from the unassociated tracks which were wrongly assigned to the event. On the other hand badly measured tracks with large momentum errors could introduce considerable smearing to various kinematical parameters.

The hadrons from hadronic shower are normally produced with a limited transverse momentum relative to the final state hadron vector or the beam direction in contrast to unassociated

tracks which have large transverse to longitudinal momentum. To reduce this background the tracks were rejected if

i) $E - p_X > 2.0$ GeV

where E and $p_X$ are the energy and the longitudinal momentum of the particle in the beam direction. The badly measured tracks normally appear to have unreasonably large momenta ($P_{track}$) and fractional error on the momenta ($\Delta p/p$). In order to reduce this background tracks were rejected if one of the following was satisfied:

i) $P_{track} > 500$ GeV/c;

ii) $\Delta p/p > 100\%$.

An insight into the quality of the track measurements is provided by the distribution of the fractional error on the momentum of identified muons, charged hadrons, flagged electrons and measured photons as shown in figure 14. The large track length of the muons (and momentum improvement of badly measured ones using IPF and EMI data) gives a good estimate of its momentum with $\langle \Delta p/p \rangle \sim 3\%$. The charged hadron momentum is also well measured with $\langle \Delta p/p \rangle \sim 5\%$. The flagged electrons have $\langle \Delta p/p \rangle \sim 30\%$. The photons likewise generally have a poor measurement of their momentum. This is mainly due to bremsstrahlung and subsequent spiralling of electron from converted gammas providing a relatively short length of electron track for momentum estimate.

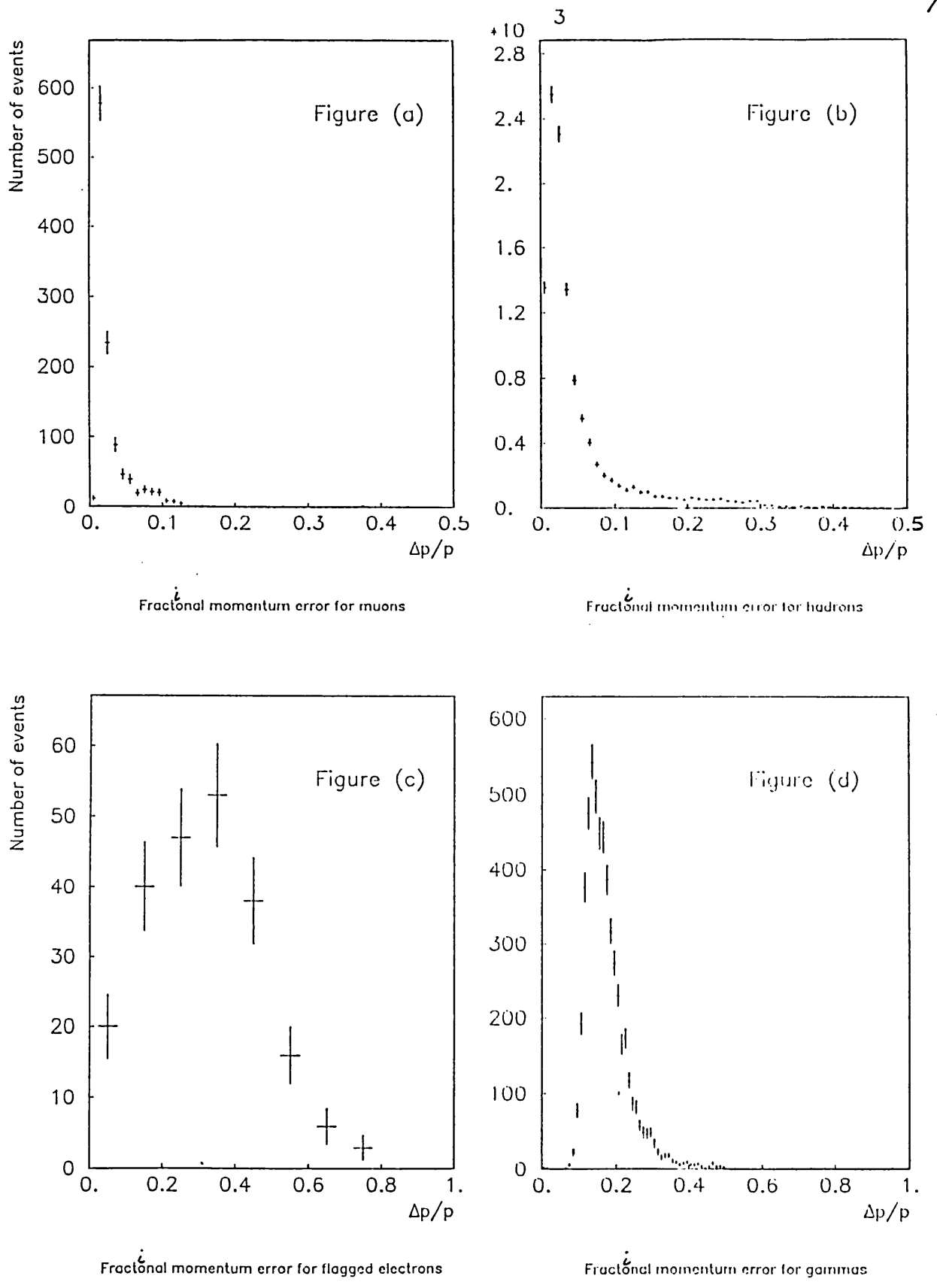



Figure 14: Distribution of measurement errors on track types.

## 5.2 EVENT SELECTION

The main background to neutrino events was from the so called "fake neutral current" events due to neutral hadrons either coming from the interactions in front and on the periphery of BEBC or from neutrino events inside the chamber resulting in the so called $n^*$ events (see 4.6). These events were normally characterised by their low energies and the exponential fall in the number of these events with increasing distance in the chamber (i.e. the distance covered by the particle in the liquid before its interaction). By applying a suitable energy cut, or using kinematical techniques, it was possible to exclude majority of this background.

The events associated with cosmic ray interactions constituted another background for NC events. Cosmic ray tracks entered the chamber from above in the field direction and interacted in the liquid resulting in events characterised by their badly measured tracks (the tracks momenta and angles could not be determined properly since they were generated in the field direction), and large transverse to longitudinal momentum ratios. In order to reduce this background the events were rejected if:

i) $\Sigma p_X < 0.3$ GeV/c or

ii) $\Sigma p_Z / \Sigma p_X > 2$

where the sum was taken over all good tracks as defined in the previous section.

All events were required to be inside the fiducial volume (see 2.4). The events on two rolls were rejected because BEBC was running under half magnetic field at the time. Two more rolls were excluded from data analysis because the EMI was not functioning properly. In addition the data obtained in a short test run with 1/2 density target were excluded from any analysis. There were additional hardware conditions required at the data taking stage [13] which were applied.

## 5.3 EVENT CLASSIFICATION

The neutrino events were classified as follows:

a) Muon neutrino events : All events with an EMI identified muon with momentum above 3 GeV/c and no electron candidate with a transverse momentum relative to the beam larger than the muon;

b) Electron neutrino events : All events with an identified electron with momentum above 0.8 GeV/c and no muon candidate with a transverse momentum relative to the beam larger than the electron;

c) Neutral Current candidates : All events with no observed secondary lepton candidates.

Using the above criteria, a total of 2391 events were selected for physics analysis. Of these, 1325 were identified as charged currrent events. The remaining ones were classified as neutral current candidates. Table 7 shows the classification of the final

data samples obtained in runs carried out with full and 1/3 density dumps with no energy cuts.

TABLE 7

Raw number of events observed with no energy cut

| Density: | Full | 1/3 |
|---|---|---|
| Muon neutrino | 379 | 442 |
| Muon antineutrino | 122 | 151 |
| Electron neutrino | 105 | 70 |
| Electron antineutrino | 31 | 25 |
| Neutral current | 521 | 545 |

## 5.4 THE X AND Y DISTRIBUTION OF CC EVENTS

i) The muon CC sample: This sample consists of 821 events with a $\mu^-$ at the final state and 273 events with a $\mu^+$ which were interpreted as $\nu_\mu$ and $\bar{\nu}_\mu$ charged current interactions respectively. The muons required to have a momentum above 3 GeV/c. Figures 15 and 16 show the x and y distributions for muon events with both density data combined. The distributions agree well with the usual expectation from the quark-parton model for $\nu_\mu$ and $\bar{\nu}_\mu$ interactions [22].

ii) The electron CC sample: There are 175 $\nu_e$ and 56 $\bar{\nu}_e$ identified charged current interactions with the electron momentum above 0.8 GeV/c. The x and y distributions for the electron events are shown in figures 15 and 16. The $e^-$ data shows an excess at low $x < 0.1$, however, because of usual difficulties in measuring the electron momenta due to bremsstrahlung etc, this excess can be attributed to measurement errors.

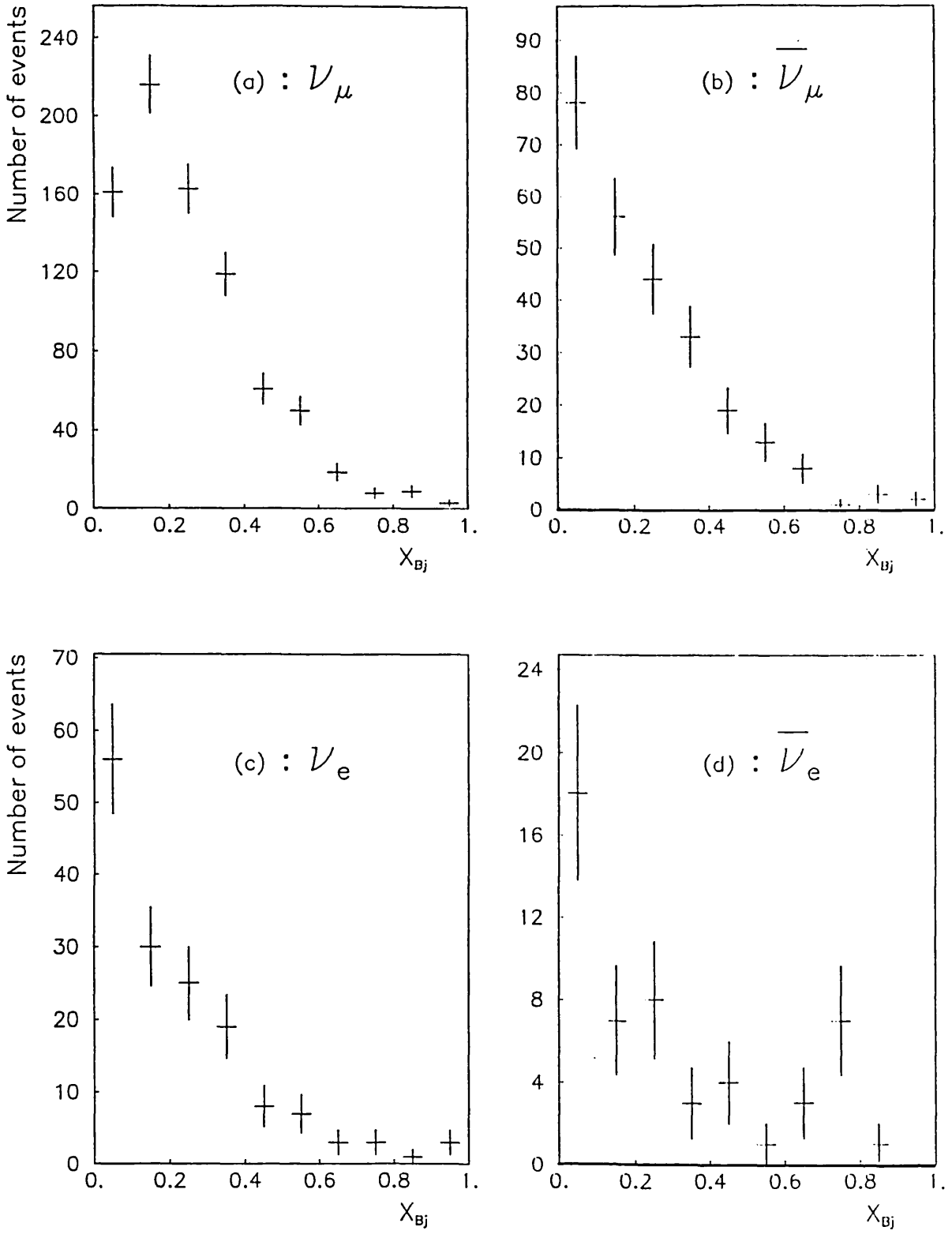



Figure 15: The Bjorken x distribution for CC events

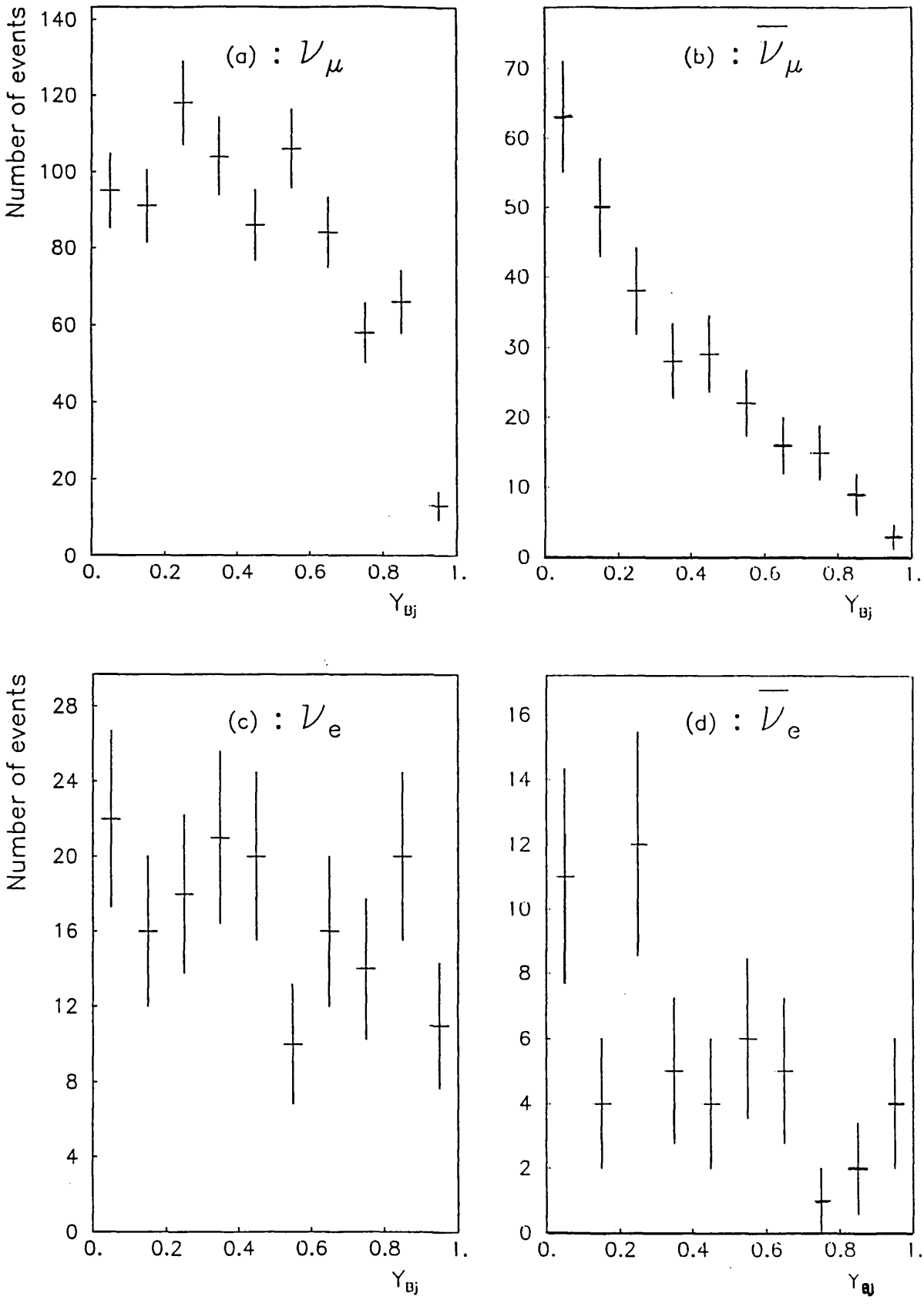



Figure 16: The Bjorken y distribution for CC events

## 5.5 CORRECTED EVENT RATES

Taking into account various efficiencies described in the previous chapter the observed charged current event sample was corrected for all type losses including the systematic uncertainties. The corrected absolute and normalised values for runs with the full and 1/3 density dumps are given for two different energy cuts in tables 8, 9, 10 and 11. The first row gives the observed number of events. The second row gives the corrected number of events with statistical and systematic errors. The third row is the event rate normalised to $10^{18}$ protons and 1 ton of detector.

TABLE 8

The CC event rate for full density dump with $E_\nu$ > 10 GeV

| $\mu^+$ | $\mu^-$ | $e^+$ | $e^-$ |
|---|---|---|---|
| 108 | 344 | 28 | 100 |
| 121.8±11.8±4.5, | 414±22.6±10.3, | 30.3±5.7±1.0, | 109.3±10.9±3.7 |
| 5.5±0.5±0.2, | 18.9±1.0±0.5, | 1.4±0.3±0.1, | 5.0±0.5±0.2 |

TABLE 9

The CC event rate for full density dump with $E_\nu > 20$ GeV

| $\mu^+$ | $\mu^-$ | $e^+$ | $e^-$ |
|---|---|---|---|
| 81 | 282 | 22 | 96 |
| 89.8±10±2.9, | 325.4±19.5±8.0, | 23.7±5.1±0.8, | 104.7±10.7±3.6 |
| 4.1±0.5±0.1, | 14.8±0.9±0.4, | 1.1±0.2±0.1, | 4.8±0.5±0.2 |

TABLE 10

The CC event rate for 1/3 density dump with $E_\nu > 10$ GeV

| $\mu^+$ | $\mu^-$ | $e^+$ | $e^-$ |
|---|---|---|---|
| 134 | 410 | 24 | 67 |
| 155.8±13.7±5.7, | 500.2±25.1±12.5, | 26.3±5.4±1.0, | 74.2±9.1±2.5 |
| 16.7±1.5±0.6, | 53.7±2.7±1.3, | 2.8±0.6±0.1, | 8.0±1.0±0.3 |

The systematic errors were taken into account by varying the input parameters and comparing the results. For the absolute and normalised rates the systematic errors are added in quadra-

TABLE 11

The CC event rate for 1/3 density dump with $E_\nu > 20$ GeV

| $\mu^+$ | $\mu^-$ | $e^+$ | $e^-$ |
|---|---|---|---|
| 101 | 331 | 20 | 60 |
| 115.9±11.8±3.7, | 387.9±21.6±9.5, | 21.8±4.9±0.8, | 66.1±8.5±2.3 |
| 12.4±1.3±0.4, | 41.7±2.3±1.0, | 2.3±0.5±0.1, | 7.1±0.9±0.2 |

ture. It can be seen that on the whole the statistical errors dominate. The more important individual absolute systematic contibutions from different sources are given in tables 12, 13, 14, 15, 16, 17, 18 and 19 for both densities and two energy cuts. The quoted numbers are absolute values. The notations used are: Scan effic = Scan efficiency, EMI elect = EMI electronic efficiency, EMI geomt = EMI geometrical efficiency, Electron det efficiency = The overall electron detection efficiency and $\beta$ parameter is defined in (4.20).

TABLE 12

The systematic corrections for full density muon CC events with $E_\nu$ > 10 GeV.

| | Scan effic. | EMI elect. | EMI geomt. | β corrected value |
|---|---|---|---|---|
| $\mu^+$ | 1.9 | 2.6 | 1.3 | 2.8 |
| $\mu^-$ | 2.6 | 8.7 | 4.4 | 2.1 |

TABLE 13

The systematic corrections for full density electron CC events with $E_\nu$ > 10 GeV.

| | Scan effic. | Electron det efficiency | β corrected value |
|---|---|---|---|
| $e^+$ | 0.3 | 1.0 | 0.2 |
| $e^-$ | 1.1 | 3.6 | 0.1 |

TABLE 14

The systematic corrections for full density muon CC events with $E_\nu > 20$ GeV.

| | Scan effic. | EMI elect. | EMI geomt. | β corrected ~~value~~ |
|---|---|---|---|---|
| $\mu^+$ | 1.4 | 1.9 | 0.9 | 1.5 |
| $\mu^-$ | 2.0 | 6.9 | 3.4 | 1.1 |

TABLE 15

The systematic corrections for full density electron CC events with $E_\nu > 20$ GeV.

| | Scan effic. | Electron det efficiency | β corrected ~~value~~ |
|---|---|---|---|
| $e^+$ | 0.2 | 0.8 | 0.1 |
| $e^-$ | 1.1 | 3.4 | 0.1 |

TABLE 16

The systematic corrections for 1/3 density muon CC events with $E_\nu$ > 10 GeV.

| | Scan effic. | EMI elect. | EMI geomt. | β ~~value~~ corrected |
|---|---|---|---|---|
| $\mu^+$ | 2.5 | 3.3 | 1.7 | 3.5 |
| $\mu^-$ | 3.1 | 10.5 | 5.3 | 2.7 |

TABLE 17

The systematic corrections for 1/3 density electron CC events with $E_\nu$ > 10 GeV.

| | Scan effic. | Electron det efficiency | β ~~value~~ corrected |
|---|---|---|---|
| $e^+$ | 0.3 | 0.9 | 0.1 |
| $e^-$ | 0.8 | 2.4 | 0.1 |

TABLE 18

The systematic corrections for 1/3 density muon CC events with $E_\nu$ > 20 GeV.

| | Scan effic. | EMI elect. | EMI geomt. | β corrected ~~value~~ |
|---|---|---|---|---|
| $\mu^+$ | 1.8 | 2.4 | 1.3 | 1.8 |
| $\mu^-$ | 2.4 | 8.2 | 4.1 | 1.3 |

TABLE 19

The systematic corrections for 1/3 density electron CC events with $E_\nu$ > 20 GeV.

| | Scan effic. | Electron det efficiency | β corrected ~~value~~ |
|---|---|---|---|
| $e^+$ | 0.2 | 0.7 | 0.1 |
| $e^-$ | 0.7 | 2.2 | 0.1 |

## Chapter VI

## THE PROMPT CHARGED CURRENT SAMPLE

One of the most important features of beam dump experiments is that other processes may in principle become recognizable above the suppressed conventional background. Of the most important of these processes are; the production and semileptonic decay of heavier hadrons with smaller production cross-section and much shorter lifetimes (eg. charmed hadrons) and the production in the decay of such hadrons of new neutrinos which could be detected through their interactions or decays in the chamber. We refer to these neutrinos and their interactions as prompt neutrinos and prompt events respectively. This chapter considers the characteristics of prompt CC neutrinos.

The magnitude of a prompt flux component may be determined either by subtraction or extrapolation method. These methods will be discussed later, but, it should be mentioned here that both of these methods are more sensitive to a prompt electron neutrino flux than to a prompt muon neutrino flux, because of much smaller conventional background for the electron neutrino events.

In order to understand the prompt rates we will consider the calculated conventional background in the run with the full den-

sity dump and the contribution to each neutrino type from the conventional sources. It will be shown that that the observed CC event spectrum can not be explained by the flux of conventionally produced neutrinos.

## 6.1 THE SOURCE OF CONVENTIONAL NEUTRINOS

The flux of conventional neutrinos from decays of pions, kaons and hyperons during their flight path of about one absorption length in the dump was calculated in [23] using the measured hadron spectra from proton copper interactions at 400 GeV/c [24]. The muon rates obtained in the solid state detectors in the muon shielding (see 2.3) were used to calibrate the Monte Carlo which estimated the number of conventional events inside BEBC. The neutrino and antineutrino cross-section slopes used were $0.657 \times 10^{-38}$ cm$^2$/GeV and $0.309 \times 10^{-38}$ cm$^2$/GeV respectively [21]. The estimated systematic uncertainty was 6% for muon neutrino, 9% for muon antineutrino and 12% for electron neutrino (antineutrino) events [1]. Table 20 lists the estimated conventional neutrino events in the full density data normalised to $10^{18}$ protons and 1 ton of detector. The bulk of conventional muon neutrinos is from the purely leptonic decays of pions and kaons with the following branching ratios

$$\pi \rightarrow \mu\nu_\mu \qquad 100\% \qquad (6.1)$$

$$K \rightarrow \mu\nu_\mu \qquad 63.5\% \qquad (6.2)$$

TABLE 20

Estimated conventional event rates in the full density dump in units of $10^{18}$ and 1 ton of detector.

| | $\mu^+$ | $\mu^-$ | $e^-$ | $e^+$ |
|---|---|---|---|---|
| $E_\nu > 20$ | 3.10 | 13.80 | 0.72 | 0.32 |

The electron neutrinos are produced in the semileptonic decays of hadrons. The number of electron neutrino events from various conventional sources above 20 GeV neutrino energy is listed in table 21

TABLE 21

The contribution to the full density electron neutrino sample from various conventional sources. The given numbers are normalised to $10^{18}$ protons and 1 ton of detector.

| Source | $K^+$ | $K^-$ | $K^0$ | $\overline{K^0}$ | $\Lambda^0$ | $\Sigma^-$ |
|---|---|---|---|---|---|---|
| $\nu_e$ | 0.31 | 0.0 | 0.41 | 0.0 | 0.0 | 0.0 |
| $\overline{\nu}_e$ | 0.0 | 0.05 | 0.0 | 0.10 | 0.08 | 0.09 |

It can be seen from this table that charged and neutral kaons make up the source of prompt $\nu_e$ whereas the contribution to $\bar{\nu}_e$ mainly comes from $\bar{K}^0$, $\Lambda^0$ and $\Sigma^-$.

## 6.2 OBSERVED EVENTS AND THE EXPECTED CONVENTIONAL BACKGROUND

Table 9 lists the raw and corrected number of CC events obtained in the run with the full density dump with $E_\nu > 20$ GeV. The interest is: How many of each neutrino type make the prompt flux? and: at which energies do they occur ? The answer to the first question is likely to put limits on the dynamics of the neutrino production process, while the spectrum of the prompt flux provides information about the kinematics involved.

We will consider the event rates from the muon neutrinos and electron neutrinos. The energy distribution of observed events will be compared with the predicted energy distribution of conventional ones for each neutrino type. In order to compare the observed and the predicted conventional rates, only the observed event rates from the full density run will be used.

### 6.2.1 The muon neutrino and antineutrino samples

Figures 17 and 18 display the visible energy distributions of the full density muon neutrino and muon antineutrino events respectively, corrected for detection efficiencies and lepton momentum cuts. The mean energies are 64±3 GeV for muon neutrinos and 53±4 GeV for muon antineutrinos for events with $E_\nu > 20$ GeV.

The distributions are superimposed onto the predictions from the conventional sources integrated over the total protons on the target and the mass of the detector. As can be seen from these figures, the observed number of events in both muon neutrino and muon antineutrino samples are compatible with the predictions from the conventional background for energies below 60 GeV. However for energies above 60 GeV the observed events appear to be higher than those expected from the conventional sources. This is specially true in antineutrino sample for energies between 60 and 100 GeV.

### 6.2.2 The electron neutrino and antineutrino samples

The energy distribution of electron neutrino and electron antineutrino events in full density are shown in figures 19 and 20 respectively together with the estimated conventional background in each sample. As can be seen from these figures, the observed event rates are higher than what is expected from the conventional sources in all energy bins indicating the existence of other electron (anti) neutrino sources.

The cleanest evidence for the existence of the prompt neutrino source comes from the observed electron sample where a difference of more than 4 standard deviations between the observed and the predicted conventional events is seen for neutrino energies between 30 and 100 GeV. The effect is less pronounced in the antielectron neutrino sample, although a difference of more

than 2.5 standard deviations can be seen in the third bin. The mean energies are 69±5 GeV for electron neutrinos and 70±6 GeV for electron antineutrinos taking events with energies above 20 GeV. From the above plots it can be seen that the observed electron events can not be explained by the estimated conventional background. Indeed a simple calculation based upon the total number of events observed and the expected total conventional background shows that the estimated conventional background accounts only for about 20% of the total electron neutrinos and electron antineutrinos. The remaining events are assumed to be due to prompt electron neutrinos.

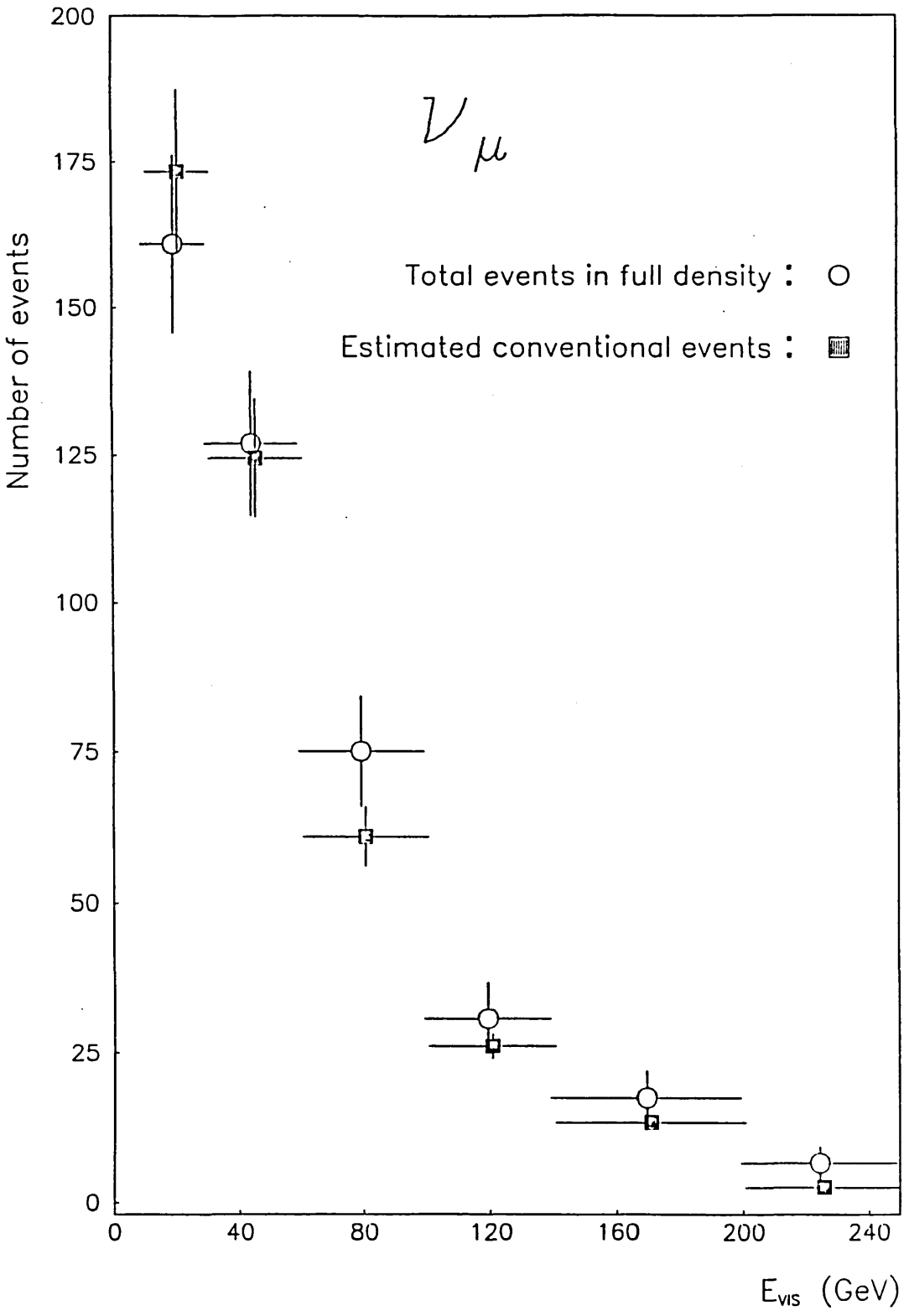



Figure 17: Energy distribution of muon neutrino events.

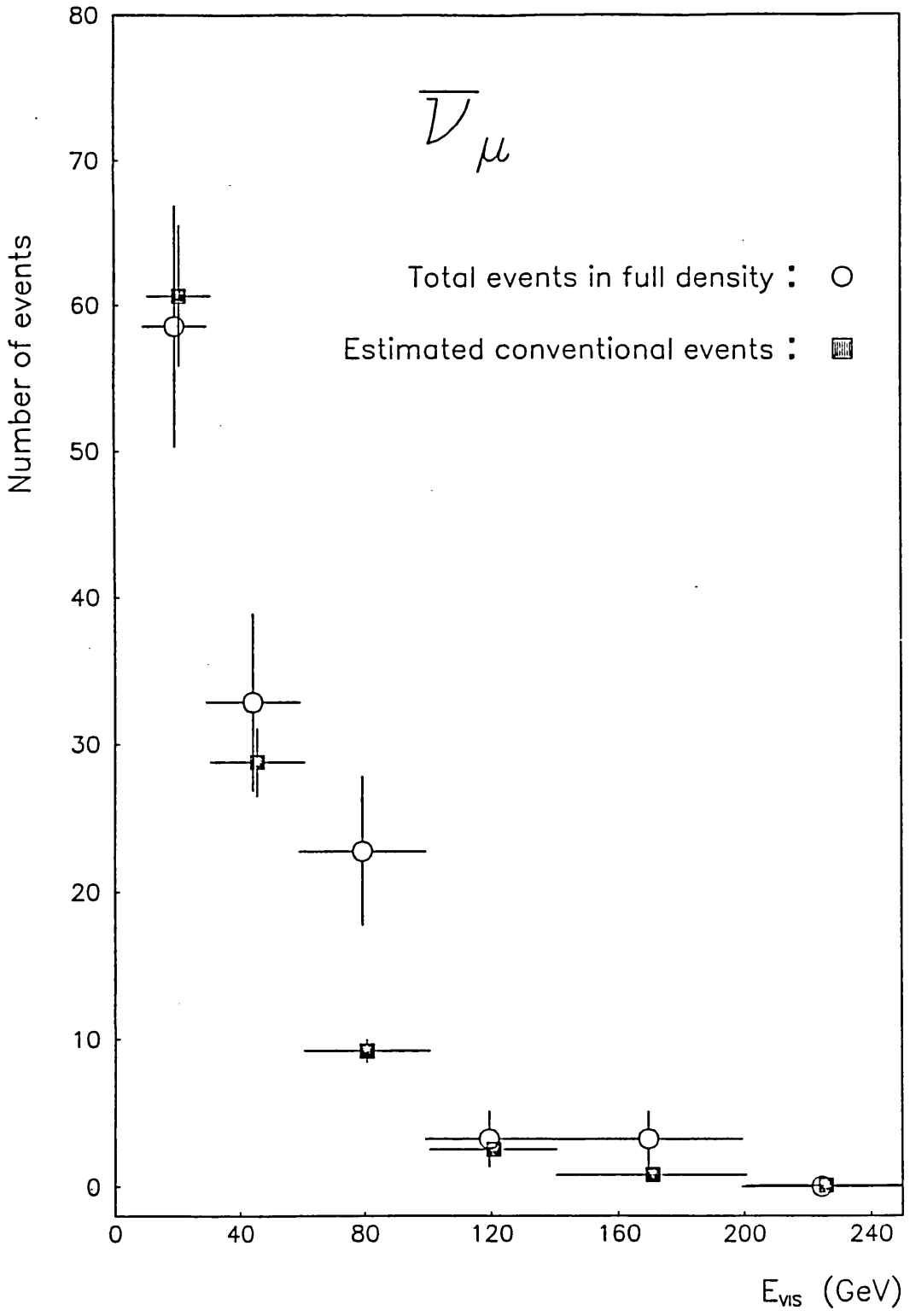



Figure 18: Energy distribution of muon antineutrino events.

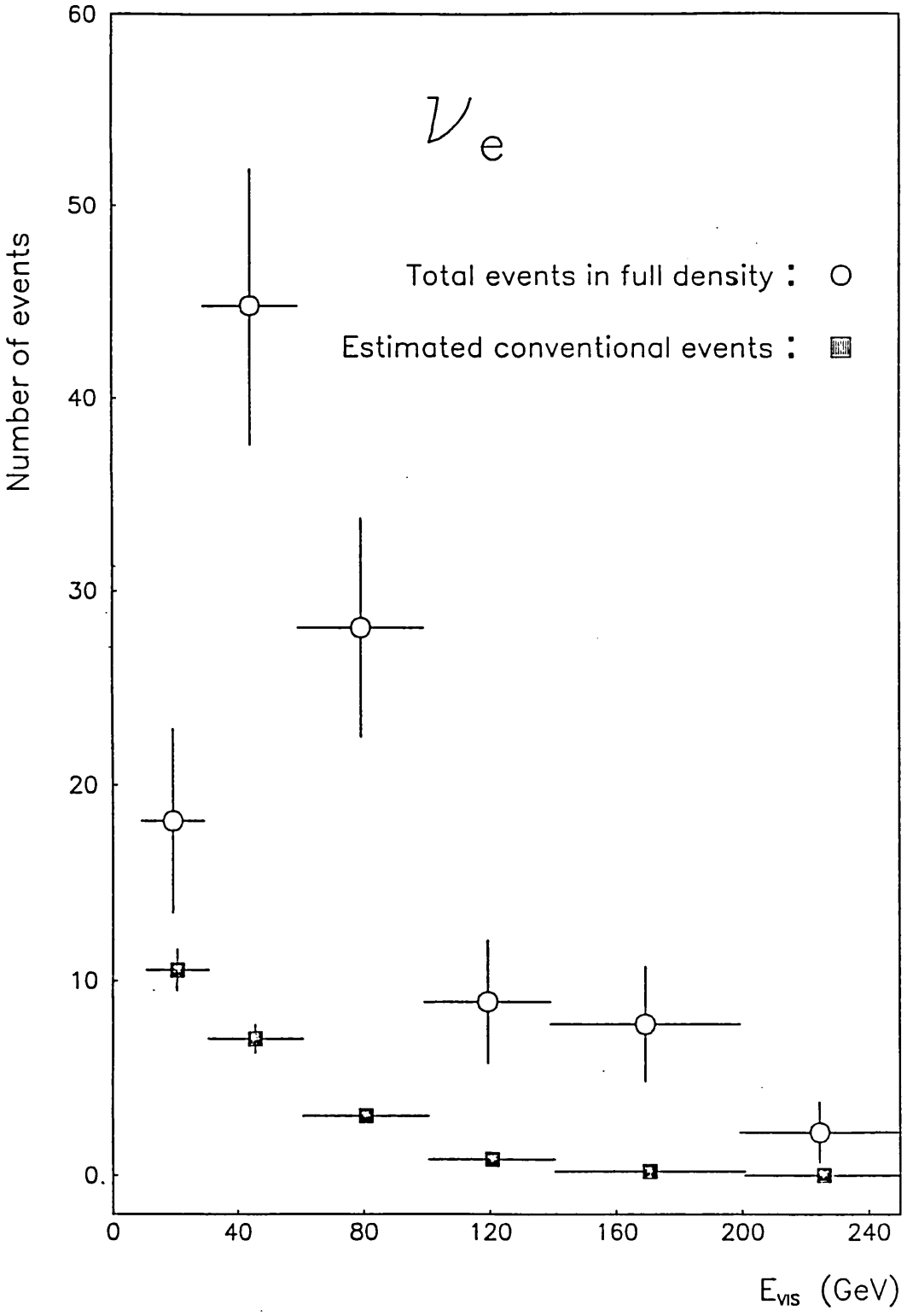



Figure 19: The energy distribution of electron neutrino events.

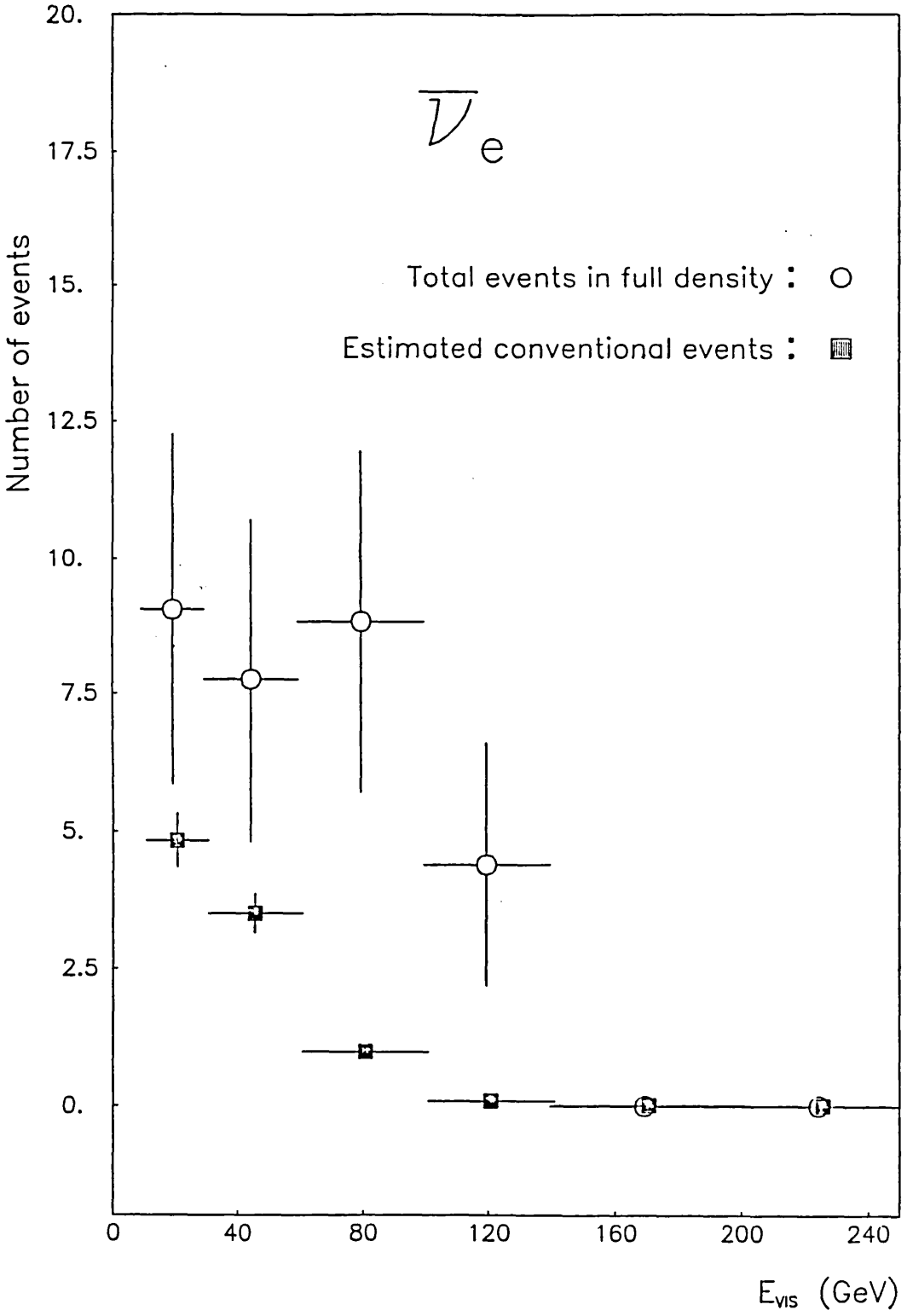



Figure 20: The energy distribution of electron antineutrino events.

## 6.3 ESTIMATE OF THE PROMPT RATES

The prompt neutrino rates are estimated by two methods; these are:

1. The subtraction method where the expected neutrino flux from the conventional sources is predicted and the prompt rate is obtained by subtracting the conventional background from the observed event rates;
2. The extrapolation method where normalised event rates in the full and 1/3 density dumps are plotted as a function of the inverse dump density and the prompt rate is estimated by extrapolating the event rate to infinite density.

Method 1 requires the knowledge of the conventional neutrino sources and measured conventional hadron spectra from proton copper interactions at 400 GeV/c. On the other hand method 2 requires a test of linearity of event rates with the inverse dump density. Both methods are described below.

### 6.3.1 The prompt rates from the subtraction method

Integrating over the spectrum of the observed and the estimated conventional events in figures 17, 18, 19, and 20 and subtracting the conventional background from the observed events the following prompt estimates are made in units of 1 ton and $10^{18}$ protons.

TABLE 23

Prompt charged current event rates for $E_\nu > 20$ GeV in units of events per ton and $10^{18}$ protons from the subtraction method.

| $\mu^+$ | $\mu^-$ | $e^+$ | $e^-$ |
|---|---|---|---|
| 1.0±0.5±0.3, | 1.0±0.9±0.9, | 0.8±0.2±0.1, | 4.1±0.5±0.2 |

### 6.3.2 The prompt rates from the extrapolation method

Compared to the subtraction method, the extrapolation method has the advantage of being nearly independent of background calculations. The gain in systematics, however is traded off by a large increase in the statistical error.

The extrapolation method relies on the fact that the prompt signal is independent of the density of the target, while the conventional background flux is inversely proportional to the density of the target. In other words, we expect to observe three times more background events in the run with the 1/3 density dump compared to the full density run. Using this simplified assumption the prompt rate will be obtained from

$$n_{prompt} = 1.5 \times R_1 - 0.5 \times R_3 \qquad (6.3)$$

where $R_1$ and $R_3$ are the observed number of neutrino events in full and 1/3 density dumps respectively.

The above equation is over simplified, because other factors had to be taken into account in evaluating the prompt rates. These were:

a) The existence of faked prompt neutrinos due to the beam interactions with the material upstream of the dump;

b) The leakage of hadrons in the 1/3 density dump.

Point (a) arises from the fact that any beam interaction with the material upstream of the dump resulted in the background for the prompt neutrino flux since the hadrons produced in these interactions had decay paths much longer than the hadrons produced in the dump. This background was independent of the density of the dump and therefore simulated a prompt signal. This background was estimated to be ($\beta = 0.7 \pm 0.1$)% of the conventional background in the full density [1].

The second point was due to the way the 1/3 density dump was manufactured. The 1/3 density dump had alternative 2.5cm copper, 5.0cm air gaps and as a result the effective copper length in 1/3 density dump was only 1m followed by the 3m long catcher. The end of nuclear cascade was absorbed in the catcher. The effect of this leakage was that a small fraction of the conventional flux appeared to be prompt or in other words the average density did not correspond to exactly 1/3 density. This effect was estimated by removing the catcher behind the dump allowing the leaking hadrons about 23 times longer decay length compared with the full density dump. Comparing the muon flux

for the two conditions, the effective inverse density was determined to be $(2.92\pm0.02)\ (gm/cm^3)^{-1}$ rather than $(3.0\ (gm/cm^3)^{-1}$ and the leakage was detemined to be [$\alpha = (4\pm1)\%$] of the conventional flux from the full density dump [1].

Accounting for the upstream interaction and the leakage corrections in equation (6.3) and introducing $\varepsilon$ as the overall correction factor for effects described above [$\varepsilon = (4.7\pm1.0)\%$], we obtain the rates in the full and 1/3 density data:

$$R_1 = R_P + (1+\beta)R_C$$

$$R_3 = R_P + \frac{(3 + \alpha + \beta + \alpha\beta) \times R_C}{1 + \alpha}$$

where $R_P$ and $R_C$ refer to prompt and conventional rates respectively. These equations may be jointly solved for $R_P$ and $R_C$. By redefining $R_C \rightarrow (1+\beta)R_C$ and approximating $\alpha\beta = 0$ one can derive the conventional and the prompt rates as follows:

$$R_C = \tfrac{1}{2} \times (R_3 - R_1)(1 + \varepsilon)$$
$$R_P = \tfrac{1}{2} \times [(3 + \varepsilon)R_1 - (1 + \varepsilon)R_3] \qquad (6.3A)$$

Table 24 gives the estimated prompt rates in units of 1 ton and $10^{18}$ protons.

TABLE 24

Prompt charged current event rates for $E_\nu > 20$ GeV in units of events per ton and $10^{18}$ protons from the extrapolation method.

| $\mu^+$ | $\mu^-$ | $e^+$ | $e^-$ |
|---|---|---|---|
| -0.3±1.0±0.1, | 0.8±1.8±0.1, | 0.4±0.5±0.0, | 3.5±0.9±0.1 |

## 6.4 THE THROUGH-GOING MUONS

As can be seen from tables 23 and 24, the small prompt muon signal is badly determined by the limited statistics available from muon neutrino interactions in BEBC. Using also through-going muons, however, increases the statistics by a factor of 14. Two different through-going muons were used;

i) "Faraway" muons from interactions in the CERN west area upstream of the veto plane, within ~ 50m from BEBC. These muons were detected as five-fold coincidences between all electronic detectors and their momenta reconstructed to within ~ 10% by using the data from these detectors alone. The sample consists of 4065 $\mu^+$ and 10257 $\mu^-$ with momenta above 10 GeV/c. While the overall acceptance is not very reliably known, the ratios of the different rates are well determined. Because of ranging out effects there are corrections to account

for the different energy spectra of prompt and conventional flux, and for the difference in y-distribution between $\mu^-$ and $\mu^+$ events. These corrections, based on a Monte Carlo calculation assuming charmed particle decay as the prompt source, introduce systematic errors which can be kept small (~ 10%), since the momentum spectra of the through-going muons greatly constrain the neutrino production models [1]. Table 25 shows various ratios as obtained by extrapolating through-going muon data and the corresponding ratios corrected to apply to event rates inside BEBC. Highly significant prompt signals are obtained in both $\mu^+$ and $\mu^-$ data;

ii) "Nearby" muons from between the veto plane and the upstream picket fence (four-fold coincidences) were found using the EMI-IPF system and were measured inside BEBC. The statistics is comparable to the event numbers inside BEBC (343 $\mu^+$ and 1180 $\mu^-$ with momenta above 10 GeV/c). The corrections to event ratios are smaller than for the faraway muons since the interactions took place immediately upstream of BEBC. The statistical errors dominate and the nearby muons do not contribute very strongly to the final result. Table 25 also gives the results for the nearby muons.

TABLE 25

Ratios of through-going muon rates

$P_\mu$ > 10 GeV/c, $E_\nu$ > 20 GeV, P = prompt, C = conventional
Statistical and systematic errors are added in quadrature

| | Faraway muons | | Nearby muons | |
|---|---|---|---|---|
| | μ ratio | event ratio | μ ratio | event ratio |
| $P^-/C^-$ | 0.35±0.05 | 0.26±0.05 | 0.14±0.11 | 0.13±0.10 |
| $P^+/C^+$ | 1.16±0.15 | 0.69±0.12 | 0.62±0.33 | 0.70±0.38 |
| $C^+/C^-$ | 0.28±0.02 | 0.21±0.03 | 0.23±0.04 | 0.16±0.04 |
| $P^+/P^-$ | 0.92±0.12 | 0.56±0.11 | 1.02±0.84 | 0.85±0.70 |

## 6.5 FITTING PROMPT RATES

It is possible to obtain a unique set of prompt rates by fitting the prompt event rates inside BEBC together with the calculated conventional background and the through-going muon rates in a generalised least squares fit to equations (6.3A). A detailed description of this fit is given in ref 1; a short description and discussion of the results is given below. The following inputs were used for this fit:

i) Corrected charged current event rates in BEBC for full and 1/3 density;

ii) The 'Monte Carlo calculated' for conventioanl background rates, C, in each bin;

iii) The extrapolated prompt and conventional rates of through-going muons, corrected to apply inside BEBC. The overall normalisations were considered unknown.

Table 26 gives the results of the fit to data for $E_\nu > 20$ GeV. The $\chi^2$ per degree of freedom was 15.1/10.

TABLE 26

Prompt charged current event rates for $E_\nu > 20$ GeV in units of events per ton and $10^{18}$ protons from the generalised least squares (global) fit.

| $\mu^+$ | $\mu^-$ | $e^+$ | $e^-$ |
|---|---|---|---|
| 1.71±0.21 | 2.94±0.47 | 0.96±0.25 | 4.36±0.48 |

The fit is the best determination of the prompt rates, as it combines all available information. It does not, however, distinguish between statistical and systematic errors.

## 6.6 THE SOURCE OF PROMPT NEUTRINOS

The prompt neutrinos are generally attributed to the hadroproduction of charmed hadrons through the reaction of the type

$$PP \rightarrow cc' + X \tag{6.4}$$

and subsequent leptonic and semileptonic decay of these hadrons [7-9]. In the above equation c (and also c') stands for either a charmed meson or a charmed hadron. This is indeed plausible, if one takes into account the lifetime of charmed particles. The charm lifetime can be estimated on the basis of the spectator diagram compared to the muon decay diagram, although the spectator quark diagram is probably not the only significant contribution to the decay rate, but it suffices for a rough estimate. Comparison of (a) and (b) in figure 21 leads to the ratio of decay rates:

$$\Gamma_c / \Gamma_\mu = 5( m_c / m_\mu )^5$$
$$\tau_c = 1/5 \, ( m_\mu / m_c )^5 \times \tau_\mu \tag{6.5}$$

where the light quark mass is neglected and the factor 5 takes account of the 3 colors plus 2 lepton types into which the W can decay and $m_c$ is the mass of the charm quark. Taking $m_c \sim 1.5$ GeV/$c^2$ (roughly half the mass of $J/\psi$) the typical charmed state lifetime is estimated at:

$$\tau_c \sim 8 \times 10^{-13} \text{ s} \tag{6.6}$$

This agrees well with measurements of charmed particle lifetimes listed in [19].

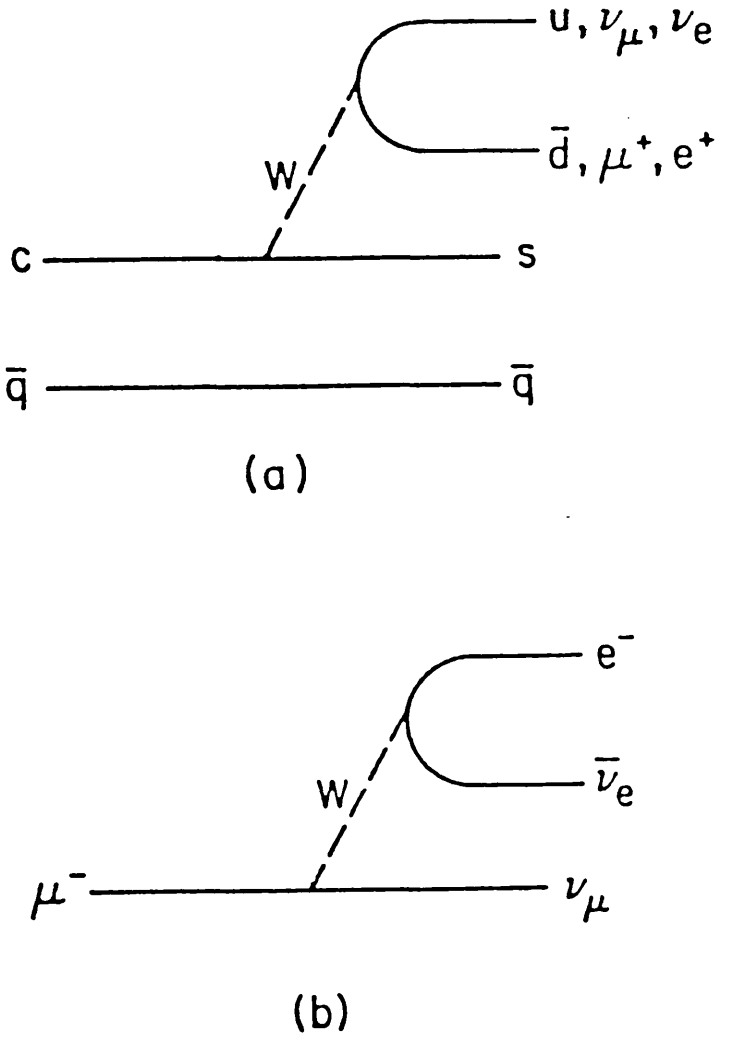



Figure 21: Comparison of charm decay (a) and muon decay (b) diagrams.

As a result the expected decay distance of high energy charmed particles are vastly shorter than those of strange particles and charmed hadrons will have an almost 100% chance of de-

cay before they are absorbed in the target. Other possible sources of prompt neutrinos are the heavy lepton production by the Drell-Yan type process or associated beauty particles but because of the large mass of heavy leptons and smallness of the beauty production cross-sections, the contribution from these sources to the prompt neutrino events is expected to be negligible [25].

Assuming charmed hadrons to be the source of prompt neutrinos, then the semileptonic decays of charmed particles can be described in terms of spectator diagrams as shown in figure 22, where the antiquark $\bar{q}$ can be $\bar{d}$, $\bar{u}$ or $\bar{s}$ resulting in formation of $D^+$, $D^0$ and $D_s^+$ (previously called F) mesons respectively. In the case of charmed baryons the lightest possible candidate is $\Lambda_c^+$. Heavier charmed hadrons could be produced in the collision but will decay to one of these ground states. The spectator decay diagram for $D^-$, $D^0$ and $D_s^-$ can be obtained by replacing c by $\bar{c}$ and $\bar{q}$ by d, u or s respectively.

The purely leptonic decay modes can be obtained from the quark fusion diagrams as shown in figure 23. Figure 23(a) shows the Cabbibo favoured W-annihiliation of $D_s^+$ decay and figure 23(b) shows the Cabbibo suppressed W-annihiliation $D^+$ decay. Assuming neutrinos have zero mass, the decay rates for figures 23(a) and (b) are

$$\Gamma(D_s \to \ell\nu) = (G^2 F_{D_s}^2/4\pi) m_\ell^2 m_{D_s} (1-m_\ell^2/m_{D_s}^2)^2 \cos^2\theta_c \qquad (6.7)$$

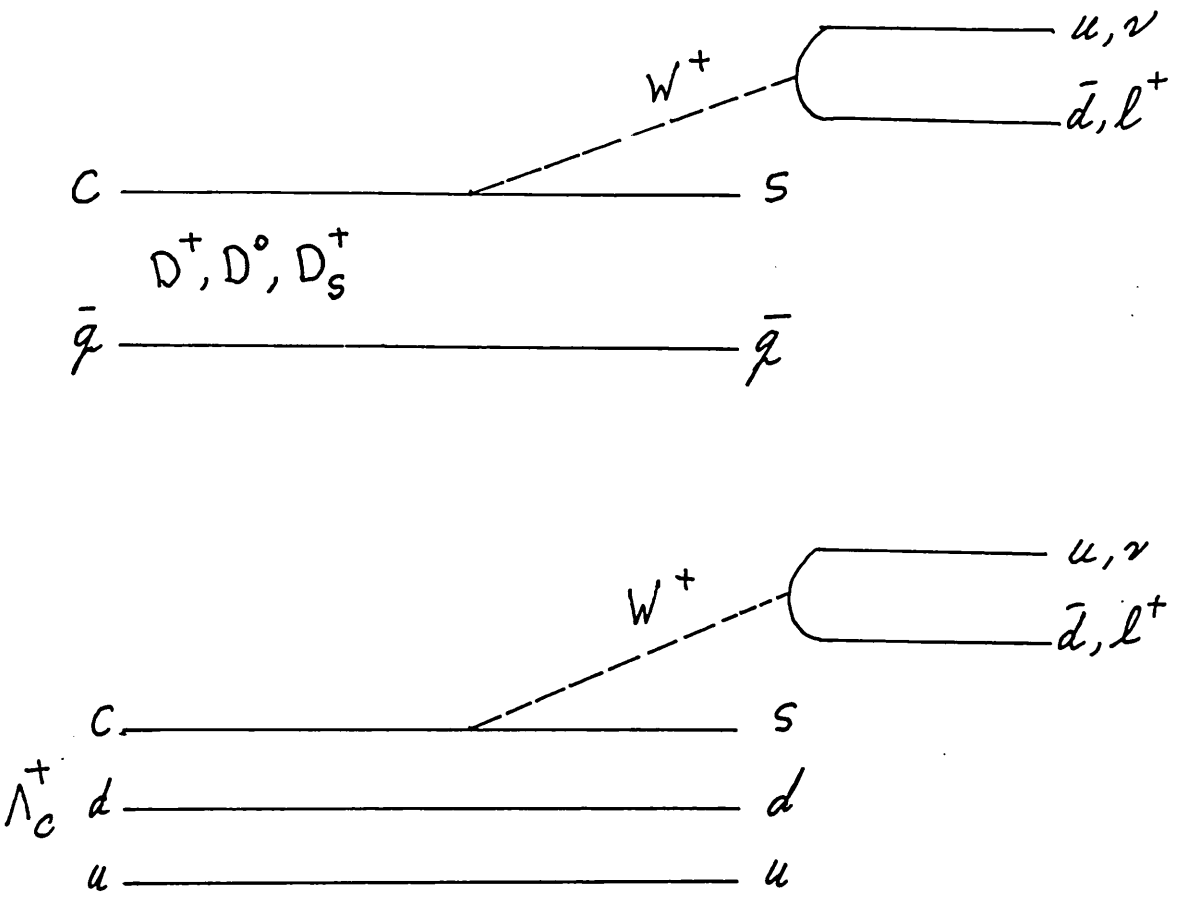



Figure 22: Semileptonic decay of charmed hadrons in the spectator quark model.

$$\Gamma(D \to \ell\nu) = (G^2 F_D{}^2/4\pi) m_\ell{}^2 m_D (1-m_\ell{}^2/m_D{}^2)^2 \sin^2\theta_c \qquad (6.8)$$

where $m_\ell$ is the mass of the charged lepton $\ell$. $\theta_c$ is the Cabbibo angle for the charm to strange transition and $f_{D_S}$ and $f_D$ are the $D_s$ meson and D meson weak decay constants. Because $m_\tau >> m_\mu >> m_e$, the above equations favour heavier lepton production. For example

$$\Gamma(D^{\pm} \to e^{\pm}\nu)/(D^{\pm} \to \mu^{\pm}\nu) \simeq (m_e/m_\mu)^2 \simeq 2.3\times10^{-5} \qquad (6.9)$$

Comparing the $D_s$ meson decay rates to $\mu\nu$ and $\tau\nu$

$$\Gamma(D_s \to \tau\nu)/(D_s \to \mu\nu) = (m_\tau/m_\mu)^2 \times [(m^2_{D_s}-m^2_\tau)/(m^2_{D_s}-m^2_\mu)]^2 \sim 9.4 \qquad (6.10)$$

One can consider the contribution from the decay $D \to \mu\nu$ relative to the semileptonic decay of $D \to \mu\nu X$. This ratio can be estimated by comparing $D \to \mu\nu$ decay width with $\pi \to \mu\nu$:

$$\Gamma(D^{\pm} \to \mu\nu)/\Gamma(\pi^{\pm} \to \mu\nu) = (f_D/f_\pi)^2 \times (m_D/m_\pi)(1-m_\mu^2/m_D^2)^2(1-m_\mu^2/m_\pi^2)^{-2}\tan^2\theta_c \qquad (6.11)$$

taking $(f_D/f_\pi)^2 = 4$ as given in [26] and $\sin\theta_c=0.23$ [19], we obtain

$$\Gamma(D^{\pm} \to \mu^{\pm}\nu)/\Gamma(\pi^{\pm} \to \mu^{\pm}\nu) \sim 16. \qquad (6.12)$$

The width for $\Gamma(\pi \to \mu\nu)$ is well established. Using the measured $D^{\pm}$ lifetime [19]:

$$\tau_{D^{\pm}} = (9.2^{+1.3}_{-1.0})\times10^{-13} \text{ sec} \qquad (6.13)$$

the branching ratio of $D \to \mu\nu$ becomes:

$$BR = \Gamma\times\tau \sim (6.2\times10^{8})\times(9.2\times10^{-13}) = 5.7\times10^{-4} \qquad (6.14)$$

The semileptonic branching fraction $D^{\pm} \to e^{\pm}\nu X$ is measured at $(18.2\pm1.7)\%$ [19], assuming an identical value for $D^{\pm} \to \mu^{\pm}\nu X$, one obtains

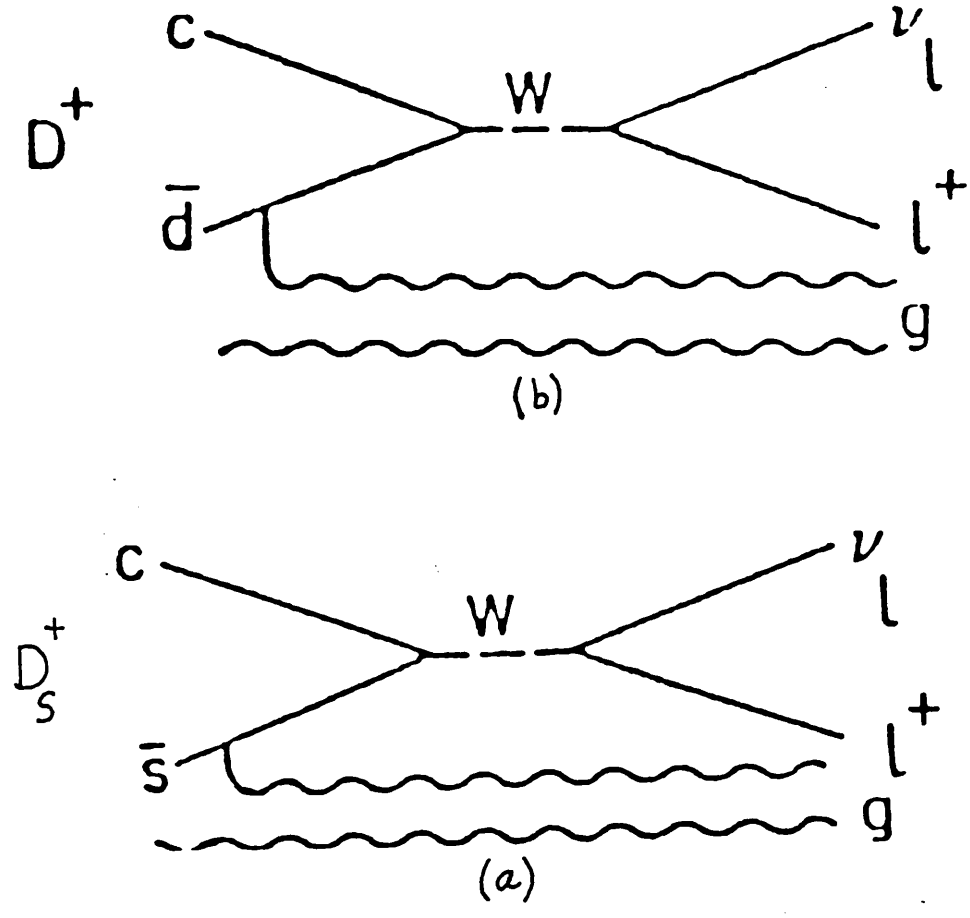



Figure 23: quark fusion diagrams for production of prompt leptons

$$\Gamma(D^{\pm} \to \mu^{\pm}\nu)/\Gamma(D^{\pm} \to \mu^{\pm}\nu X) \sim 3\times10^{-3} \qquad (6.15)$$

and

$$\Gamma(D \to e\nu)/\Gamma(D \to e\nu X) \sim (2.3\times10^{-5})(3\times10^{-3}) = 6\times10^{-8}. \qquad (6.16)$$

using (6.9) and (6.15).

From the above relations one can deduce that the contribution from the decay of $D^{\pm} \rightarrow e^{\pm}\nu$ to the prompt electron neutrino flux is practically non existent. On the other hand with the estimated $BR(D \rightarrow \mu\nu) \sim 5.7 \times 10^{-4}$, and the reported upper limit on this ratio < 2% [19], one expects a negligible contribution to the prompt muon neutrino flux from this decay mode. Also the neutral D's do not have any purely leptonic decay modes.

With the above discussion, it is plausible to assume that the semileptonic decay modes of charmed mesons overwhelm the purely leptonic modes. Moreover, the charmed hadrons semileptonic branching fractions presumably obey simple electron-muon universality. The test of this universality is of great interest and has profound implications on the assumptions made about the production mechanism of prompt neutrinos.

## 6.7 ELECTRON-MUON UNIVERSALITY

Following the discussion of previous section, the interpretation of the prompt neutrino fluxes observed is to assume they come from the semileptonic decays of charmed hadrons produced in proton hadron collisions. In spectator quark model in which the c-quark decays independently of the presence of other quarks (fig 22), the resultant $W^{\pm}$ will have a total decay rate $W \rightarrow \ell\nu_{\ell}$ given in the rest frame of W [27]:

$$\Gamma_W = (GM^3_W/6\sqrt{2}\pi)\ (1-m^2_{\ell}/M^2_W)^2(1+m^2_{\ell}/2M^2_W) \qquad (6.17)$$

The measured mass of the W [19]:

$$M_W = (81.8 \pm 1.5)\ GeV/c^2$$

i.e. $M_W >> m_\ell$ where $\ell$ is e or $\mu$. Thus for either decay modes the decay rate satisfies

$$\Gamma_W \sim GM^3_W / 6\sqrt{2}\pi \sim 239\ MeV \qquad (6.18)$$

The implication of this result is that the decay widths to $e\nu_e$ and $\mu\nu_\mu$ are the same. In that case $\nu_e$ and $\nu_\mu$ fluxes should essentially be equal. In principle one can test the validity of this asssumptions by studying the asymmetry in the number of prompt $\nu_e$ and $\nu_\mu$ events. We define this asymmetry '$A_{e\mu}$' to be:

$$A_{e\mu} = ( N_e - N_\mu ) / ( N_e + N_\mu ) \qquad (6.19)$$

where $N_e$ and $N_\mu$ are the total prompt electron and prompt muon neutrino events respectively. The above parameter is prefered over the simple prompt electron to muon ratio 'R' since the error is more symmetric. One should stress in here that the asymmetry parameter '$A_{e\mu}$' is not a direct measure of asymmetry in the prompt $\nu_e$ and $\nu_\mu$ fluxes. Because the neutrino interaction cross-section is proportional to neutrino energy, the number of prompt events estimated is proportional to neutrino energy times the prompt flux. The parameter '$A_{e\mu}$' provides asymmetry in the flux only if the energy dependence of the prompt electron (anti) neutrino flux is identical to that for prompt muon (anti) neutrino. Equal neutrino and antineutrino fluxes would yield event rates in the ratio $r = \sigma(\bar{\nu})/\sigma(\nu) = 0.49 \pm 0.02$ [21]. We define the asymmetry between neutrino and antineutrino events to be:

$$A_{\nu\bar{\nu}} = ( rN_{\ell^-} - N_{\ell^+} ) / ( rN_{\ell^-} + N_{\ell^+} ) \qquad (6.20)$$

where $\ell$ refers to electrons or muons. The asymmetry between $e^-$ and $\mu^-$ is given by:

$$A^-_{e\mu} = ( N_{e^-} - N_{\mu^-} ) / ( N_{e^-} + N_{\mu^-} ) \qquad (6.21)$$

similar defintion applies for asymmetry between $e^+$ and $\mu^+$.

## 6.8 DISCUSSION OF THE PROMPT RATES

The 1979 experiments suggested that the prompt electron neutrino and prompt muon neutrino fluxes might be different. The asymmetry for the 1979 BEBC beam dump was[†] [7]:

$$A_{e\mu} = -0.08^{+0.44}_{-0.27} \qquad (6.22)$$

for neutrino energies above 20 GeV, using prompt rates from table 26 gives

$$A_{e\mu} = 0.07 \pm 0.08 \qquad (6.23)$$

in good agreement with expectation and fully consistent with e-μ universality. One has to bear in mind that for the correction of the through-going muon rates charm production models have been assumed which might hide new production mechanisms for prompt neutrinos (specially at the low end of the energy range) [1]. Omitting the faraway muons (the most model dependent

[†]The 1979 asymmetry $A_{e\mu}$ was updated using the new measurements of conventional background [24] and presented in reference 1.

part of the analysis) yields [1]:

$$A_{e\mu} = 0.33^{+0.20}_{-0.16} \qquad (6.24)$$

using the event rates in BEBC (tables 23 and 24), For $E_\nu > 20$ GeV, the asymmetry from subtraction is:

$$A_{e\mu} = 0.41 \pm 0.20 \pm 0.20 \qquad (6.25)$$

the asymmetry from extrapolation is:

$$A_{e\mu} = 0.78 \pm 0.65 \pm 0.05 \qquad (6.26)$$

and the combined asymmetry from (6.25) and (6.26) is:

$$A_{e\mu} = 0.47 \pm 0.19 \pm 0.05 \qquad (6.27)$$

For energies above 20 GeV, using global prompt rates, the asymmetry between neutrinos and antineutrinos (6.20) for muon neutrinos and electron neutrinos combined is:

$$A_{\nu\bar{\nu}} = 0.15 \pm 0.08 \qquad (6.28)$$

For muon neutrinos and electron neutrinos separately the asymmetries are:

$$A^{\mu}_{\nu\bar{\nu}} = -0.09 \pm 0.11 \qquad (6.29)$$

and

$$A^{e}_{\nu\bar{\nu}} = 0.38 \pm 0.14 \qquad (6.30)$$

The asymmetries between leptons of same charge are:

$$A^{+}_{e\mu} = -0.28 \pm 0.14 \qquad (6.31)$$

and

$$A^{-}_{e\mu} = 0.19 \pm 0.10 \qquad (6.32)$$

From the above results it can be seen that there is 2.6 standard deviation difference between $A^{e}_{\nu\bar{\nu}}$ and $A^{\mu}_{\nu\bar{\nu}}$. On the other hand, comparing $A^{-}_{e\mu}$ and $A^{+}_{e\mu}$, the difference is unlikely to be explained in terms of systematic errors. While it is not possible to explain any deviation from the expected $A^{-}_{e\mu} = A^{+}_{e\mu} = 0$ by known physics, the data favour $A^{-}_{e\mu} > 0 > A^{+}_{e\mu}$. Although the effect is not strong enough to allow definite conclusion which would require a radically different interpretation of the experimental situation, involving new physics. Given this, the interpretation in terms of statistical fluctuations appears more appropriate.

## 6.9 COMPARISON WITH OTHER EXPERIMENTS

### 6.9.1 Comparison with 1979 rates from CERN beam dump experiments

Due to change in the position of the dump in the present setup, the total rates from the 1979 CERN beam dump experiments [7-9] are not directly comparable with the present ones. If there are no distance dependent effects, such as neutrino oscillations or decays, and if the solid angle coverage is the same, the rates scale as (distance from dump)$^{-2}$. Table 27 shows the ratios be-

tween the present BEBC beam dump rates and that of 1979 CERN beam dump experiments for muon events. The first line gives the so called dilution factor from pure geometry. It can be seen from this table that the full density $\mu^-$ rate in the present BEBC experiment appears low compared to 1979 $\mu^-$ rates, despite of improved muon detection in the present experiment.

TABLE 27

Comparison of the present BEBC beam dump rates and that of 1979 CERN beam dump experiments for muon events with $E_\nu$ > 20 GeV.

| | BEBC/BEBC79 | BEBC/CDHS79 | BEBC/CHARM79 |
|---|---|---|---|
| geo. factor | 4.08 | 4.81 | 5.03 |
| $\mu^+$ (1/1) | 2.79±0.70 | 4.51±0.63 | 3.47±0.60 |
| $\mu^-$ (1/1) | 2.56±0.34 | 3.24±0.23 | 3.73±0.35 |
| $\mu^+$ (1/3) | 5.69±2.00 | 4.94±0.63 | 7.34±1.64 |
| $\mu^-$ (1/3) | 3.47±0.55 | 3.82±0.26 | 4.42±0.41 |

### 6.9.2 Rates from the present CERN beam dump experiments

Table 28 summarises the relative ratios of the present BEBC beam dump rates to that of CDHS and CHARM [28], for muon neutrinos. The rates from CDHS and CHARM are preliminary.

The first line gives the dilution factors from pure geometry. The second and third lines refer to Monte Carlo calculation [28] of dilution factors for conventional and prompt fluxes respectively, taking into account the event kinematics and the angular acceptences. Again it can be seen that the present BEBC $\mu^-$ rate in the full density data is less than expected. This is also true of the CHARM rate in 1/3 density, since the ratio BEBC/CHARM82 = 1.48±0.09 is higher than expected. On the other hand, the charm full density muon rate is higher than expected (BEBC/CHARM82 = 1.11±0.07), which will show up in the prompt muon rates.

TABLE 28

Comparison of the present BEBC beam dump muon rates with those of CDHS and CHARM for events with $E_\nu$ > 20 GeV.

| | BEBC/CDHS82 | BEBC/CHARM82 |
|---|---|---|
| geometrical factor | 1.31 | 1.44 |
| conventional flux | 1.33±0.013 | 1.34±0.019 |
| prompt flux | 1.32±0.013 | 1.44±0.030 |
| $\mu^+$ (1/1) | 1.31±0.17 | ----- |
| $\mu^-$ (1/1) | 1.18±0.08 | ----- |
| $\mu^+ + \mu^-$ (1/1) | 1.20±0.07 | 1.11±0.07 |
| $\mu^+$ (1/3) | 1.70±0.19 | ----- |
| $\mu^-$ (1/3) | 1.30±0.08 | ----- |
| $\mu^+ + \mu^-$ (1/3) | 1.38±0.07 | 1.48±0.09 |

### 6.9.3 Comaprison of the prompt rates

The prompt rates for the present CERN beam dump experiments are given in table 29 for $E_\nu$ > 20 GeV, per ton and $10^{18}$ protons on target scaled to the BEBC position. For the BEBC the prompt rates from the global fits (table 26) are given. The CDHS and CHARM rates are preliminary extrapolation results [28]. One can observe a factor of two more prompt muons in

the CHARM compared to BEBC and CDHS reflecting the higher absolute rates in the full density, and a lower absolute rates in the 1/3 density data from this experiment. The electron data agree despite of the different ways the data are obtained.

TABLE 29

Comparison of the present BEBC beam dump prompt rates with those of CDHS and CHARM for events with $E_\nu$ > 20 GeV.

| | BEBC82 | CDHS82 | CHARM82 |
|---|---|---|---|
| $\mu^+$ | 1.71±0.21, | 1.25±0.24±0.11 | ------ |
| $\mu^-$ | 2.94±0.47, | 3.36±0.52±0.44 | ------ |
| $\mu^+ + \mu^-$ | 4.65±0.51, | 4.61±0.57±0.45, | 9.94±1.10±0.80 |
| $e^+$ | 0.96±0.25, | ------ | ------ |
| $e^-$ | 4.36±0.48, | ------ | ------ |
| $e^+ + e^-$ | 5.32±0.54, | 4.05±0.32±0.59, | 5.07±0.37±0.25 |

Using the prompt $\mu^+$ and $\mu^-$ rates from CDHS and prompt $e^+$ and $e^-$ rates from BEBC, the asymmetries for like sign leptons become:

$$A^+_{e\mu} = -0.13 \pm 0.17 \qquad (6.33)$$

and

$$A^{-}_{e\mu} = 0.13 \pm 0.11 \qquad (6.34)$$

in better agreement with the expected value of zero than the corresponding values from BEBC alone [compared with results (6.31) and (6.32)].

### 6.9.3.1 Prompt $\nu_e$-$\nu_\mu$ asymmetry

Table 30 shows the prompt e-μ asymmetries for the CERN experiments and the Fermilab experiment E613 [29] for $E_\nu > 20$ GeV. The results for CDHS and CHARM are preliminary [28]. The values given are consistent with no asymmetry, with the exception of the CHARM extrapolation value. Excluding this value which clearly disagrees with other estimates, a least squares fit gives a global e-μ asymmetry of

$$A_{e\mu} = -0.005 \pm 0.044 \qquad (6.35)$$

with $\chi^2$/d.o.f of 0.35 which is compatible with no asymmetry.

TABLE 30

$\nu_e$-$\nu_\mu$ asymmetries from CERN and Fermilab experiments for events with $E_\nu$ > 20 GeV.

| Method: | extrapolation | subtraction | global fits |
|---|---|---|---|
| BEBC82 | ----- | ----- | 0.07±0.08 |
| CDHS82 | -0.07+0.12-0.11, | -0.06±0.15 | ----- |
| CHARM82 | -0.32±0.08 | -0.02±0.13 | ----- |
| E613 | -0.027±0.064±0.04 | ----- | ----- |

### 6.9.3.2 Prompt neutrino-antineutrino asymmetry

Table 31 shows the prompt $\bar{\nu}$ to $\nu$ ratios for the two CERN experiments; BEBC82 and CDHS82. The neutrino rates are weighted by factor r as given in (6.20). The result from the Fermilab experiment E613 is also quoted [29]. It can be seen from this table that the muon ratios are compatible with 1 whereas the BEBC electron rate is less than unity indicating an excess of prompt $\nu_e$ flux, which can possibly reflect an asymmetric parent production process such as associated production of fast charmed baryons with slow charmed antimesons, in analogy to the associated production of strange particles leading to a large excess of conventional $\nu$ over $\bar{\nu}$.

TABLE 31

prompt $\bar{\nu}$ to $\nu$ ratios for events with $E_\nu > 20$ GeV

| experiment: | BEBC82 | CDHS82 | E613 |
|---|---|---|---|
| $\bar{\nu}_\mu/\nu_\mu$ | 1.19±0.24 | 0.76±0.22 | 1.17±0.23±0.10 |
| $\bar{\nu}_e/\nu_e$ | 0.45±0.13 | ------ | ----- |

## Chapter VII

## THE NEUTRAL CURRENT SAMPLE

The weak neutral current, a necessary component of the Weinberg-Salam theory of electro-weak interactions [30], has been the subject of intense experimental investigation since its discovery in 1973 (31). In particular, the study of inclusive neutral-current scattering from the isoscalar targets, protons and neutrons can illuminate the structure of this weak current. Moreover, in a beam dump experiment, the study of the characteristics of the neutral currents and more importantly an estimate of their numbers through the usual neutral current to charged current cross-sections ratio is of particular interest since they can reveal the contamination of the NC sample by other types of interactions.

The neutral current reaction

$$\nu + N \rightarrow \nu + \text{hadrons} \qquad (7.1)$$

is difficult to study because the outgoing neutrino, which typically carries half the interaction energy, can not be detected, in contrast to the charged current reaction

$$\nu + N \rightarrow \ell + \text{hadrons} \qquad (7.2)$$

in which the charged lepton '$\ell$' is readily detected. The 'y' distribution of neutral current events is hard to measure directly since it requires knowledge of the incoming neutrino energy, which is only partially possible with narrow-band beams and not available for wide-band and beam dump experiments.

A much easier task is the direct comparison of neutral current and charged current event distributions by measuring the ratios:

$$R_{\nu N} = \frac{N(\nu + N \rightarrow \nu + X)}{N(\nu + N \rightarrow \ell^- + X)}$$

and

$$R_{\nu N} = \frac{N(\bar{\nu} + N \rightarrow \bar{\nu} + X)}{N(\bar{\nu} + N \rightarrow \ell^+ + X)}$$

They follow directly from event analysis and are essentially independent of neutrino flux uncertainties. The measurement requires a minimal hadron energy cut to establish a minimal energy for neutral current events. This complicates the interpretation of the experimental results and even their direct comparison because the hadron energy cut limits the accessible y distribution.

The observed neutral current sample is contaminated by various backgrounds due to variety of sources some of which are of great interest in this experiment. Traditionally in normal neutrino experiments, the observed NC sample is contaminated by two major backgrounds; these are:

a) the 'neutral hadron' interactions in the liquid simulating neutral current events;

b) the unidentified charged current events where the outgoing lepton is not identified.

In addition in a beam dump experiment, the neutral current sample is expected to be enhanced by the following sources:

1. The CC tau neutrino interactions resulting in an outgoing $\tau$ lepton which decayed ~ 65% of the time into a semileptonic final state within a few millimeters (0.056mm / GeV) of the vertex simulating a neutral current type event;
2. the decays or interactions of supersymmetric particles such as axions, gluinos or heavy neutrinos resulting in neutral current type events.

The search for these two types of events specially the search for tau neutrino interactions has been one of the main objectives of this beam dump experiment and will be considered later. This chapter will discuss methods used for correcting the raw number of neutral currents and estimate of contamination in the NC sample due to sources mentioned in (a) and (b) above.

## 7.1 ESTIMATE OF HADRONIC BACKGROUND IN THE NC SAMPLE

One of the major problems in estimating the number of genuine neutral currents is the existence of "fake neutral current" events due to neutral hadrons either coming from interactions in front and on the periphery of BEBC or from neutrino events in-

side the chamber resulting in the so called "neutron star" background. In general most of these hadronic events have low energies and by applying a suitable energy cut majority of them can be excluded from the analysis.

The problem arises when one tries to estimate the neutral hadronic background below visible energy 10 GeV, because this is where most of these background events occur. One way of estimating this background is to make use of the different characteristic behaviour of neutrino and hadronic events as explained below.

### 7.1.1 Method

We rely on the spatial distribution of hadronic interactions in order to distinguish them from genuine neutrino events.

In a bubble chamber experiment filled with heavy liquid such as the one under consideration, the probability of interaction for neutral hadrons (n*'s, $K^0_L$ etc) will be markedly different than that for neutrinos. Given the shape of the bubble chamber one can define two kinematical variables directly related to the spatial distribution of the observed events in the fiducial volume. These are:

i) x : the distance from the beam entry to the fiducial volume up to the interaction point;

ii) $\ell$ : the potential length (i.e. the distance in the beam direction from entry into fiducial volume up to the exit from that volume);

iii) $\bar{X}$ : the effective interaction length in the liquid.

These variables are shown in figure 24.

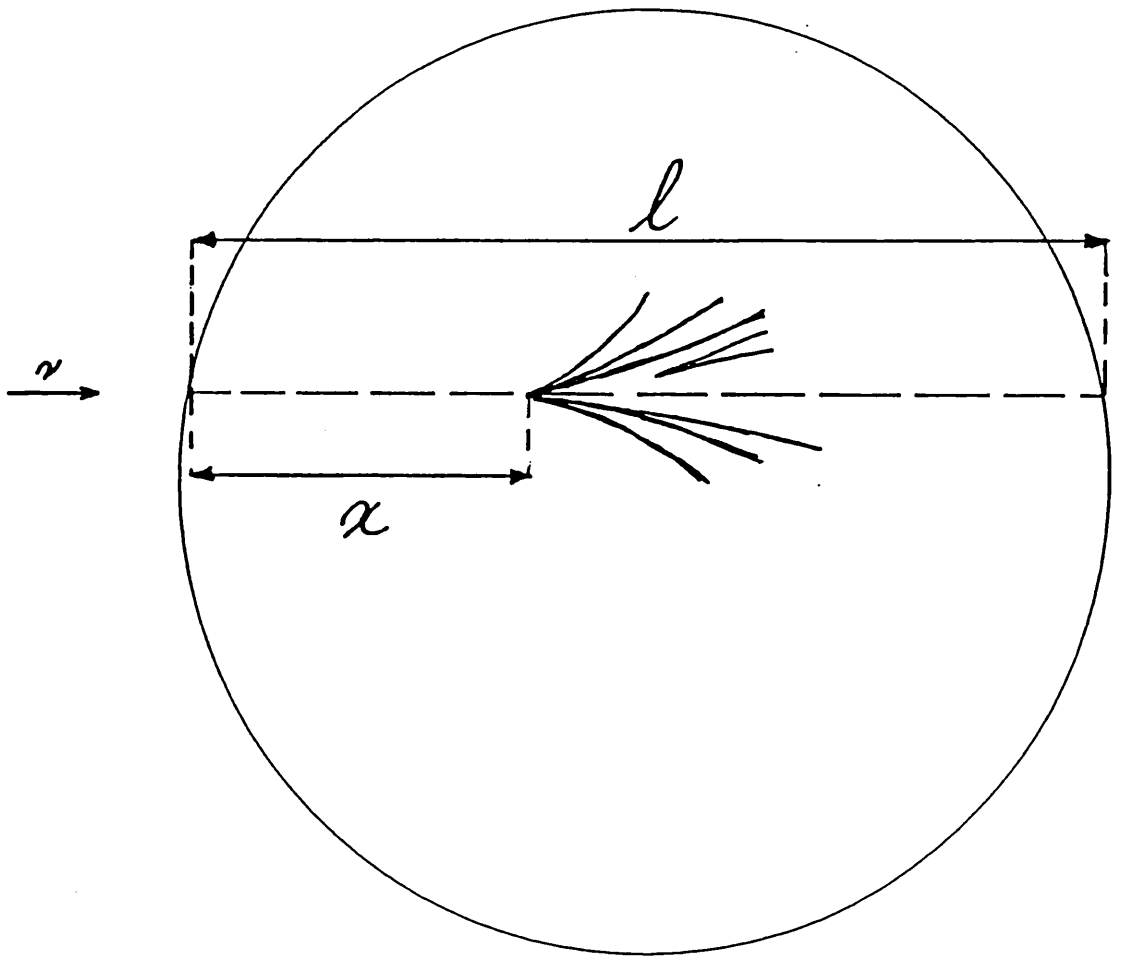



Figure 24: The definition of kinematical variables x and ℓ

In general the above variables depend on the direction in which the incoming beam (neutrino or neutral hadrons) is defined. In order to be consistent in defining this direction, all events were assumed to be originating from the dump (i.e. parallel beam) and the distances for both x and ℓ were taken in the beam direction.

Knowing the exact position of the dump with respect to the centre of bubble chamber and the dump distance from this centre a unit vector in the beam direction could be determined as

$$\hat{r} = 0.914\hat{i} + 0.403\hat{j} + 0.042\hat{k}$$

where $\hat{i}$, $\hat{j}$ and $\hat{k}$ are the unit vectors in the bubble chamber coordinates. Note that this assumption is not necessarily true for hadronic events, since the majority of neutral hadrons were coming from interactions in front of the chamber in different directions and in general the potential length distributions for hadronic events is different than that of neutrino events. However, this effect was investigated by defining the final state hadron vector as the beam direction (in general this direction is better defined for hadronic interactions since the final state hadron vector is a fair representation of the direction of incoming neutral hadron, on the other hand for neutrino events this definition is certainly biased since it ignores the direction of the outgoing lepton, given that in an ideal case the direction of the incoming neutrino is defined as the vector sum of all the final state particles including the detected charged lepton or the missing outgoing neutrino in a NC event) and comparing the potential length distribution of NC events with the corresponding distribution, assuming the events originating from the dump. The potential length distributions for both definitions are shown in figures 25a and 25b respectively.

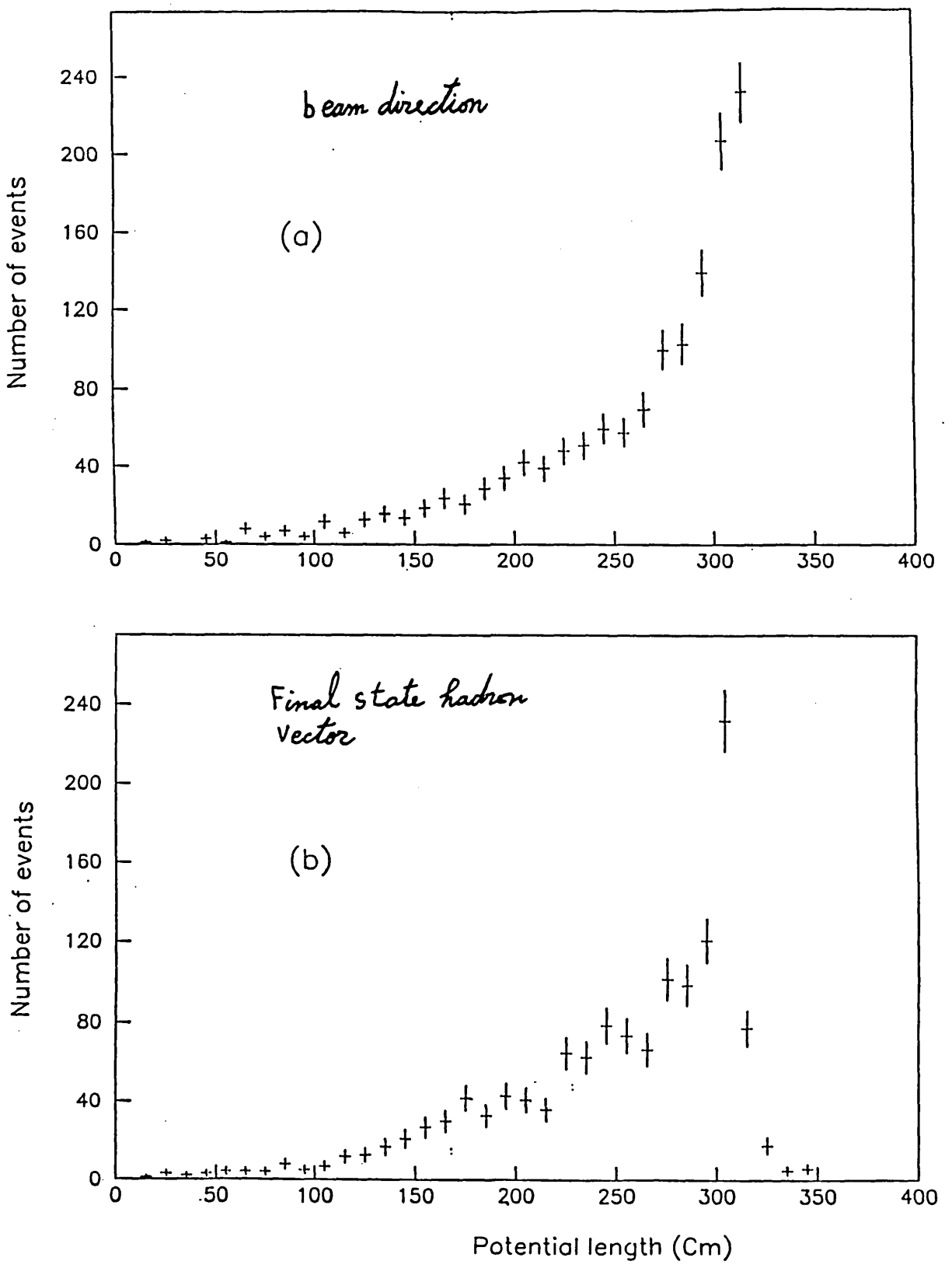



Figure 25: The potential length distribution for NC candidates

As can be seen from figure 25b, taking the final state hadron vector as the beam direction flattens the spectrum and introduces a tail for $\ell > 300$ C.m, but this effect is small and one can assume that as long as the number of hadronic events is small, their potential length distribution will be similar to that for neutrino events.

**Given the above argument, we thereafter assume that all events are originating from the dump in the direction defined by the unit vector above.** We are now in a postion to consider the neutrino and hadronic interactions separately, and try to work out a mechanism in order to estimate the hadronic background in the NC sample. Figure 26 shows the potential length distribution for muon CC events. Note that these events are genuine neutrino events since the muon is identified by the EMI-IPF system.

a) **The neutrino interactions**

We define the joint probability density function (PDF) for x and $\ell$ to be $f(x,\ell)$. For $\nu$ events, given the neutrino interaction cross-section, one can assume that the effective interaction length $\bar{X} \simeq \infty$. This assumption implies that for a slab bubble chamber the spatial spread of the $\nu$ events is expected to be uniform independent of x and $\ell$. In other words we expect a flat $\ell$ and x distributions for neutrino events. Taking $\bar{X} \simeq \infty$, for a given $\ell$, we assume a flat 'x' distribution given by a constant $\alpha$, i.e.

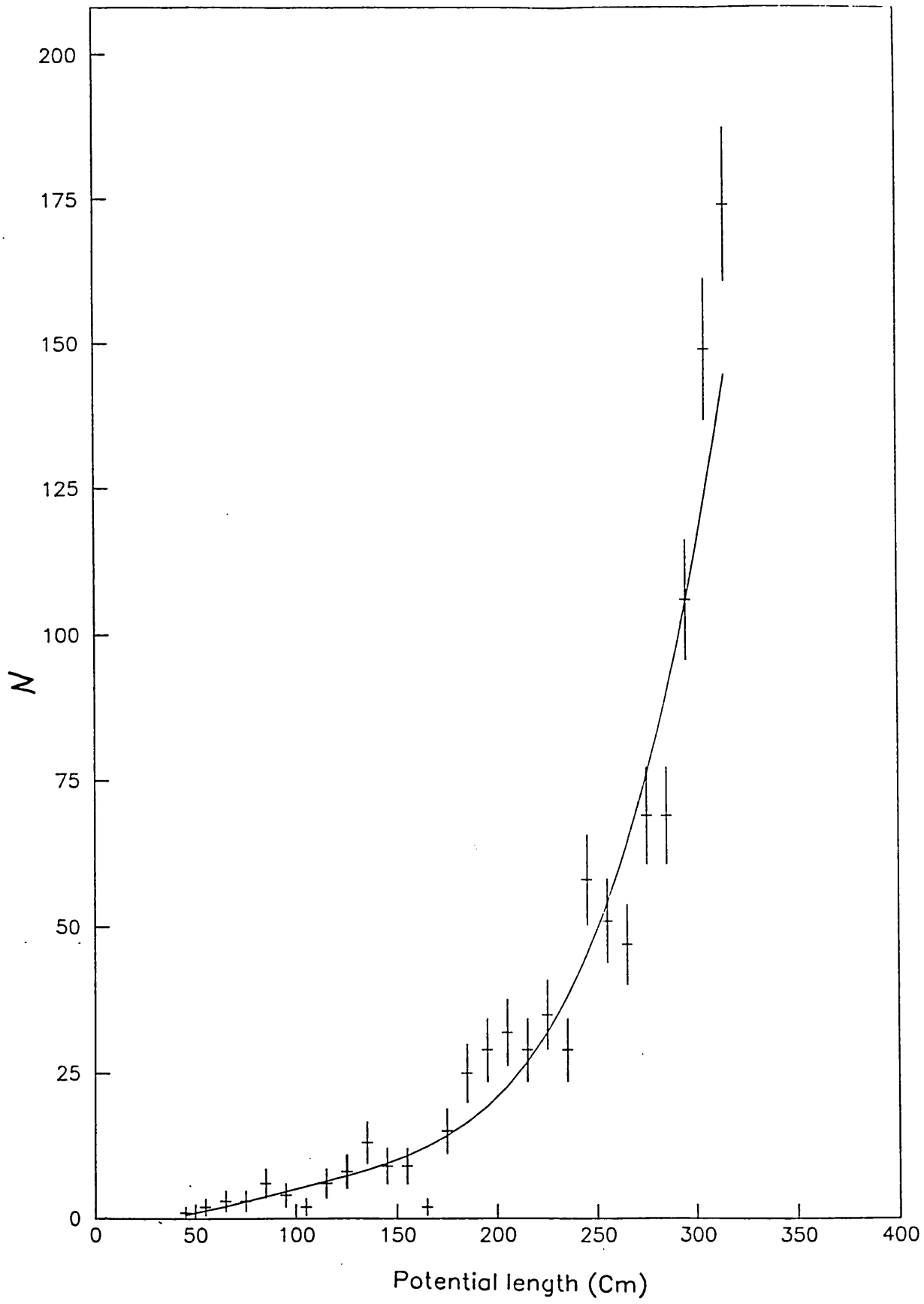



**Figure 26: The potential length disttribution for muon CC events**

$$f(x,\ell) = \alpha\rho(\ell) \qquad 0 < x < \ell \tag{7.3}$$

where $\rho(\ell)$ is the potential length distribution for neutrino events assumed to be the same for hadronic events. From (7.3) one can obtain the projection in $\ell$

$$g(\ell) = \int_0^{\ell} f(x,\ell)dx = \int_0^{\ell} \alpha\rho(\ell)dx = \alpha\ell\rho(\ell) \tag{7.4}$$

If one introduces a new set of variables $\eta = x/\ell$ and $\ell$, then one requires to find the PDF for these variables given by

$$\Psi(\eta,\ell) = f(x,\ell).|J| \tag{7.5}$$

where 'J' is the jacobian determinant of the transformation given by

$$|J| = \partial(x,\ell)/\partial(\eta,\ell) = \ell \tag{7.6}$$

so

$$\Psi(\eta,\ell) = \ell f(x,\ell) \tag{7.7}$$

then the distribution in $\eta$ and $\ell$ becomes

$$\Psi(\eta,\ell) = \alpha\ell\rho(\ell) \tag{7.8}$$

(in other words, a distribution $f(x,\ell)$ independent of x leads to a distribution $\Psi(\eta,\ell)$ independent of $\eta$). The projection in $\eta$ becomes

$$\Phi(\eta) = \int_0^{\ell_{max}} \Psi(\eta,\ell)d\ell = \alpha \int_0^{\ell_{max}} \ell\rho(\ell)d\ell \tag{7.9}$$

but

$$\int_0^{\ell_{max}} \ell\rho(\ell)d\ell = <\ell> \qquad (7.10)$$

so

$$\Phi(\eta) = \alpha <\ell> \qquad (7.11)$$

**i.e. a constant flat distribution independent of $\eta$ for neutrino events.**

Equation (7.11) implies that for neutrino events the distribution in $\eta$ is a constant and proportional to the mean potential length in the bubble chamber. As a result of this one expects a flat $\Phi(\eta)$ distribution for neutrino events.

b) **Hadronic interactions**

The joint probability density function is

$$f(x,\ell) = \beta.\exp(-x/\bar{X}).\rho(\ell) \qquad (7.12)$$

where $\bar{X}$ is the effective interaction length for neutral hadrons. The exponential term above reflects the fall in the number of hadronic events as x increases. the projection in $\ell$ becomes

$$g(\ell) = \int_0^{\ell} f(x,\ell)dx = \int_0^{\ell} \beta.\exp(-x/\bar{X}).\rho(\ell)dx$$
$$= \beta\bar{X}(1 - \exp(-\ell/\bar{X})).\rho(\ell) \qquad (7.13)$$

again if we introduce $\eta = x/\ell$, then the distribution in $\eta$ and $\ell$ becomes

$$\Psi(\eta,\ell) = \ell f(x,\ell) = \ell\beta.\exp(-\eta\ell/\bar{X}).\rho(\ell) \qquad (7.14)$$

and the projection in $\eta$ becomes

$$\Phi(\eta) = \int_0^{\ell_{max}} \Psi(\eta,\ell)d\ell = \int_0^{\ell_{max}} \ell\beta.\exp(-\eta\ell/X).\rho(\ell)d\ell \qquad (7.15)$$

In order to evaluate (7.15) one needs the potential length distribution for hadronic events. As mentioned earlier we assume that $\rho(\ell)$ will be similar for hadronic and $\nu$ events (this remains approximately true, even if there is evidence that the angular distribution of the hadronic events is different from the $\nu$ events, because of the rough spherical geometry of the chamber) and for this reason the potential length distribution for CC muon events was used. A polynomial of the form

$$\rho(\ell) = \alpha\ell + \beta\ell^2 + \gamma\ell^3 + \delta\ell^4 \qquad (7.16)$$

was fitted to the distribution of figure 26. The fitted curve obtained is also shown in figure 26. The fit corresponds to a $\chi^2$ of 47 with 23 degrees of freedom.

The effective interaction length $\bar{X}$ for neutral hadrons was taken to be

$$\bar{X} = \bar{X}_\pi \frac{\sigma(\pi^\pm)}{\frac{1}{2}[\sigma(K^+) + \sigma(k^-)]} = 200 \text{ Cm}$$

for $K^0_L$s and

$$\bar{X} = \bar{X}_{\pi} \frac{\sigma(\pi^{+})}{\sigma(P)} = 120 \text{ Cm}$$

for neutrons using the estimated effective interaction length for charged hadrons of 164cm (see 4.3.3.1), and the measured total cross-section for $\pi^{\pm}P$ and $k^{\pm}P$ interactions [19].

The $\eta$ distribution for hadronic events is evaluated from equation (7.15). Figures 27 and 28 show the shape of $\eta$ spectra using $\bar{X}$ = 120cm and 200cm respectively. Note that for neutrinos we expect a flat $\eta$ distribution. We apply a least squares fit of the form

$$A + \beta\Phi_{\ell}(\eta) \qquad (7.17)$$

to the $\eta$ spectrum of apparent NC events, using equations (7.11) and (7.15), and from the fit one estimates the neutrino and hadronic components for different hadronic energy intervals. Table 32 summarises the neutrino and hadronic components obtained.

The ratio of hadronic events to total are given in column 4 of table 32. As can be seen from this column the backgound is highest below hadron energy 10 GeV. The background falls considerably above 10 GeV and is almost negligible above 20 GeV.

TABLE 32

The neutrino and hadronic components in the NC sample

| $E_h$ / GeV | Neutrino | $N^*$ | $N^*$/total |
|---|---|---|---|
| 5-10 | 166±38 | 30.0±41.0 | 0.15±0.21 |
| 10-20 | 175±18 | 20.0±11.0 | 0.10±0.06 |
| 20-40 | 174±14 | 5.5±3.5 | 0.03±0.02 |
| >10 | 489±29 | 25.5±11.5 | 0.05±0.02 |
| >20 | 308±18 | 5.5±3.5 | 0.02±0.01 |

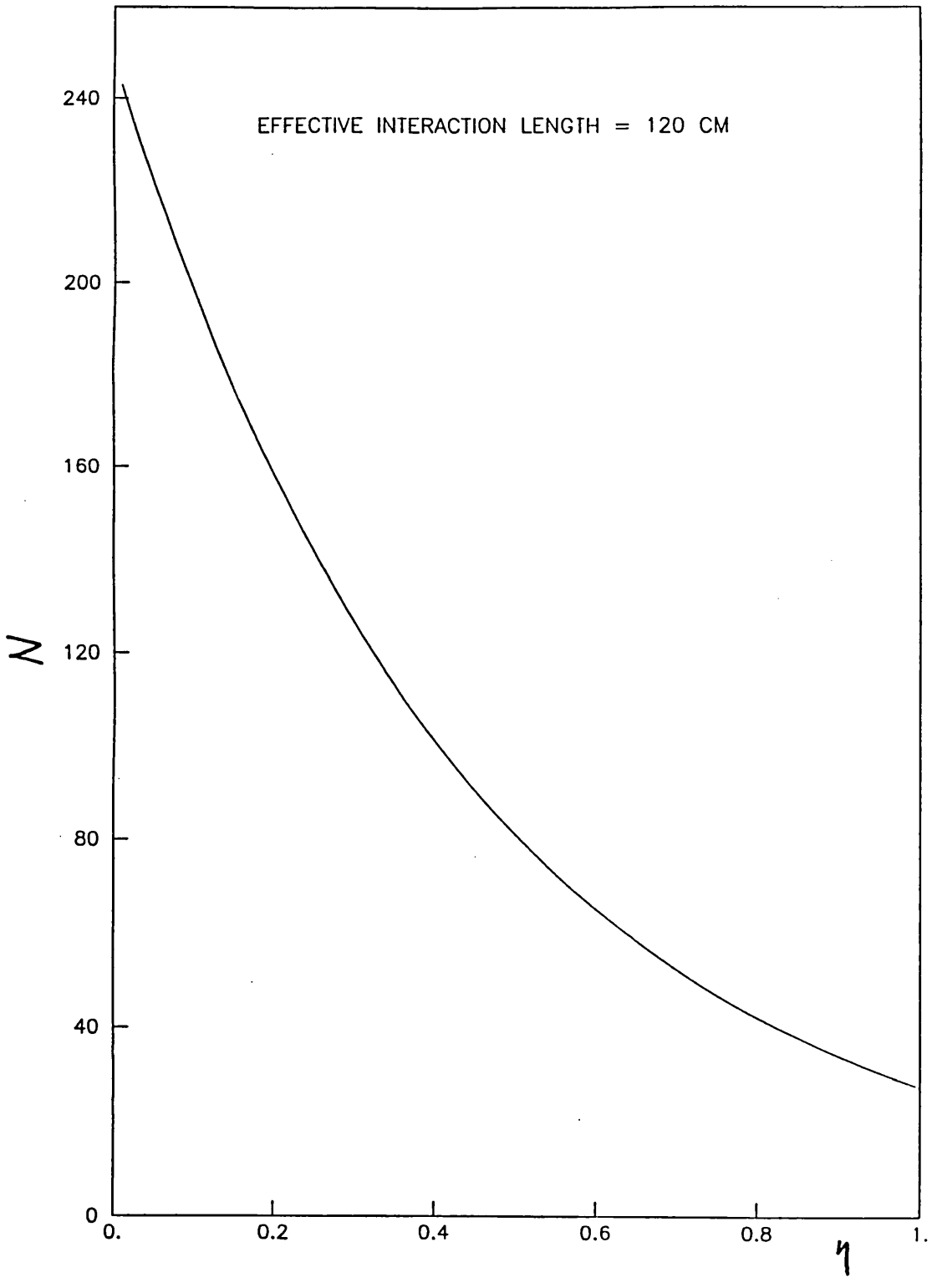



Figure 27: η distribution for hadronic events with x = 120cm

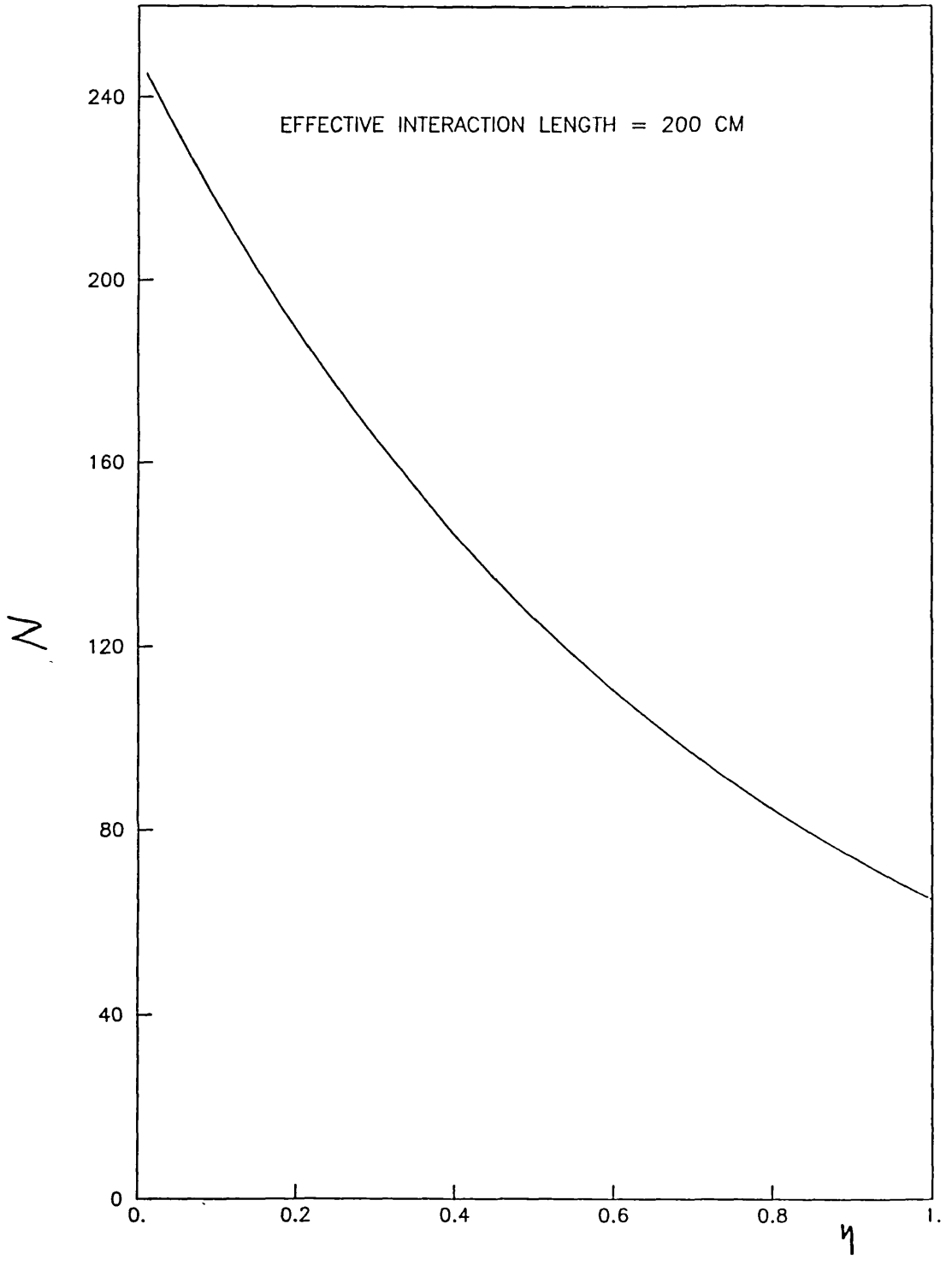



Figure 28: η distribution for hadronic events with x = 200cm

## 7.2 CORRECTION FOR MISIDENTIFIED CHARGED CURRENT EVENTS

The sample of NC candidates is contaminated by several backgrounds due to misidentified CC events. These are:

a) CC muon events with muons below 3 GeV/c;

b) CC electron events with electrons below 0.8 GeV/c;

c) CC events with muon above 3 GeV/c where the muon was not identified by the EMI-IPF system;

d) CC electron events with electrons above 0.8 GeV/c where the electron was not identified because of lack of clear signature.

In order to estimate the contamination of the NC sample due to above CC backgrounds, individual corrections described in chapter 4 and used in chapter 5 to correct the observed CC sample were applied to the NC sample for various hadronic energy cuts.

## 7.3 THE NEUTRAL CURRENT TO CHARGED CURRENT RATIOS

The uncertainties in the above mentioned corrections for hadronic backgrounds and misidentified CC events are large; they can, however, be reduced drastically using the so called transverse momentum method [32]. This method relies on the fact that in neutrino-nucleon scattering, the momenta, transverse to the neutrino direction , of both the outgoing lepton $P_T^{\ell}$ and the outgo-

ing observed hadron system $P_T^H$ are in general large and in the opposite direction as seen in fig. 29a. Any CC event, which is misidentified as NC will give an apparent $P_T^H$ which is on average small, as the lepton is included with the hadrons, and would be zero if all neutral particles were detected (fig. 29b.) In addition, because of the limited transverse momenta of hadrons relative to the direction of the hadronic shower, the transverse momentum of individual hadrons is much smaller that that of the total hadronic system. Thus, events induced by neutral hadrons inside the bubble chamber will also have small values of $P_T^H$ (fig. 29c) (note that this does not apply to those neutral hadrons entering the bubble chamber from outside). Hence, a selection of events with $P_T^H$ above a suitable value will substantially reduce the contamination of the NC candidates. By measuring a ratio of the number of NC and CC events with $P_T^H$ above a given ($P_T^{min}$) the CC background can be strongly reduced. At the same time the hadronic background is also reduced.

In figures 30, 31, 32, and 33, the raw and the corrected values of $R_{\nu N}$ where $R_{\nu N} = \sigma(NC)/\sigma(CC)$ for $\nu N$ and $\bar{\nu} N$ interactions are shown as a function of the $P_T^{min}$ cut for hadron energies $5 < E_H < 10$ GeV, $E_H > 10$ GeV and $E_H > 20$ GeV respectively. It can be seen that the corrected ratios are constant within errors as functions of the $P_T^{min}$ cut. We choose a value of $R_{\nu N}$ corresponding to a certain $P_T^{min}$ such that at this $P_T^{min}$ the

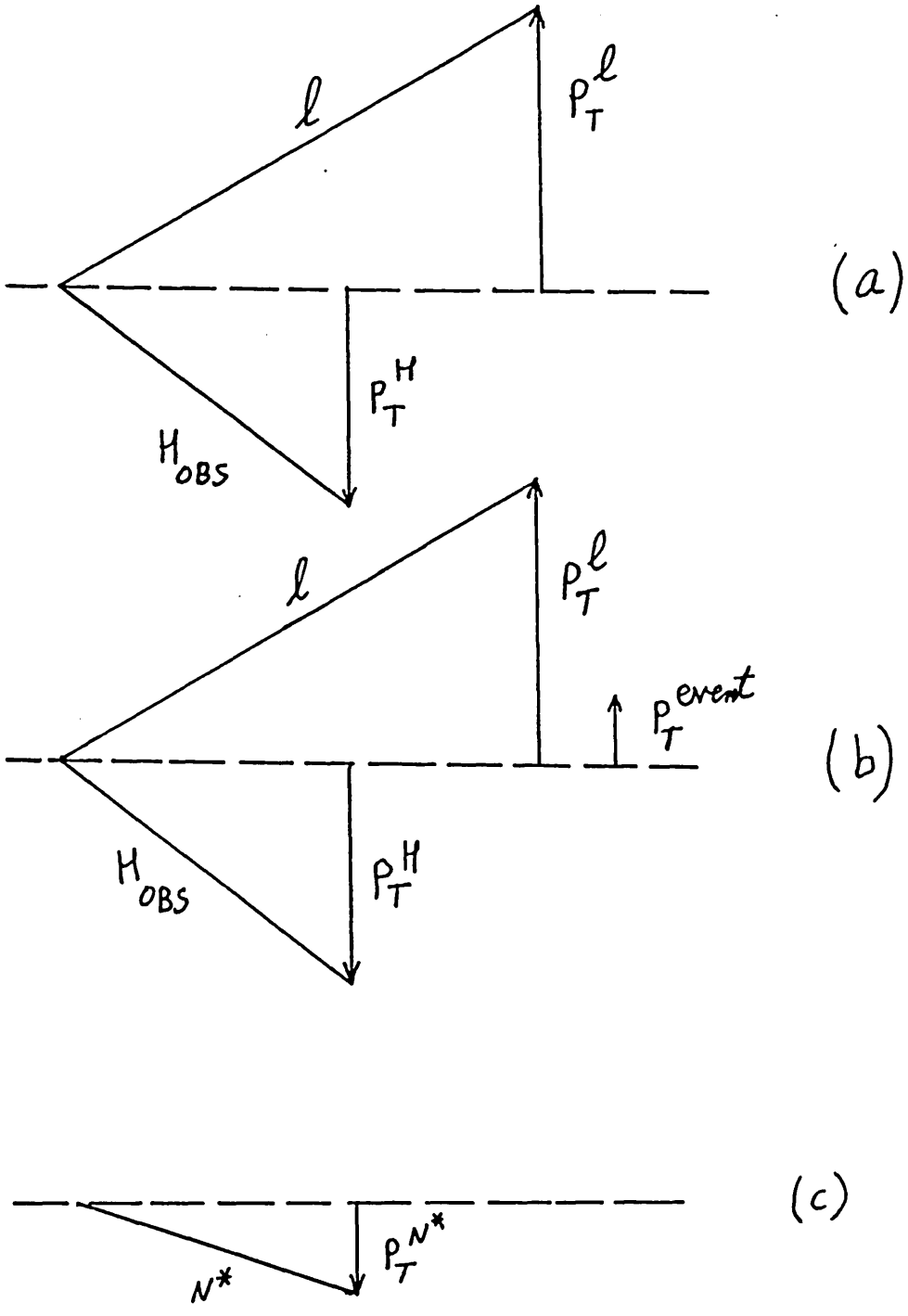



Figure 29: (a) The defintion of transverse momentum with respect to neutrino direction of lepton and the detected hadronic system in CC events, (b) the transverse momentum of all tracks, including the lepton in CC events, (c) the transverse momentum of neutral hadrons.

observed $R_{\nu N}$ flattens and a platau is observed, indicating a reduction in systematic errors. In addition any further cut above this $P_T^{min}$ will not improve the systematics whereas it will increase the statistical errors and the uncertainty on the cross-sections ratio. From these figures it can be seen that a cut-off of $P_T^{min} > 1$ GeV/c will satisfy the above criteria.

The raw event numbers and the various corrections[+] are summarised in tables 33, 34, 35, 36, 37 and 38 for all events with hadron energies between 5 and 10 GeV, for full density events > 10 GeV, for 1/3 density events > 10 GeV, for full density events between 10 and 20 GeV, for 1/3 density events between 10 and 20 GeV and for all events above 20 GeV respectively. The given errors in the corrected number of NC and CC events are statistical only. Note that because of correlation, only the overall statistical errors are quoted. The resulting values for the neutral to charged current cross-section ratios are given in table 39. The first error is statistical and the second systematic. It can be seen that the limitation is on statistics rather than systematics.

---

[+]See section 3.2 for definition of XYW events.

TABLE 33

Raw numbers and corrections for events with $5 < E_H < 10$ GeV and $P_T^{min} > 1.0$ GeV/c using full and 1/3 density data.

| Event type | CC | NC |
|---|---|---|
| Event numbers before correction | 148 | 60 |
| CC-events with $P_\ell > P_{cut}$ | 12.0 | -0.3 |
| CC-events with $P_\ell < P_{cut}$ | 24.2 | -1.5 |
| Hadron induced events | --- | -4.0 |
| Events lost due to XYW cut | 7.0 | 3.0 |
| Corrected event numbers | 191±16 | 57±10 |

TABLE 34

Raw numbers and corrections for events with $E_H > 10$ GeV and $P_T^{min} > 1.0$ GeV/c using full density data only.

| Event type | CC | NC |
|---|---|---|
| Event numbers before correction | 294 | 119 |
| CC-events with $P_\ell > P_{cut}$ | 15.9 | -6.5 |
| CC-events with $P_\ell < P_{cut}$ | 15.6 | -7.9 |
| Hadron induced events | --- | -4.1 |
| Events lost due to XYW cut | 12.2 | 5.0 |
| Corrected event numbers | 338±20 | 105±12 |

TABLE 35

Raw numbers and corrections for events with $E_H > 10$ GeV and $P_T^{min} > 1.0$ GeV/c using 1/3 density data only.

| Event type | CC | NC |
|---|---|---|
| Event numbers before correction | 314 | 137 |
| CC-events with $P_\ell > P_{cut}$ | 22.1 | -6.7 |
| CC-events with $P_\ell < P_{cut}$ | 19.1 | -12.7 |
| Hadron induced events | --- | -4.4 |
| Events lost due to XYW cut | 17.0 | 7.4 |
| Corrected event numbers | 372±22 | 121±13 |

TABLE 36

Raw numbers and corrections for events with $10 < E_H < 20$ GeV and $P_T^{min} > 1.0$ GeV/c using full density data only.

| Event type | CC | NC |
|---|---|---|
| Event numbers before correction | 76 | 41 |
| CC-events with $P_\ell > P_{cut}$ | 3.3 | -1.2 |
| CC-events with $P_\ell < P_{cut}$ | 5.9 | -2.5 |
| Hadron induced events | --- | -3.4 |
| Events lost due to XYW cut | 3.1 | 1.7 |
| Corrected event numbers | 88±10 | 35±7 |

TABLE 37

Raw numbers and corrections for events with $10 < E_H < 20$ GeV and $P_T^{min} > 1.0$ GeV/c using 1/3 density data only.

| Event type | CC | NC |
|---|---|---|
| Event numbers before correction | 111 | 45 |
| CC-events with $P_\ell > P_{cut}$ | 6.5 | -1.4 |
| CC-events with $P_\ell < P_{cut}$ | 10.4 | -5.9 |
| Hadron induced events | --- | -5.0 |
| Events lost due to XYW cut | 6.0 | 2.4 |
| Corrected event numbers | 134±13 | 35±8 |

TABLE 38

Raw numbers and corrections for events with $E_H > 20$ GeV and $P_T^{min} > 1.0$ GeV/c using full and 1/3 density data.

| Event type | CC | NC |
|---|---|---|
| Event numbers before correction | 421 | 170 |
| CC-events with $P_\ell > P_{cut}$ | 28.2 | -10.6 |
| CC-events with $P_\ell < P_{cut}$ | 18.4 | -12.4 |
| Hadron induced events | --- | -1.9 |
| Events lost due to XYW cut | 20.0 | 8.0 |
| Corrected event numbers | 488±24 | 153±14 |

TABLE 39

Summary of NC to CC ratios with $P_T^{min} > 1.0$ GeV/c

| Energy cut / GeV | Data used | $R_{\nu N} = \sigma(NC)/\sigma(CC)$ |
|---|---|---|
| $5 < E_H < 10$ | all | $0.300 \pm 0.058 \pm 0.052$ |
| $E_H > 10$ | full density | $0.312 \pm 0.039 \pm 0.017$ |
| $E_H > 10$ | 1/3 density | $0.324 \pm 0.039 \pm 0.018$ |
| $10 < E_H < 20$ | full density | $0.396 \pm 0.093 \pm 0.076$ |
| $10 < E_H < 20$ | 1/3 density | $0.260 \pm 0.060 \pm 0.053$ |
| $E_H > 20$ | all | $0.315 \pm 0.032 \pm 0.021$ |

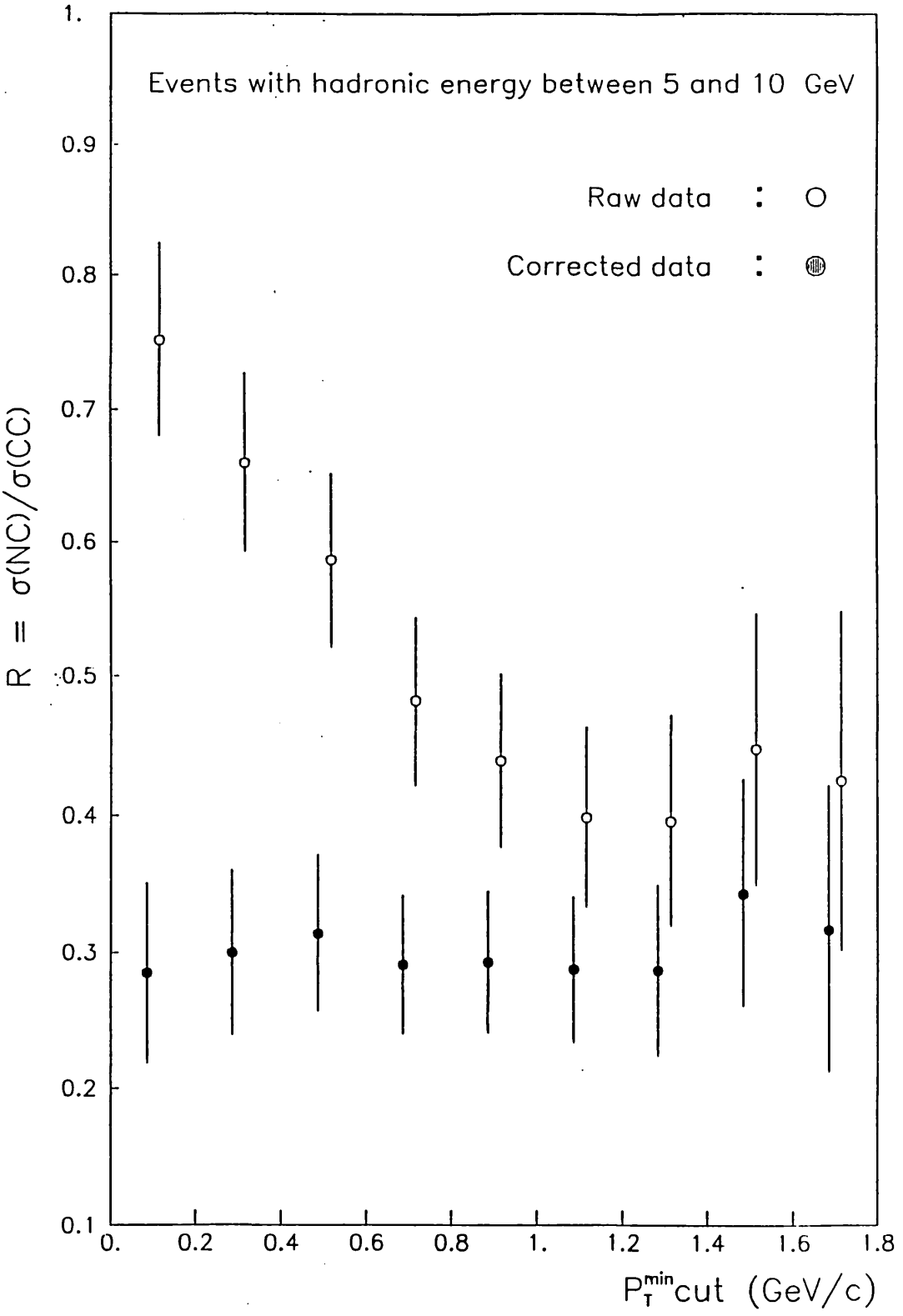



**Figure 30: NC to CC ratio as a function of $P_T^{min}$ for all events with hadronic energies between 5 and 10 GeV.**

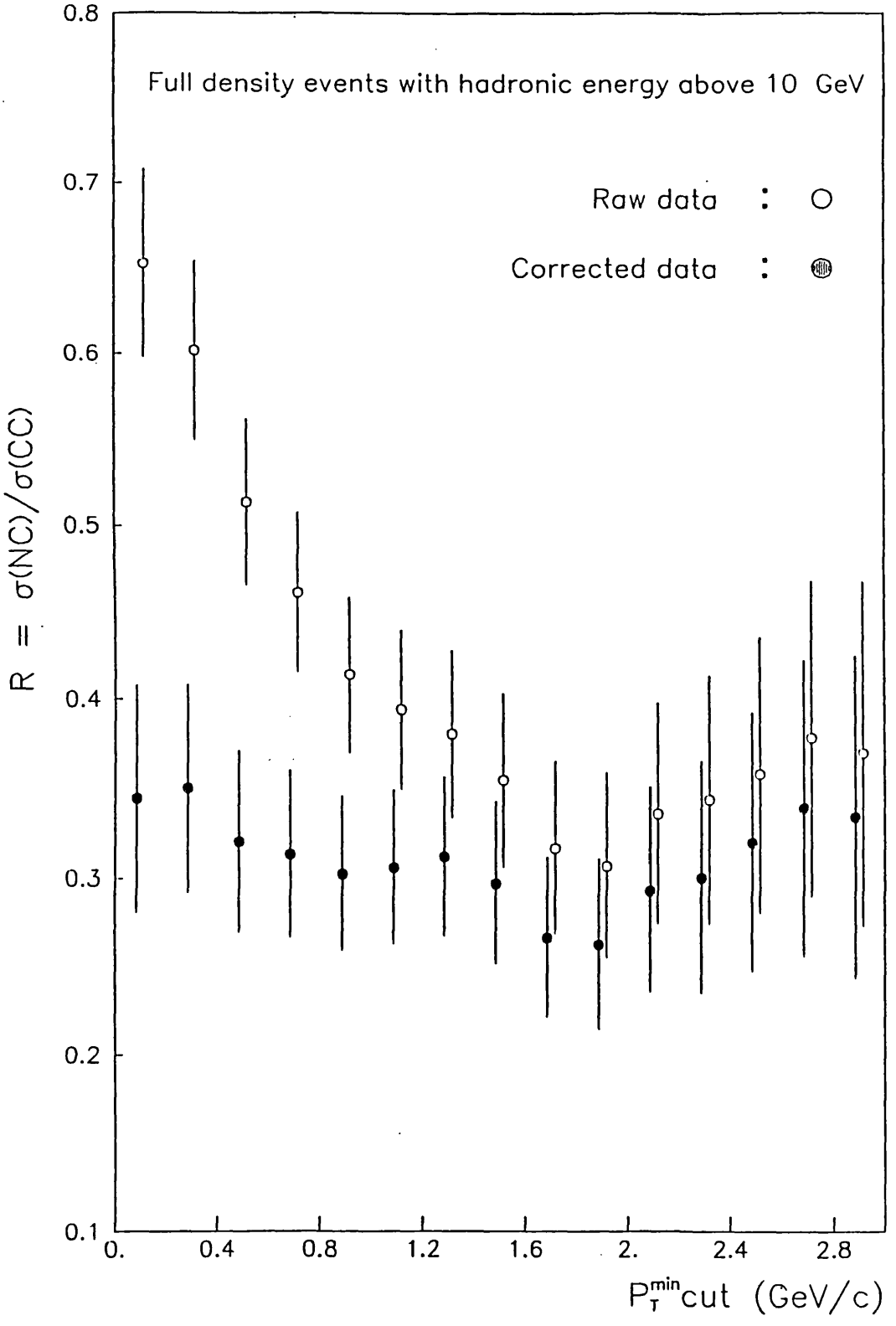



Figure 31: NC to CC ratio as a function of $P_T^{min}$ for full density events with hadronic energies above 10 GeV.

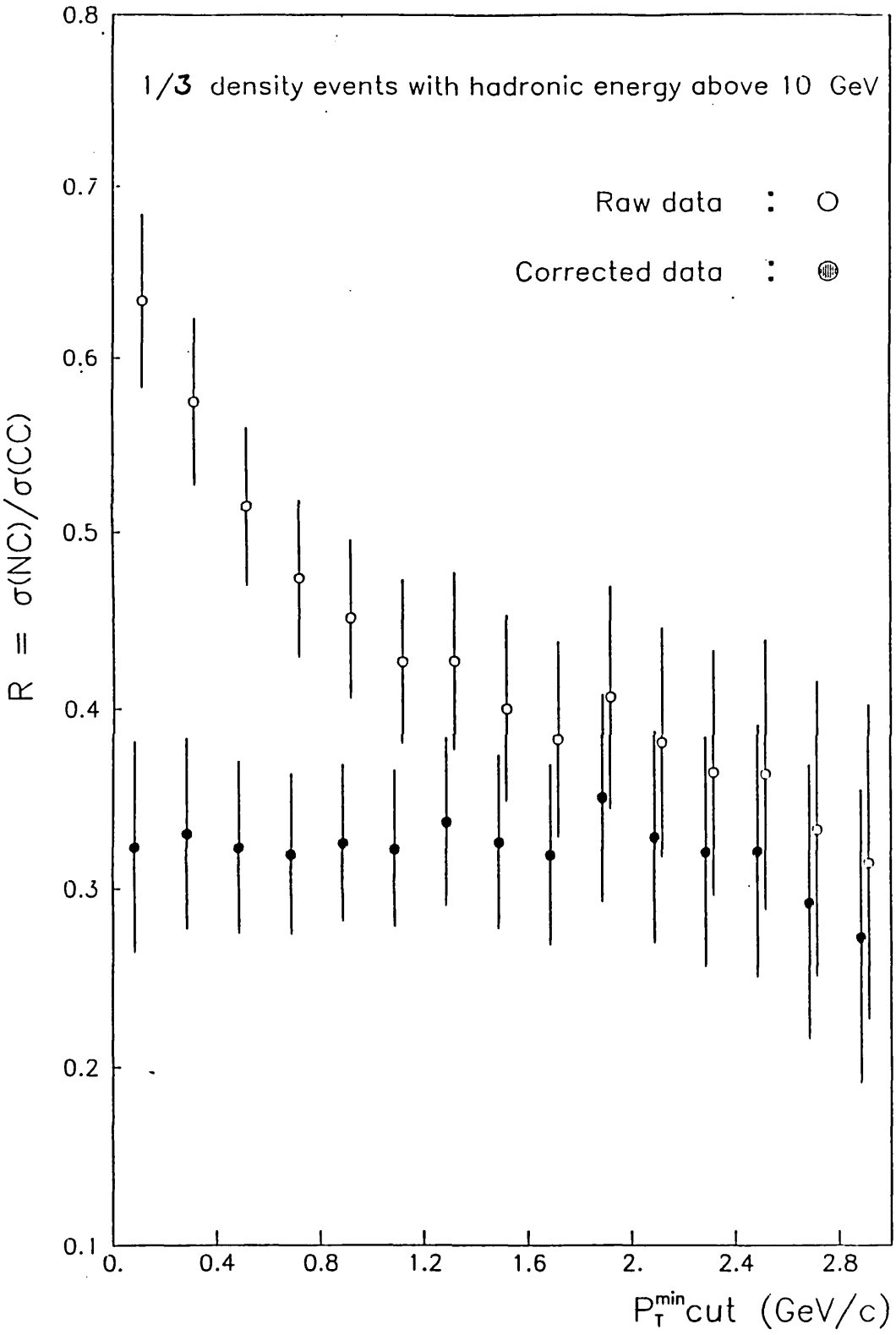



Figure 32: NC to CC ratio as a function of $P_T^{min}$ for 1/3 density events with hadronic energies above 10 GeV.

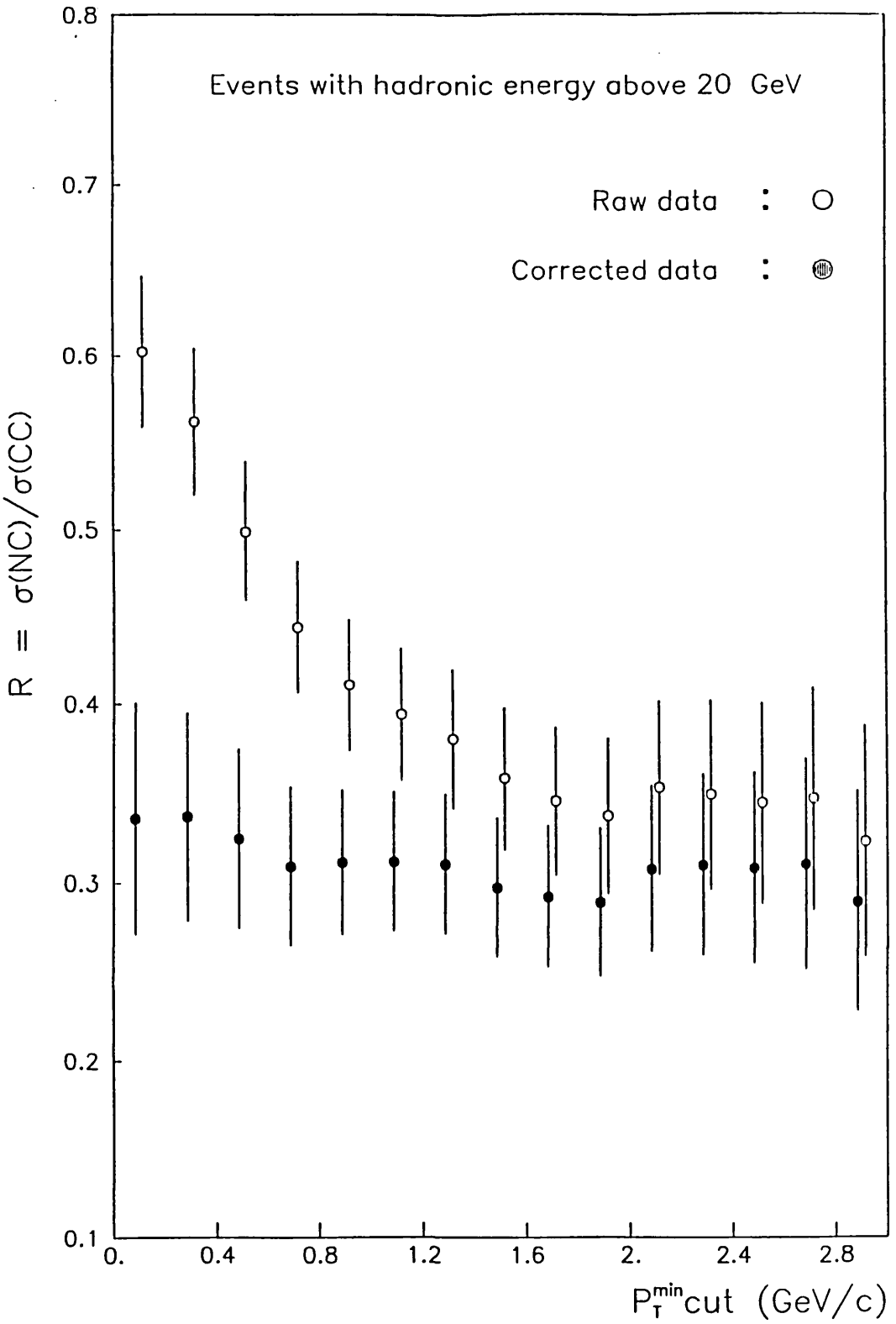



Figure 33: NC to CC ratio as a function of $P_T^{min}$ for all events with hadronic energies above 20 GeV.

### 7.3.1 NC to CC ratio for electron neutrinos

Given the considerable number of electron neutrino events in our sample and the well measured neutral current to charged current ratios for $\nu_\mu$ events, it is possible to measure the NC/CC ratio for electron neutrinos by subtracting the $\nu_\mu$ induced NC events from the total number of neutral current events and thus obtain the NC/CC for electron neutrinos. The most precise estimate of neutral current to charged current ratios for muon neutrinos are 0.301±0.007 and 0.363±0.015 for $\nu_\mu$ and $\bar{\nu}_\mu$ respectively [33] with a mean NC/CC ratio of 0.312±0.008 for our $\nu_\mu$ and $\bar{\nu}_\mu$ combined. Table 40 summarises the NC to CC ratios estimated for for $\nu_e$ induced events.

TABLE 40

NC to CC ratios for $\nu_e$ events with $P_T^{min} > 1.0$ GeV/c

| Energy cut / GeV | Data used | $R_{\nu N} = \sigma(NC)/\sigma(CC)$ |
|---|---|---|
| $E_H > 10$ | full density | 0.312 ± 0.154 ± 0.121 |
| $E_H > 10$ | 1/3 density | 0.380 ± 0.257 ± 0.140 |

The results are in good agreement with muon case, although caution should be taken since this procedure assumes that there are no contribution to the NC sample from $\nu_\tau$, gluino or other neutral induced events which have NC like interactions.

### 7.3.2 Comparison with conventional neutrino experiments

As can be seen the NC/CC ratios obtained are compatible with the observed values in normal neutrino experiments [34]. If there was a contamination of CC or NC samples due to other possible sources as mentioned above, then the obtained ratios would differ from the normal ratios.

### 7.3.3 Excess of low energy NC events

The CHARM collaboration reported an excess of 54 ± 19 (statistical) ± 9 (systematic) prompt muonless events, with shower energy in the range from 2 to 20 GeV, in excess of electron and muon neutrino interactions expected from D and $\bar{D}$ meson decay, in their 1979 data [8]. If true this excess should show up in our neutral current sample at hadron energies below 20 GeV. Taking the corrected number of CC events for hadron energy in the range 5 to 10 GeV and 10 to 20 GeV from tables 33 and 36, and using the mean ratio of NC/CC = 0.312±0.008, we estimate an excess of -3±11 NC type events for hadron energy between 5 and 10 GeV using both full and 1/3 density data[†].

[†]Because of lack of statistics, data from both full and 1/3 density runs were used for this estimate (signal to noise ratio is

Similarly for full density events between hadron energy 10 and 20 GeV, the excess corresponds to 7.5±8 NC type events. Thus from the above numbers it can be deduced that we are compatible with no excess of leptonless events between hadron energies 5 and 20 GeV.

---

three times worse in 1/3 density data). Also because of severe background in the NC sample no reliable estimate could be made for excess of NC events below 5 GeV.

## Chapter VIII

## SEARCH FOR TAU NEUTRINO INTERACTIONS

The nature of the lepton spectrum constitutes an old and still outstanding puzzle in elementary particle physics. In 1946 it was found that the particle discovered in 1937 was not the long awaited pion, but rather a new kind of lepton. Since then, one of the greatest puzzles in particle physics is, why this new lepton, called muon, exists. The generation puzzle, introduced with the discovery of the muon, remained one of the most intriguing questions of physics and we have no clue of a solution yet.

Since the muon happens to exist in nature, it is natural to ask whether there are further heavy leptons. The first experimental hint for such a new heavy lepton was the observation of an anomalously high rate of e $\mu$ events in $e^+e^-$ collisions at SPEAR by Perl and collaborators [35] in 1975.

This observation was confirmed in 1976 by the results of an independent measurement by PLUTO at DORIS [36]. A final proof that these e $\mu$ events were not due to charm decay was the observation of $\tau$ production below charm threshold at the $\psi'$ resonance by the DASP collaboration [37]. The most natural way to explain those events was to assume pair production of a new heavy lepton.

Today the existence of the $\tau$ as a new lepton is firmly established and many of its properties have been measured accurately [19,39]. All measurements agree very well with the interpretaion of the $\tau$ as a new sequential heavy lepton. In addition, there are strong experimental and theoretical reasons for supposing that there exists an associated neutrino $\nu_\tau$.

At present however, there is no experimental evidence of the interactions of tau neutrinos. On the contrary, upper limits have been set on the production of tau neutrinos and on oscillations of muon and electron neutrinos into tau neutrinos based on the absence of tau-neutrino interactions in conventional neutrino beams [38] and in beam dump experiments [4-9]. This chapter is going to give an estimate of $\nu_\tau$ production in the pesent BEBC beam dump experiment. It will present a novel and efficient kinematical method for determining the number of $\nu_\tau$ interactions and compare the results obtained from this method with other currently used methods.

## 8.1 POSSIBLE SOURCES OF TAU NEUTRINOS

It is now widely believed that the most probable source of tau neutrinos in hadron-hadron collisions is the weak decays of charmed hadrons which are heavier than the tau. Other possible sources such as direct lepton production by Drell-Yan type processes or beauty decays are expected to have negligible contributions to $\nu_\tau$ production ( see section 6.6).

The lightest possible candidate for $\nu_\tau$ production in beam dump experiments is the decay of $D_s$ mesons produced by interactions in the dump, for example:

$$P + Cu \rightarrow D_s + \bar{D}_s + X \tag{8.1}$$

followed by:

$$D_s \rightarrow \tau\nu_\tau \quad \text{and} \quad \tau \rightarrow \nu_\tau + X \tag{8.2}$$

The total cross-section for producing a $\nu_\tau$ pair is given by

$$\sigma = \sigma_{D_S} BR(D_s \rightarrow \tau\nu_\tau) \tag{8.3}$$

followed by

$$BR(D_s \rightarrow \tau\nu_\tau) = \Gamma(D_s \rightarrow \tau\nu_\tau)\tau_{D_S}$$

where $\Gamma$ is the decay rate and $\tau$ the lifetime.

The decay mode $D_s \rightarrow \tau\nu_\tau$ has not been observed but the decay rate can be predicted from the $\pi$-decay rate, assuming zero mass for the $\nu_\tau$,

$$\Gamma(D_s \rightarrow \tau\nu)/\Gamma(\pi \rightarrow \mu\nu) = (f_{D_S}/f_\pi)^2 \, (m_\tau/m_\mu)^2 \, (m_{D_S}/m_\pi) \times [\, (1-(m_\tau/m_{D_S})^2)/(1-(m_\mu/m_\pi)^2) \,]^2 \tag{8.4}$$

taking $m_{D_S} = 1970.5$ MeV [19], $m_\tau = 1784.2$ MeV [19], $\tau_{D_S} = (3.5^{+0.6}_{-0.5})\times10^{-13}$ s [39] and assuming $(f_{D_S}/f_\pi)^2 = 4$ [26] and using

$$BR(D_s \rightarrow \tau\nu)/BR(\pi \rightarrow \mu\nu) = (\tau_{D_S}/\tau_\pi) \, (\Gamma_{D_S}/\Gamma_\pi) \tag{8.5}$$

we obtain:

$$BR(D_s \rightarrow \tau\nu_\tau) = (3.9 \pm 0.7)\%. \qquad (8.6)$$

Theoretical estimates of the ratio $\sigma(PN \rightarrow D_s^+X)/\sigma(PN \rightarrow D^+X)$ vary between 0.1 and $(m_D/m_{D_s})^2$ [40]. For a $\bar{D}$ production cross-section of 17μb per nucleon [1], for example this gives a $\bar{D}_s$ production cross-section estimates between 1.7-15 μb.

## 8.2 SIMULATION OF THE EXPECTED TAU NEUTRINO FLUX

In order to estimate the $\nu_\tau$ interaction in BEBC, to study the acceptance of our detector for these neutrinos, and the energy distribution of $\nu_\tau$ flux using different production parameters, a Monte Carlo program simulating $D_s$ production in the target with subsequent $D_s$ decay into $\tau\nu_\tau$ and $\tau \rightarrow \nu_\tau + X$ was developed. From Eq. (8.2) it can be seen that the $\nu_\tau$ production due to $D_s$ decay is a two stage process. The first $\nu_\tau$ is produced directly in the $D_s$ decay and another one from the subsequent $\tau$ decay. We thereafter refer to these two neutrinos as primary and secondary neutrinos respectively.

The production of the $D_s$ meson was assumed to be described by the phenomenological differential cross-section:

$$d^3\sigma/d^3p \sim (1 - |x|)^n e^{-2p_t} \qquad (8.7)$$

where p, x and $p_t$ are the momentum, Feynman x and transverse momentum of the $D_s$ meson respectively. In order to study the

effect of various production assumptions on $\nu_\tau$ flux, the parameter n was varied according to recent estimates of charm production in hadron-hadron collisions (see later). The cross-section for $D_s^+$ and $D_s^-$ was assumed to be identical. The decay of $D_s \to \tau\nu_\tau$ is isotropic. The branching ratios for $\tau$ decays were taken from measurements [19], the values used were:

$$\tau^- \to e^-\bar{\nu}_e\nu_\tau \qquad 17.4\% \qquad (8.8)$$

$$\tau^- \to \mu^-\bar{\nu}_\mu\nu_\tau \qquad 17.6\% \qquad (8.9)$$

$$\tau^- \to \pi^-\nu_\tau \qquad 10.8\% \qquad (8.10)$$

$$\tau^- \to \rho^-\nu_\tau \qquad 23.7\% \qquad (8.11)$$

$$\tau^- \to \pi^+\pi^-\pi^-\nu_\tau \qquad 8.1\% \qquad (8.12)$$

$$\tau^- \to \pi^+\pi^-\pi^-\pi^0\nu_\tau \qquad 5.3\% \qquad (8.13)$$

$$\tau^- \to \pi^-\pi^0\pi^0\nu_\tau \qquad 11.0\% \qquad (8.14)$$

$$\tau^- \to \pi^-\pi^0\pi^0\pi^0\nu_\tau \qquad 6.1\% \qquad (8.15)$$

The decay of $\tau^- \to K^-\nu_\tau$ (0.67±0.17)% [19] was approximated by (8.11). The non resonant decay of $\tau^- \to \pi^-\pi^0\nu_\tau$ (0.3±0.3)% and the decay $\tau^- \to K^-\pi^0\nu_\tau$ (1.0±0.3)% [19] were added to (8.11). The decay of $\tau^- \to \pi^-\rho^0\nu_\tau$ ( 5.4±1.7)% [19] was added to (8.14).

The expected angular distributions for $\tau \to \nu_\tau + X$ are given below assuming zero mass for $\nu_\tau$.

### 8.2.1 The decay of $\tau^- \rightarrow e^-\bar{\nu}_e\nu_\tau$

The purely leptonic decays of $\tau$ can be estimated from the decay of $\mu^- \rightarrow e^-\bar{\nu}_e\nu_\mu$. The energy and angular distribution of the electron from an arbitrarily polarized $\tau^-$ is given in the rest frame of $\tau$ as [41]:

$$d^2\Gamma = (G^2M^5_\tau/3x2^7\pi^4)[3-2x - (\vec{W}.\hat{p}_e)(2x-1)]x^2dxd\Omega_e \quad (8.16)$$

where 'G' is the Fermi Coupling Constant, 'x' is $E/E_{max}$ of the electron with $E_{max}$ =1/2 $M_\tau$, '$\vec{W}$' is the polarization vector of the tau and $\hat{P}_e$ is the unit vector along the direction of the electron. $d\Omega_e$ is the element of the solid angle given by $d\Omega = d\cos\theta d\psi$, where $\theta$ is the angle between the tau polarization vector and the electron momentum ($\vec{W}.\hat{p}_e = \cos\theta$) and $\psi$ is the azimuthal angle. Note that the mass of the electron is ignored in (8.16). The polarization dependent term $\vec{W}.\hat{p}_e$ is due to the parity non conservation. The decay of $\tau^+ \rightarrow e^+\nu_e\bar{\nu}_\tau$ can be obtained from (8.16) by changing the sign in front of ($\vec{W}.\hat{p}_e$) term.

### 8.2.2 The decay of $\tau^- \rightarrow \mu^-\bar{\nu}_\mu\nu_\tau$

When the mass of the muon is not ignored, the energy-angle distribution of the muon can be written as [41]:

$$d^2\Gamma = (G^2M^5_\tau/3x2^7\pi^4)(8/M^4_\tau)(p^2)[\,3M_\tau - 4E - 2M^2_\mu/E + 3M^2_\mu/M_\tau - (\vec{W}.\hat{p}_\mu)(p/E)(4E - M_\tau - 3M^2_\mu/M_\tau)\,]dpd\Omega_\mu \quad (8.17)$$

where p and E are the momentum and energy of the muon respectively, and $\hat{p}_\mu$ is the unit vector along the direction of the muon. Again the $\tau^+$ decay can be obtained by changing the sign in front of $(\vec{W}.\hat{p}_\mu)$ term.

### 8.2.3 The decay of $\tau^- \to \pi^- \nu_\tau$

This decay mode can be calculated from the knowledge of $\pi^- \to \mu^- \nu_\mu$. The Feynman diagrams for the two decays are shown in figure 34. Lepton universality implies that W coupling to $\mu\nu_\mu$, $e\nu_e$, and $\tau\nu_\tau$ have the same strength g given by $g^2/M^2_W = G/\sqrt{2}$. The coupling constant between W and $\pi$ is given by $gf_\pi \cos\theta_c$, where $\theta_c$ is the Cabbibo angle. The angular distribution of $\pi^-$ from the decay of a polarised $\tau^-$ can be computed from the Feynman diagram of fig. 34 [41].

$$d\Gamma = (G^2 f^2_\pi \cos^2\theta_c/16\pi) M^3_\tau (1 - M^2_\pi/M^2_\tau)^2 x \\ (1 - \vec{W}.\hat{p}_\pi)/4\pi \, d\Omega_\pi \qquad (8.18)$$

where $\hat{p}_\pi$ is the unit vector in the direction of the pion. We notice that the energy dependent terms are missing because in the two body decay the energy of each particle is fixed in the rest frame of $\tau$: $E_\pi = (M^2_\tau + M^2_\pi)/2M_\tau$ and $E_\nu = (M^2_\tau - M^2_\pi)/2M_\tau$. Again the invariance under CP implies that the angular distribution of $\tau^+ \to \pi^+ \bar{\nu}_\tau$ can be obtained from that of $\tau^- \to \pi^- \nu_\tau$ by changing the sign of $\vec{W}$.

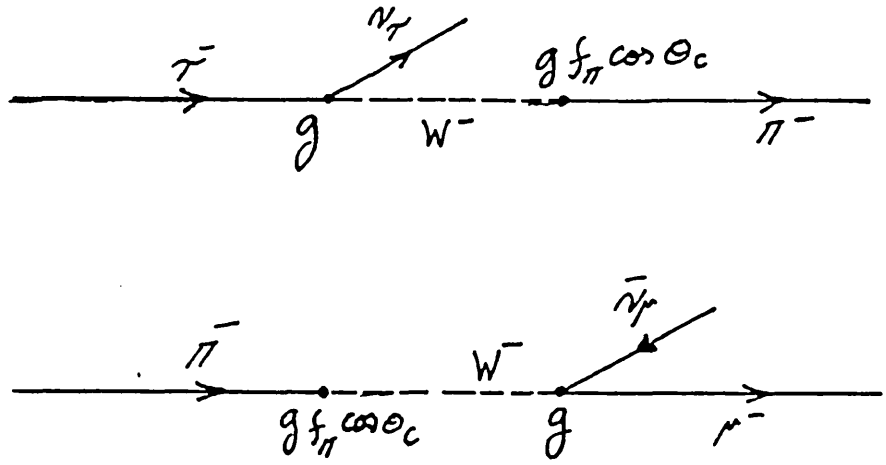



Figure 34: The Feynman diagram for decay of $\tau^- \to \pi^- \nu_\tau$

### 8.2.4 The decay of $\tau^- \to \rho^- \nu_\tau$

The interest in this decay is its high branching ratio of 21.8% plus a contribution of 0.3% from $\tau^- \to \pi^-\pi^0(\text{non-res.})\nu_\tau$ decay. The angular distribution for this decay is complicated by the vector structure of the $\rho$ meson. Two different amplitudes, with $\rho$'s of helicity 0 and -1 contribute. The $\rho$ angular distribution following Tsai calculation [41] is carried out in [42]. The $\rho$ angular distribution becomes

$$d\Gamma \sim (1 - \alpha \cos\theta)d\cos\theta \qquad (8.19)$$

where $\alpha$ is:

$$\alpha = (M^2_\tau - 2M^2_\rho)/(M^2_\tau + 2M^2_\rho) \approx 0.46 \qquad (8.20)$$

The angular distribution of $\tau^+ \rightarrow \rho^+ \bar{\nu}_\tau$ can be obtained by changing the sign in front of $\alpha$.

### 8.2.5 Multipion final states

The angular distribution for the multi-pion states were approximated using the $\tau^- \rightarrow a_1 \nu_\tau$ ($a_1$ previously called $A_1$) decay mode. The angular distribution for this decay mode is given in [42] with $\alpha \simeq 0.14$ in (8.19). The multi-body final states for decay modes (8.12), (8.13), (8.14) and (8.15) were generated using the 'CERN program library' multi-body phase space generator 'GENBOD' [43], assuming zero mass for $\nu_\tau$.

### 8.2.6 The energy distribution of tau neutrino flux

The values of n in the phenomenological differential cross-section for $D_s$ production (8.7) was chosen according to estimates of charm production from this experiment [1]. Assuming a symmetric $D\bar{D}$ production only and using faraway prompt muons (see section 6.4), we obtain values of n = 4.4±1.0 for D and 5.3±0.5 for $\bar{D}$. This calculation assumes for the distribution of the centre of mass momentum of the neutrino in D decay the one measured for electrons in [44]. If the distribution is taken to be harder as in the free quark model [45], larger n values (5.2±1.0 and 6.3±0.5 respectively) are obtained. Given the above assumptions a value of n = 5.7 was chosen. The effect of varying this choice on the $\nu_\tau$ flux spectra was taken into account by reducing the above value by 2 units to n = 3.7.

The calculated energy spectra of the neutrinos reaching BEBC are shown in figure 35 for both values of n; each curve is normalised to correspond to one $\nu$ per produced $D_s$. The $\nu_\tau$ from $D_s$ decay has a much softer spectrum ($< E_\nu > = 13$ GeV for $n = 5.7$ and $< E_\nu > = 17$ GeV for $n = 3.7$) than the $\nu_\tau$ from $\tau$ decay ($< E_\nu > = 45$ GeV for $n = 5.7$ and $< E_\nu > = 58$ GeV for $n = 3.7$). As a result, most tau neutrinos interacting in BEBC would come from $\tau$ decays.

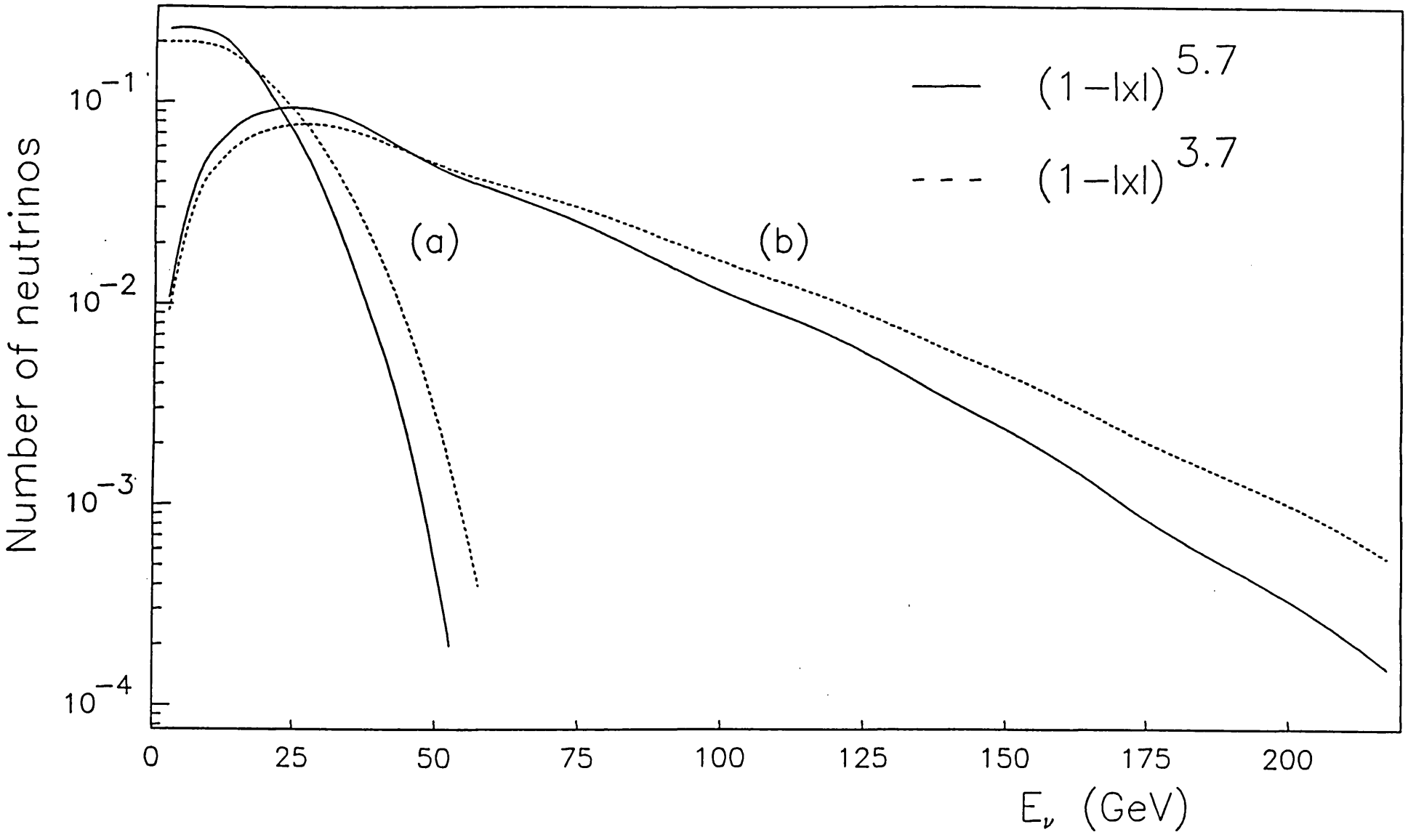



Figure 35: The energy distributions of neutrinos traversing BEBC from (a) $D_s \rightarrow \tau + \nu_\tau$ and (b) $\tau \rightarrow \nu_\tau + X$ decay.

## 8.3 THE TAU NEUTRINO CHARGED CURRENT CROSS-SECTION SUPPRESSION

The $\nu_\tau$ charged current interaction cross-section takes a more complicated form than that of $\nu_\mu$, because the heavier mass of the tau implies threshold effects. These are:

i) the accessible range of x and y is limited;

ii) the neutrino-quark cross-section is reduced by

$$P(E_\nu, x) = (s - m_\tau^2)^2 / s^2 \qquad (8.21)$$

where $\sqrt{s}$ is the invariant mass of the $\nu_\tau q$ system i.e. $s \simeq 2xME_\nu$ with M being the nucleon mass;

iii) the sensitivity of the cross-section to the neutrino production structure functions depends on the final state lepton mass.

A detailed calculation of i) and iii) is given in [46]. here, only the relevant formulae are quoted and applied to the special case of $\nu_\tau N \rightarrow \tau + X$.

The kinematical bounds for a CC tau neutrino interactions are given by:

$$m^2/2M(E_\nu - m) \leq x \leq 1, \qquad (8.22)$$

and

$$A - B \leq y \leq A + B, \qquad (8.23)$$

where:

$$A = \tfrac{1}{2}(1 - m^2/2ME_\nu x - m^2/2E_\nu{}^2) \;/\; (1 + xM/2E_\nu)$$

$$B = \tfrac{1}{2}[\; (1 - m^2/2ME_\nu x)^2 - (m/E_\nu)^2 \;]^{1/2} \;/\; (1 + xM/2E_\nu)$$

Within these limits, the differential cross-section for $\nu_\tau$ interaction is given by:

$$\begin{aligned} d^2\sigma^\nu/dxdy = P(E_\nu,x)(G^2ME/\pi)\{ &( xy + m^2/2ME )yF_1(x) \\ &+ [\; (1 - y) - (Mxy/2E + m^2/4E^2) \;]F_2(x) \\ &+ [\; xy(1 - y/2) - m^2y/4ME \;]F_3(x) \\ &+ (m/M)^2[\; (Mxy/2E + m^2/4E^2)F_4(x) - (M/2E)F_5(x) \;] \;\} \end{aligned} \quad (8.24)$$

where m is the tau mass, $E_\nu$ is the energy of the neutrino and $F_i(x)$ refer to neutrino production structure functions. The $\bar{\nu}_\tau$ cross-section is obtained by changing sign in front of $F_3(x)$. Comparing (8.24) with the differential cross-section for $\nu_\mu$ interaction (4.17), it can be noticed the addition of two structure functions $F_4(x)$ and $F_5(x)$ because of heavier mass of the $\tau$ compared to muon. The equation (8.24) can be simplified by using the Callan-Gross relation $2xF_1(x) = F_2(x)$ (4.18), and the positivity conditions further restrictiong $F_4(x)$ and $F_5(x)$ to [46]:

$$xF_5(x) = F_2(x) \text{ and } F_4(x) = 0 \quad (8.25)$$

The x dependence of the structure functions was parametrized by [19]:

$$\begin{aligned} F_2(x) &= 3.9x^{0.55}(1 - x)^{3.2} + 1.1(1 - x)^8 \text{ and} \\ xF_3(x) &= 3.6x^{0.55}(1 - x)^{3.2} \end{aligned} \quad (8.26)$$

It can be observed from relations (8.22) and (8.23) that the kinematical suppresion of the cross-sction becomes less important at high energies allowing more kinematical regions for $\nu_\tau$ interaction.

The phase space suppresion of $\nu_\tau$ relative to $\nu_\mu$:

$$S_{ps} = \frac{\sigma(\nu_\tau, \text{total})}{\sigma(\nu_\mu, \text{in the scaling region})}$$

can be calculated by integration of (4.17) and (8.24), and evaluating the cross-sections ratio as a function of $E_\nu$, taking into account the kinematical regions available for $\nu_\tau$ for a given neutrino energy. Figure 36 shows the $S_{ps}$ for both neutrinos and antineutrinos as a function of $E_\nu$. As can be seen the suppresion is highest at low energies, decreasing with increasing $\nu_\tau$ energy and approaching a platau at high energies.

Using our $\nu_\tau$ flux spectra from fig 35, we obtain for tau neutrinos:

$$< S_{ps} > = 0.53 \text{ for } n = 5.7 \qquad (8.27)$$

$$< S_{ps} > = 0.57 \text{ for } n = 3.7 \qquad (8.28)$$

and for tau antineutrinos:

$$< S_{ps} > = 0.64 \text{ for } n = 5.7 \qquad (8.29)$$

$$< S_{ps} > = 0.67 \text{ for } n = 3.7 \qquad (8.30)$$

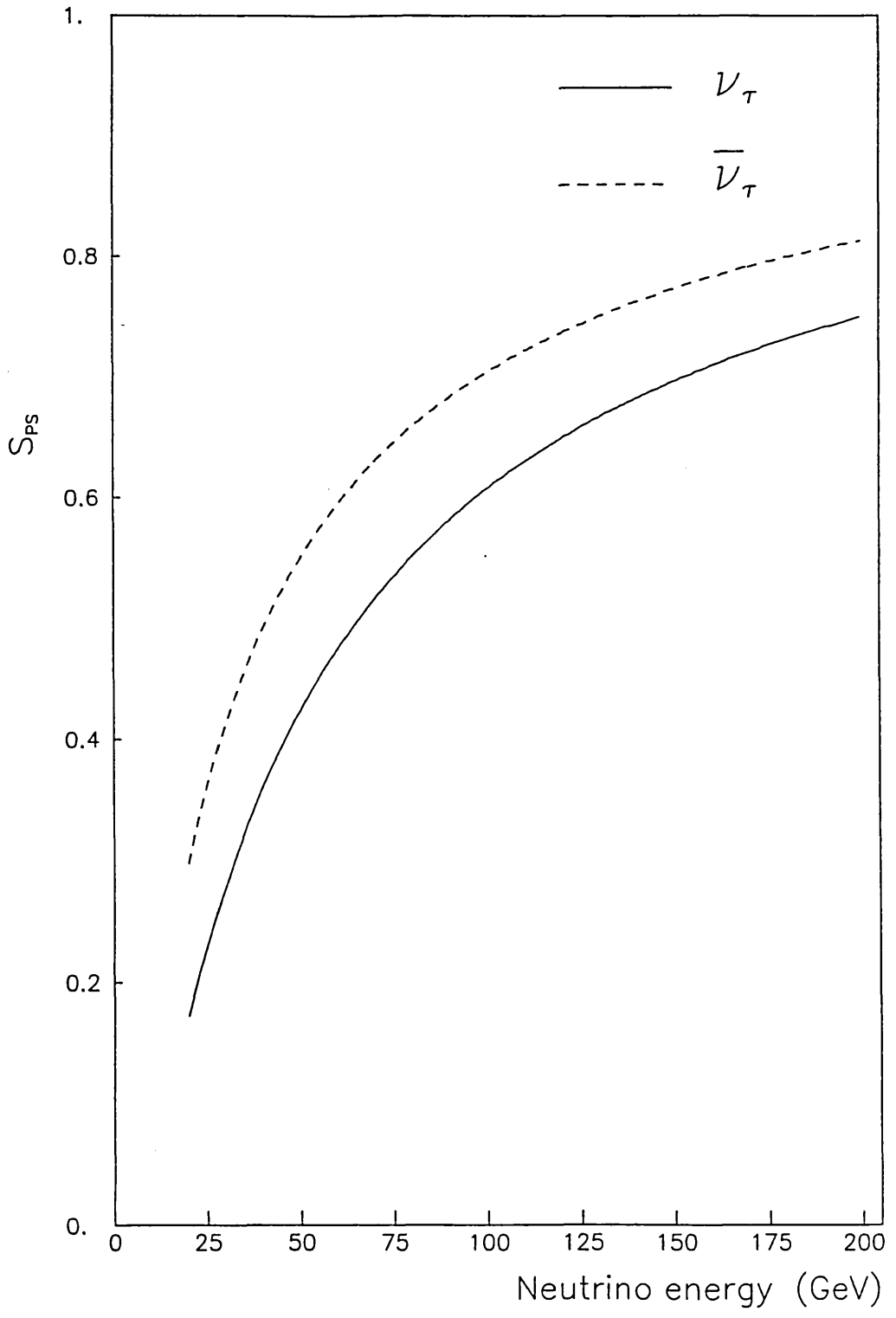



Figure 36: The tau neutrino phase space suppresion relative to muon neutrino as a function of neutrino energy.

## 8.4 SIMULATION OF $\nu_\tau$ INTERACTIONS IN BEBC

Assuming lepton universality, the $\nu_\tau$ like $\nu_\mu$ and $\nu_e$ is expected to have both CC and NC type interactions given by:

$$\nu_\tau + N \rightarrow \tau + X \tag{8.31}$$

$$\nu_\tau + N \rightarrow \nu_\tau + X \tag{8.32}$$

The measured CC muon events were used in order to simulate $\nu_\tau$ interactions in BEBC in detail:

a) weights were applied to correct the $\nu_\mu$ spectrum to the simulated $\nu_\tau$ spectrum as seen in figure 35;

b) in each event the muon was replaced by a tau. There were two possibilities: either we could take a tau 4 vector with the same energy as the muon (this does not conserve momentum) or we could choose the same 3 momentum and allow for energy non-conservation to order $m_\tau/\sqrt{s}$. Given a high event energy expected for $\nu_\tau$, either choice did not significantly change the result. So the choice was made in favour of momentum conservation bearing in mind that one was generally relying on the kinematical properties of the tau decay products in order to isolate $\nu_\tau$ interactions. The energy was calculated using the tau mass;

c) the kinematical parameters x and y of the event were required to be within the limits given by (8.22) and (8.23);

d) for a given $E_\nu$, x and y, the probability of $\nu_\tau$ relative to $\nu_\mu$ event was calculated using (8.24) and (4.17);

e) the tau decay was simulated in just the same way as described in the previous section on the $\nu_\tau$ flux using the branching ratios given in (8.8)-(8.15). In order to get sufficient statistics each measured $\mu^-$ and $\mu^+$ event was processed 50 times. To account for equal fluxes of $\nu_\mu$ and $\bar{\nu}_\mu$, the $\mu^-$ and $\mu^+$ events were weighted accordingly, using the corrected number of CC events (table 9) and the measured $\bar{\nu}_\mu$ to $\nu_\mu$ cross-section ratio [21].

## 8.5 SIMULATION OF THE TAU DECAY PRODUCTS

The simulation of the tau decays included $\rho^- \rightarrow \pi^-\pi^0$ and $\pi^0 \rightarrow \gamma\gamma$ decays in (8.11)-(8.15). In order to incorporate our experimental resolution and detection efficiencies, the products from tau decays were subject to the following procedure:

i) the interaction probabilities for charged pions were calculated from the knowledge of the decay position of the tau, and the pion's total path in the chamber, taking into account the energy loss and multiple scattering (see the track following procedure in 4.3.3);

ii) our experimental resolutions on the momenta of charged hadrons and photons were taken into account by studying the distribution of errors on the momenta of measured tracks from the data, as shown in figure 14. In

order to account for possible dependency of measurements errors on the momenta of tracks, the measured tracks were divided in momentum groups 0-5, 5-10, 10-20, 20-40 and > 40 GeV/c, and the fractional error ($\Delta p/p$) distributions were plotted. Tables 41 and 42 give $\langle \Delta p/p \rangle$ for charged hadrons and photons respectively. The fractional errors for simulated tracks from tau decay were obtained by generating a random number ($R_D$) according to the distribution of $\Delta p/p$ plots, depending on the momentum of the track. The actual (smeared) momentum was obtained from:

$$\alpha = R_D \times R_G \tag{8.33}$$

$$p' = (1 + \alpha)p \tag{8.34}$$

where $R_G$ in (8.33) was a random number from a normal distribution with zero mean and unit variance. The charged tracks from simulated tau decays were rejected if $\Delta p/p > 30\%$. The photons were rejected if $\Delta p/p > 100\%$;

iii) during the data analysis stage it was found that the most poorly measured tracks, namely associated neutral stars, all interacting or kinking tracks of length below 10cm and all charged interacting tracks whose momenta were obtained from the measurements of their secondaries (the so called synthesised tracks) were introducing

large errors to some of the kinematical parameters used to isolate tau neutrino interactions. These tracks were excluded in the analysis stage. Table 41 shows the percentage of the charged hadrons which were lost in each momentum interval. In order to be consistent, the corresponding fraction of pions were lost from simulated tau decays;

iv) because of the finite volume of the bubble chamber, the position of the vertex and the momentum, some of the photons from $\pi^0$ decays escaped detection. The photon detection efficiency for the type of target used in this experiment was estimated to be between 50 and 80% [47]. For this reason a value of 65% for photon detection efficiency was assumed. This amounted to a loss of 35% of the photons from simulated tau decay products.

TABLE 41

<Δp/p> and percentage of charged hadrons lost due to interaction, using measured hadrons in the data.

| Momentum (GeV/c) | <Δp/p> (%) | % lost |
|---|---|---|
| 0 - 5 | 4.8±0.2 | 11.2 |
| 5 - 10 | 5.8±0.5 | 7.9 |
| 10 - 20 | 5.8±0.7 | 8.1 |
| 20 - 40 | 7.4±1.3 | 10.2 |
| > 40 | 11.9±2.6 | 10.0 |

TABLE 42

<Δp/p> for measured photons in the data sample

| Momentum (GeV/c) | <Δp/p> (%) |
|---|---|
| 0 - 5 | 17.0±0.2 |
| 5 - 10 | 22.9±0.7 |
| 10 - 20 | 25.2±1.2 |
| 20 - 40 | 34.5±3.4 |
| > 40 | 36.5±6.0 |

## 8.6 SIMULATION OF THE EXPECTED BACKGROUND DISTRIBUTIONS

Backgrounds to the tau decay arise from the conventional muon and electron CC events for purely leptonic decays of the tau (8.8)-(8.9); and from genuine NC, unidentified CC and neutral hadron induced events to the semileptonic decay modes of the tau (8.10)-(8.15). Because of the nature of analysis used in searching for a tau signal (see later) we will only describe the simulation of the expected background for semileptonic decay modes of the tau.

The NC background was simulated by ignoring the muon in CC events, together with any good inner bremsstrahling candidates, i.e. any photons collinear with the muon within ±30 mr in both dip and azimuth [48]. The CC background was simulated by treating the muon as unidentified. In order to simulate the two backgrounds in the right proportion, appropriate weights were assigned to each sample. these weights were calculated from the number of unidentified CC events, estimated from the muon and electron identification inefficiencies, and from the corresponding number of genuine NC events using all events with $E_H > 20$ GeV as given in table 43. The appropriate weight for each sample is given in table 45. From table 43, it can be seen that the estimated number of neutral hadron events above $E_H > 20$ GeV in the observed full density NC sample is very small, and in any case the secondary hadron showers from such events will be adequately approximated by the NC hadron showers.

TABLE 43

The contribution to the NC sample from the background of unidentified CC events and neutral hadron interactions for events with $E_H$ > 20 GeV using full and 1/3 density data.

| |
|---|
| Contribution from unidentified CC events in all = 123.3±5.8 |
| Contribution from $N^*$ events to full density data = 2.7±1.8 |
| Contribution from $N^*$ events to 1/3 density data = 2.8±1.7 |
| Corrected NC events in full density data = 98.5±13.4 |
| Corrected NC events in 1/3 density data = 97.3±14.2 |
| Corrected CC events in full density data = 298.6±18.6 |
| Corrected CC events in 1/3 density data = 294.8±19.1 |

## 8.7 SEARCH FOR A TAU NEUTRINO SIGNAL

Various methods have been suggested and used in order to isolate $\nu_\tau$ interactions from a large background of conventional neutrino events. They range from direct observation of tau decays using high resolution techniques to statistical methods such as multivariate discriminant analysis [50]. A review of these methods is given in [25].

Because of the nature of the tau decay two distinct decay search possibilities are available. These are:

a) search for $\nu_\tau$ signal using tau leptonic decay modes;

b) search for $\nu_\tau$ signal using tau semileptonic decay modes.

The leptonic decay modes rely on the usually large missing transverse momentum in the final state due to two missing neutrinos. The semileptonic decay modes contribute more events in a smaller background. These events have the appearance of NC events (i.e. they contain no identified μ or e), unless there is a detectable distance between the τ production and decay vertices. However the energy and transverse momentum carried off by the final state neutrino are much less in the $\nu_\tau$ events.

Most of these methods were tried in the early stages of the analysis. Given our limited statistics and the resolution of the bubble chamber, majority of the methods were found not to be sensitive enough to a $\nu_\tau$ signal. Henceforth, we have developed a simple and efficient kinematical method in order to determine the number of $\nu_\tau$ CC interactions with semileptonic τ decays in a full sample of NC candidates. This sample contains genuine NC events, unidentified CC events and neutral hadron interactions. This method has been published in [51]. The method used will be described and the results obtained will be presented. A comparison will be made with other currently used techniques.

This analysis uses kinematical selection criteria and a maximum likelihood fit in order to separate the tau neutrino charged current interactions with subsequent semileptonic decay of the tau (8.10)-(8.15) from the large background of geniune NC and unidentified CC events. The criteria are designed to detect the semileptonic decay modes of the tau and rely on the transverse

momentum of hadrons from tau decay having larger than usual transverse momenta relative to the normal hadron (quark) jet. We apply this kinematical technique to find $\tau$ decays among the observed NC events from the run with the full density dump[†].

Tau neutrino events resulting in semileptonic decays will have no primary muons or electrons. The combination of charged particles from $\tau$ decay will have net charge $\pm 1$, invariant mass less than tau mass and usually a substantial fraction of the total energy of the event. The transverse momentum (relative to the incident neutrino direction) of the secondaries from $\tau$ decay will often be large and in the opposite direction to the transverse momentum of hadrons from the hadronic shower. In addition we exploit the fact the distribution of the transverse momentum of one hadron calculated with respect to the vector sum of other hadron momenta from the same source is limited. In contrast the secondaries from $\tau$ decay have a large transverse momentum relative to the neutrino direction ($P_T$) and, by conservation of transverse momentum, have an even larger transverse momentum relative to the final state hadron vector ($P^t$). These definitions are shown in figure 37.

In detail, the full procedure was the following:

1. The NC candidates were required to have a corrected hadron energy $E_H$ above 20 GeV; this cut removes nearly all of the neutral hadron interactions.

---

[†]Given that the signal to noise ratio is three times worse in 1/3 density data only full density neutral current events were used.

2. For each retained event the total final state hadron momentum vector $\vec{P}_H$ was constructed by summing the momentum vectors of all accepted tracks as defined in the previous section. Leptons in unidentified CC events may simulate hadrons from tau decay by virtue of their large transverse momenta. Therefore the leaving track (if any) with the largest transverse momentum with respect to $\vec{P}_H$ was also excluded from the sum; in addition, any photon collinear within ±30 mr in dip and ±100 mr in azimuth was also excluded [48] (to remove photons due to inner or outer bremsstrahling from unidentified leptons).
3. Of the remaining charged particles (now presumably all hadrons), the one with the largest momentum component $P^t_1$ transverse to $\vec{P}_H$ was selected first. Then the one with the largest momentum component $P^t_2$ transverse to $\vec{P}_H - \vec{P}_1$ was selected. Then the photon with the largest momentum component $P^t_3$ transverse to $\vec{P}_H - \vec{P}_1 - \vec{P}_2$ was selected. If the required particle was absent, the corresponding $P^t_i$ value was set to zero.
4. The distribution of $P^t_1$, $P^t_2$ and $P^t_3$ were plotted and fitted to the sum of the $P^t_i$ distributions expected from tau decay and from background.

The selections $P^t_1$ and $P^t_2$ allow the detection of charged pions from the tau decay specially for the decay modes where more than a single charged pion is expected. $P^t_3$ is used to de-

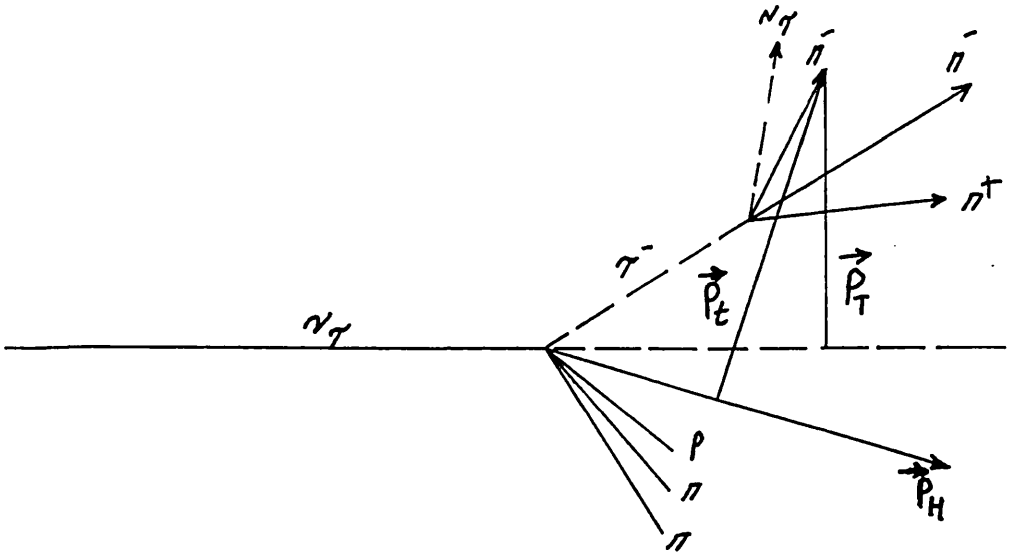



Figure 37: The definition of kinematical parameters in tau decay

tect neutral pions from the tau decay. Thus this prescription is almost equally sensitive to all of semileptonic tau decay modes. Subtracting the $\vec{P}_i$ from $\vec{P}_H$ was done to avoid correlations between the $P^t_i$ values.

Figure 38 shows the corrected visible energy distribution of $\nu_\tau$ events for tau semileptonic decay modes. The visible energy $E_{vis}$ does not account for the unseen final state tau neutrino which takes away a fraction of the total energy of the event. Because of 20 GeV cut on the NC events, only CC muon events with $E_\nu > 20$ GeV were used to simulate tau semileptonic decay modes. It can be seen from this figure that because of the energy carried away by the $\nu_\tau$ from the $\tau$ decay, a fraction of charged current $\nu_\tau$ events are lost below 20 GeV cut. This loss amounted to 12.4% of $\nu_\tau$ charged current events with subsequent semileptonic decay of the tau, or an acceptance of 87.6% for these events.

The secondary neutrino carried away an average energy of 16 GeV. Excluding events lost below 20 GeV, the mean visible energy expected from all semileptonic tau decay modes is $\langle E_{vis} \rangle$ = 60 GeV. Table 44 gives the mean momenta $\langle P_1 \rangle$, $\langle P_2 \rangle$ and $\langle P_3 \rangle$ for the observed NC, simulated tau decay and simulated background events.

TABLE 44

The mean momentum distribution in GeV/c of $P_1$, $P_2$ and $P_3$ tracks for the observed NC, simulated tau decay and simulated background events.

| Event type | $\langle P_1 \rangle$ | $\langle P_2 \rangle$ | $\langle P_3 \rangle$ |
|---|---|---|---|
| Observed NC | 5.1 | 3.7 | 3.0 |
| Simulated tau decay | 9.6 | 5.1 | 5.7 |
| background | 5.3 | 4.4 | 3.1 |

## TABLE 45

**The Mean $P_1^t$ Values and Weights of the Simulated $\nu_\tau$ Events, the Simulated Background Events and the Observed Event Sample**

| Event Type | Weight | $P_1^t$ (GeV/c) (first charged particle) | $P_2^t$ (GeV/c) (second charged particle) | $P_3^t$ (GeV/c) (photon) |
|---|---|---|---|---|
| $\tau^\pm \to \pi^\pm \nu_\tau$ | 0.108 | 0.911 | 0.393 | 0.218 |
| $\tau^\pm \to \rho^\pm \nu_\tau$ | 0.237 | 0.798 | 0.412 | 0.444 |
| $\tau^\pm \to \pi^\pm \pi^0 \pi^0 \nu_\tau$ | 0.110 | 0.788 | 0.431 | 0.534 |
| $\tau^\pm \to \pi^\pm \pi^0 \pi^0 \pi^0 \nu_\tau$ | 0.061 | 0.749 | 0.421 | 0.519 |
| $\tau^\pm \to \pi^\pm \pi^+ \pi^- \nu_\tau$ | 0.081 | 1.038 | 0.647 | 0.250 |
| $\tau^\pm \to \pi^\pm \pi^+ \pi^- \pi^0 \nu_\tau$ | 0.053 | 0.909 | 0.566 | 0.385 |
| all simulated $\nu_\tau$ events | 0.650 | 0.850 | 0.459 | 0.403 |
| simulated NC | 0.62± 0.03 | 0.518±0.014 | 0.343± 0.010 | 0.267±0.013 |
| simulated unidentified CC | 0.38± 0.03 | 0.486±0.010 | 0.304± 0.007 | 0.205±0.007 |
| all simulated background | 1.00 | 0.506±0.011 | 0.329± 0.008 | 0.244±0.010 |
| observed NC candidates | | 0.507±0.020 | 0.325± 0.015 | 0.227±0.016 |

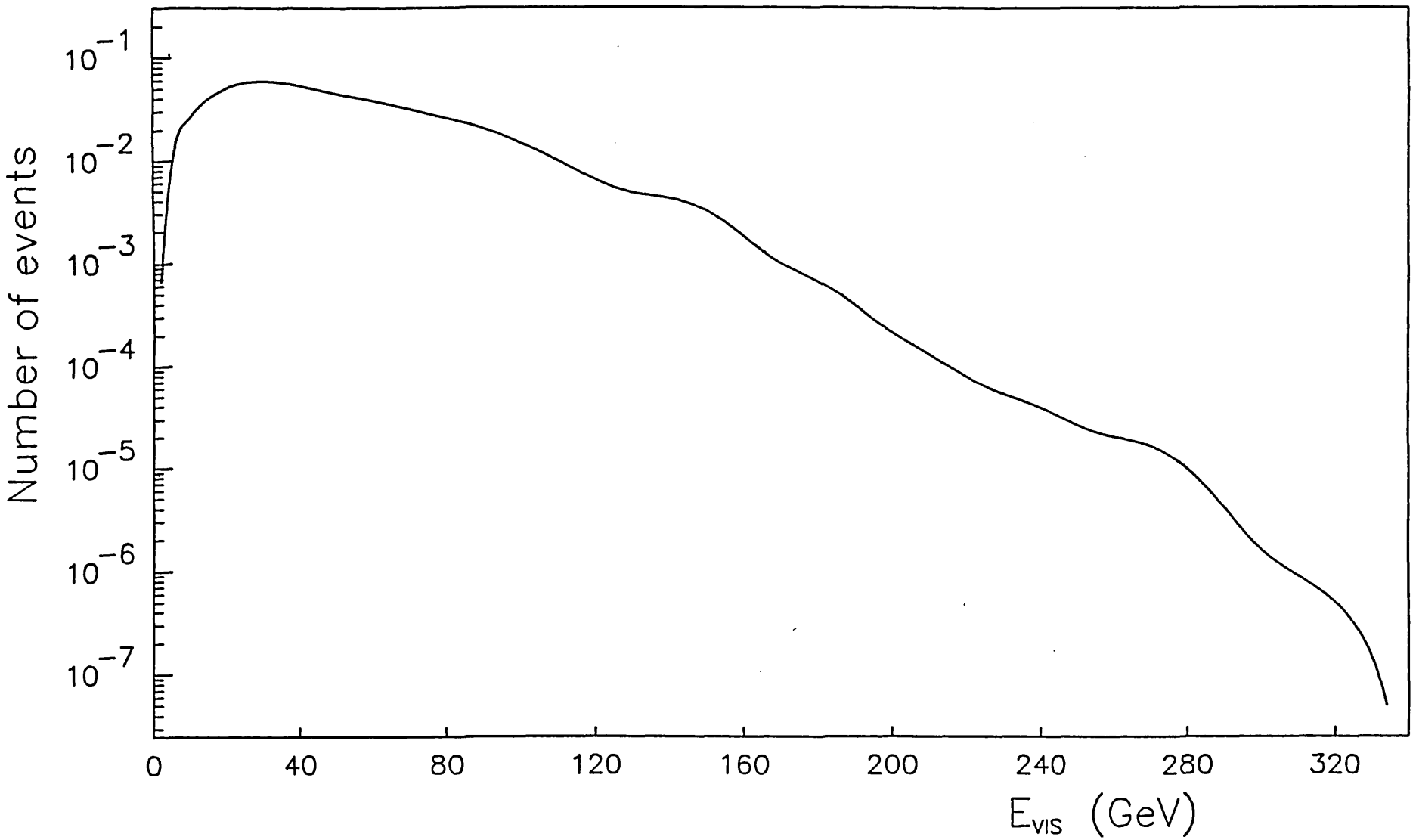



Figure 38: The expected visible energy distribution of $\nu_\tau$ events with subsequent semileptonic decays of the tau.

## 8.8 EXPERIMENTAL DISTRIBUTIONS

Figure 39 shows the $P^t_i$ distributions for the observed NC, simulated tau decay and simulated background events. The mean values of $P^t_1$, $P^t_2$ and $P^t_3$ for the simulated tau decay (individual decay modes) and the expected background from NC and unidentified CC events are given in table 45. As can be seen from figure 39 and table 45, The $P^t_{1,2,3}$ distribution of the simulated NC and unidentified CC background events are very similar because the unidentified muon was indeed usually excluded from the initially constructed $\vec{P}_H$. Consequently the results given below are insensitive to the assigned weights for the background simulation. Because of the way the $\vec{P}_i$ vectors were defined it was found to be unnecessary to simulate separately the unidentified CC events with leptons below the momentum cuts (this was investigated by comparing the $P^t_i$ values from different runs using selected muon momentum intervals. The mean $P^t_i$ values were found to be insensitive to the muon momentum). It can be seen from table 45 that the mean $P^t_i$ values for the background events are considerably lower than the corresponding values for tau decay events.

## 8.9 RESULTS

To determine the relative proportion of tau decay and background events in the observed NC sample, the distributions of $P^t_1$, $P^t_2$ and $P^t_3$ for the observed NC sample (the data points in Fig.39), were fitted as sums of the corresponding tau decay distributions (full lines) and background distributions (dashed lines) using the maximum likelihood method. Because of the limited statistics in the background distributions, only one bin was used for $P^t_1 > 1$ GeV/c, one for $P^t_2 > 0.8$ GeV/c and one for $P^t_3 > 0.6$ GeV/c.

The fraction of the observed NC sample that is due to tau neutrino CC events with subsequent semileptonic decay of the tau was thus estimated to be

$$\alpha = (-5.9 \pm 4.9)\% \qquad (8.35)$$

The $\alpha$ values obtained from the $P^t_1$, $P^t_2$ and $P^t_3$ distributions separately were (-6.2±6.4)%, (-2.9±12.4)% and (-7.7±9.9)% respectively.

There being 138† events with corrected hadron energy above 20 GeV in this NC sample, Eq. (8.35) corresponds to -8±7 such events. In order to account for purely leptonic CC $\nu_\tau$ events one needs to take into account the individual branching ratios, the suppression of $\nu_\tau$ cross-section, the antineutrino to neutrino

---

†There were initially 141 NC candidates. Three were found to be wrongly identified and subsequently excluded from the NC sample as explained below.

and the $\nu_\tau$ NC to CC cross-section ratios. The branching ratios and the $\nu_\tau$ cross-section suppresion are given in (8.8)-(8.15) and (8.27)-(8.30) respectively. The $\nu_\tau$ NC to CC ratio above a given total energy was estimated from a Monte Carlo calculation based upon the observed event spectra and Buras Gaemers structure function parametrisation [13]. the ratios obtained were:

$$\begin{aligned} R &= 0.174 \qquad \text{neutrinos} \\ R &= 0.117 \qquad \text{antineutrinos} \end{aligned} \tag{8.36}$$

The weight associated with each decay mode was calculated from:

$$f_i = W_i/\Sigma W_i$$

where $W_i$ was defined to be

$$W_i = BR \times S_{ps} \times r$$

for $\nu_\tau$ CC events, where BR is the corresponding branching ratio for the ith decay mode, $S_{ps}$ is the $\nu_\tau$ cross-section suppresion and the factor r was set to 1 and 0.49 [21] for neutrino and antineutrino events respectively. For $\nu_\tau$ NC events the W becomes:

$$W = R \times r$$

where there is no phase space suppresion for $\nu_\tau$ NC interactions. Table 46 summarises the weight factors associated with $\nu_\tau$ interactions

TABLE 46

The weight factors ($f_i$) associated with $\nu_\tau$ CC and NC interactions.

| Decay product | neutrino | antineutrino |
|---|---|---|
| $\nu_\tau N \rightarrow \tau \rightarrow e + X$ | 0.080 | 0.047 |
| $\nu_\tau N \rightarrow \tau \rightarrow \mu + X$ | 0.091 | 0.053 |
| $\nu_\tau N \rightarrow \tau \rightarrow$ hadrons $+ X$ | 0.326 | 0.190 |
| $\nu_\tau N \rightarrow \nu_\tau + X$ | 0.161 | 0.053 |

Including (a) 12.4% of the $\nu_\tau$ events lost below 20 GeV cut and (b) charged current $\nu_\tau$ events with purely leptonic $\tau$ decay from table 46, the number of $\nu_\tau$ charged current interaction with $E_\nu > 20$ GeV becomes:

$$N_\tau^{CC} = -14 \pm 12 < 17 \text{ at } 90\% \text{ c.l.} \qquad (8.37)$$

The error quoted includes the statistical errors of the simulations due to the finite number of CC muon events available. The upper limit quoted takes into account that $\alpha$ and $N_\tau^{CC}$ cannot have been negative, the 90% c.l. upper limit $C_{90}$ on $\alpha$ being defined from

$$\int_0^{C_{90}} L(\alpha)d\alpha = 0.90 \int_0^{\infty} L(\alpha)d\alpha \qquad (8.38)$$

where $L(\alpha)$ is the likelihood function that was maximised. The result is insensitive to the n value used in the production formula for $D_s$ mesons as given in Eq. (8.7). Changing n from 5.7 to 3.7 changed $\alpha$ only to $(-5.4\pm4.5)\%$.

The events giving at least one high $P^t_i$ are the most likely $\nu_\tau$ candidates. In order to check for any $\tau$ signal all events with $P^t_1 > 0.8$ GeV/c or $P^t_2 > 0.8$ GeV/c or $P^t_3 > 0.6$ GeV/c were selected. These amounted to 18 candidates. All their photographs were therefore carefully re-examined. None showed evidence of the presence of separate tau production and tau decay vertices [47,48,49]. Two events (985/2899 and 992/4982) were found to be $\nu_e$ CC events wrongly identified as NC candidates with the brems assosiated with the electron tracks giving high $P^t_3$ values. These two events were subsequently excluded from the NC sample. Another event (964/4164) was found to have a leaving track labelled as interacting on the DST, consequently failing the leaving track rejection criteria as described in section 8.7. This event was also excluded from the NC sample resulting in the selected number of NC candidates being 138 rather than 141.

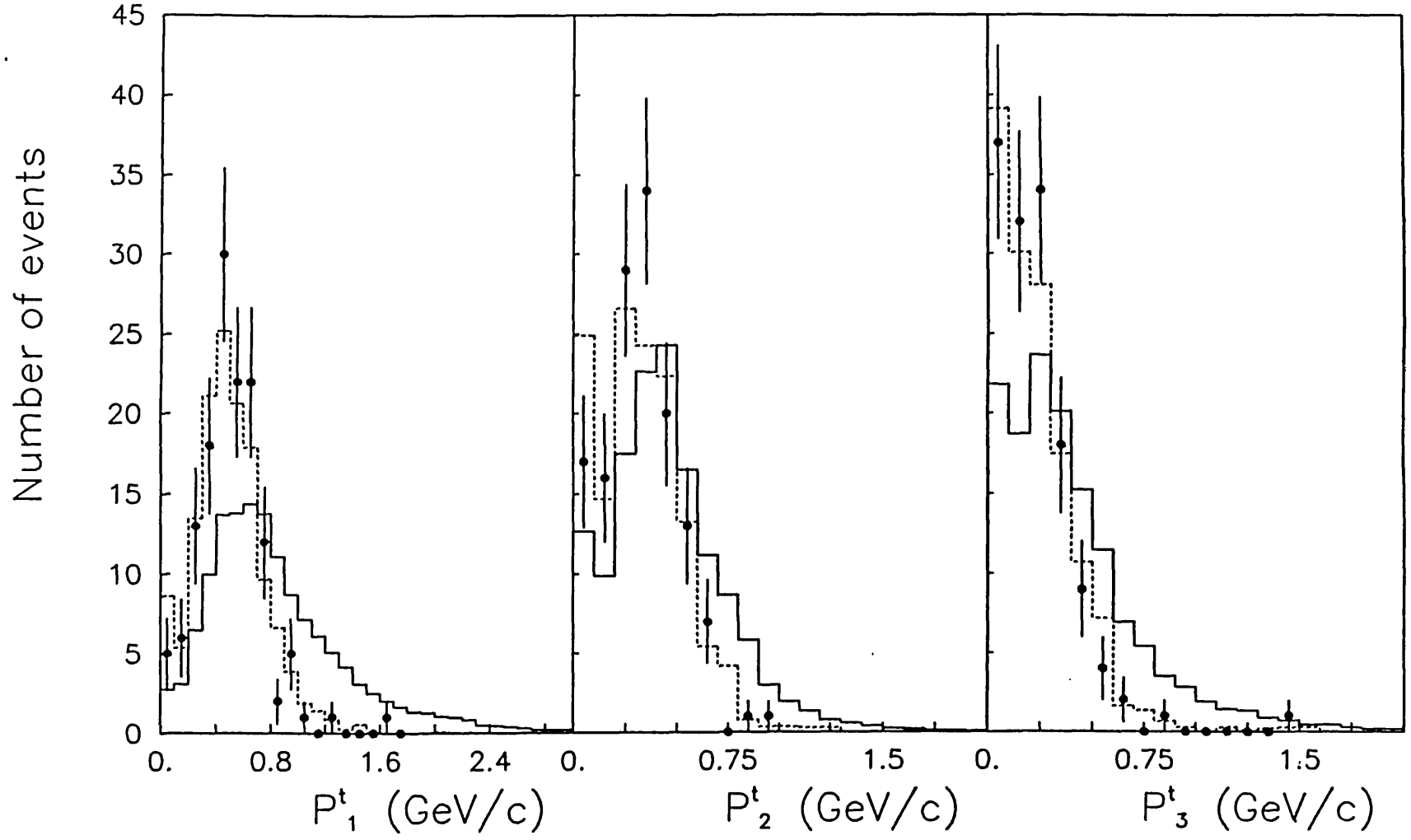



Figure 39: $P^t_i$ distribution for NC candidates (data points), simulated tau decay events (full lines) and simulated background events (dashed lines).

### 8.9.1 Comparison with other methods

As explained in section 2.4, BEBC was equipped with a high resolution camera of spatial resolution ~ 200μm. About 10% of the observed events were within the reduced volume seen by this camera and could therefore be examined for tau decays or kinks very close to the event vertex. No clear τ track connecting distinct production and decay vertices was seen among this sub sample. This would give an upper limit of 23 CC $\nu_\tau$ events (90% c.l.) if the detection efficiency for τ decays were 100%. In reality, for 200μm resolution and a lifetime of $3.3\times10^{-13}$ s [19] corresponding to a decay length of 0.056mm/GeV, the efficiency is below 10% and the upper limit in excess of 230 events.

The kinematic method of Ballagh et al [38] looks for $\tau \rightarrow 3\pi^{\pm} + X$ semileptonic decays, amounting to 13.4% of all τ decays (table 45), with an efficiency of 31% in their experiment falling to 28% in ours because of softer $\nu_\tau$ spectrum. Seeing no candidate would therefore have given an upper limit of 61 events: in fact there was 1 candidate (event 976/321 in the full density sample), giving an upper limit of 102 events at 90% c.l.

The method of Poppe [52] uses the scaling variable $\xi = P_t^2/P_\ell$, where $P_t$ and $P_\ell$ are the total transverse and longitudinal momenta of the observed hadron system. The idea of the

method relies on the fact that the transverse momentum of an event is affected in a different way than the longitudinal momentum, if we replace a neutral current event by a charged current $\nu_\tau$ interaction of identical total energy and 4 momentum transfer with semileptonic decay of the $\tau$ (fig. 40). Since, in a plane normal to the incident neutrino direction, the hadron shower from the tau decay points approximately opposite to the fragments from the primary neutrino nucleon interaction, the overall transverse momentum becomes smaller, while, simultaneously, the longitudinal momentum increases. To apply this method to our NC event sample, the $\xi$ distributions expected for the tau signal and the background were simulated as before, and the $\xi$ plots for the observed sample (the data points) were fitted as sums of the corresponding tau decay distributions (full curves) and background distributions ( dashed curves) as shown in figure 41, using a maximum likelihood fit. The result was

$$\alpha = (25.5 \pm 21)\% \tag{8.39}$$

Correcting as for Eq. (8.35), this corresponds to

$$N_\tau^{CC} = 61 \pm 50 \tag{8.40}$$

Since most $\nu_\tau$ interactions (65%) appear as NC candidates, the apparent NC/CC ratio, after correcting for unidentified CC electron and CC muon events and neutral hadron interactions, measures the $\nu_\tau$ rate if the true NC/CC ratio is assumed to be the

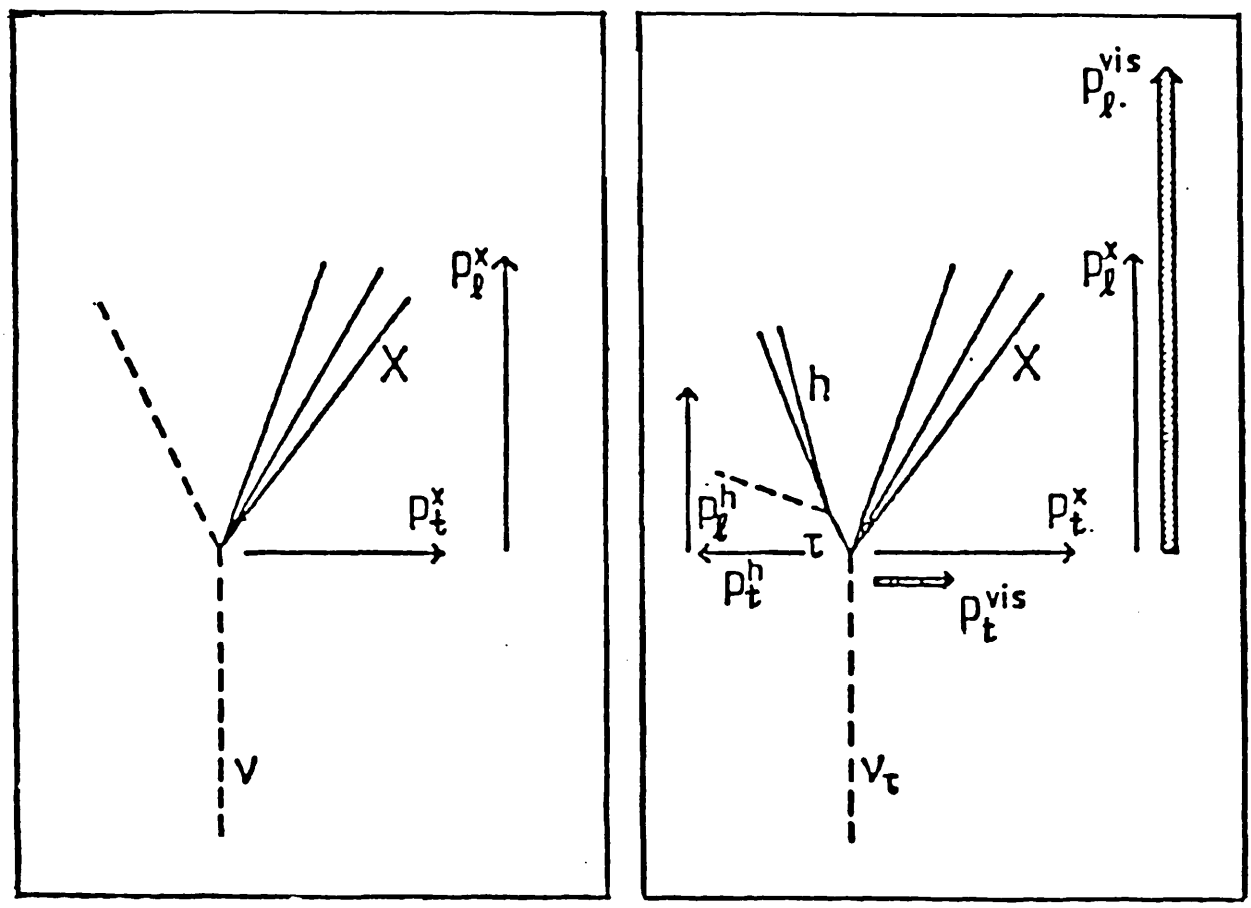



Figure 40: Comparison of true and fake neutral currents of similar neutrino energy and 4 momentum transfer. As fake neutral current produces smaller $p_t$, but larger $p_\ell$ than a geniune neutral current.

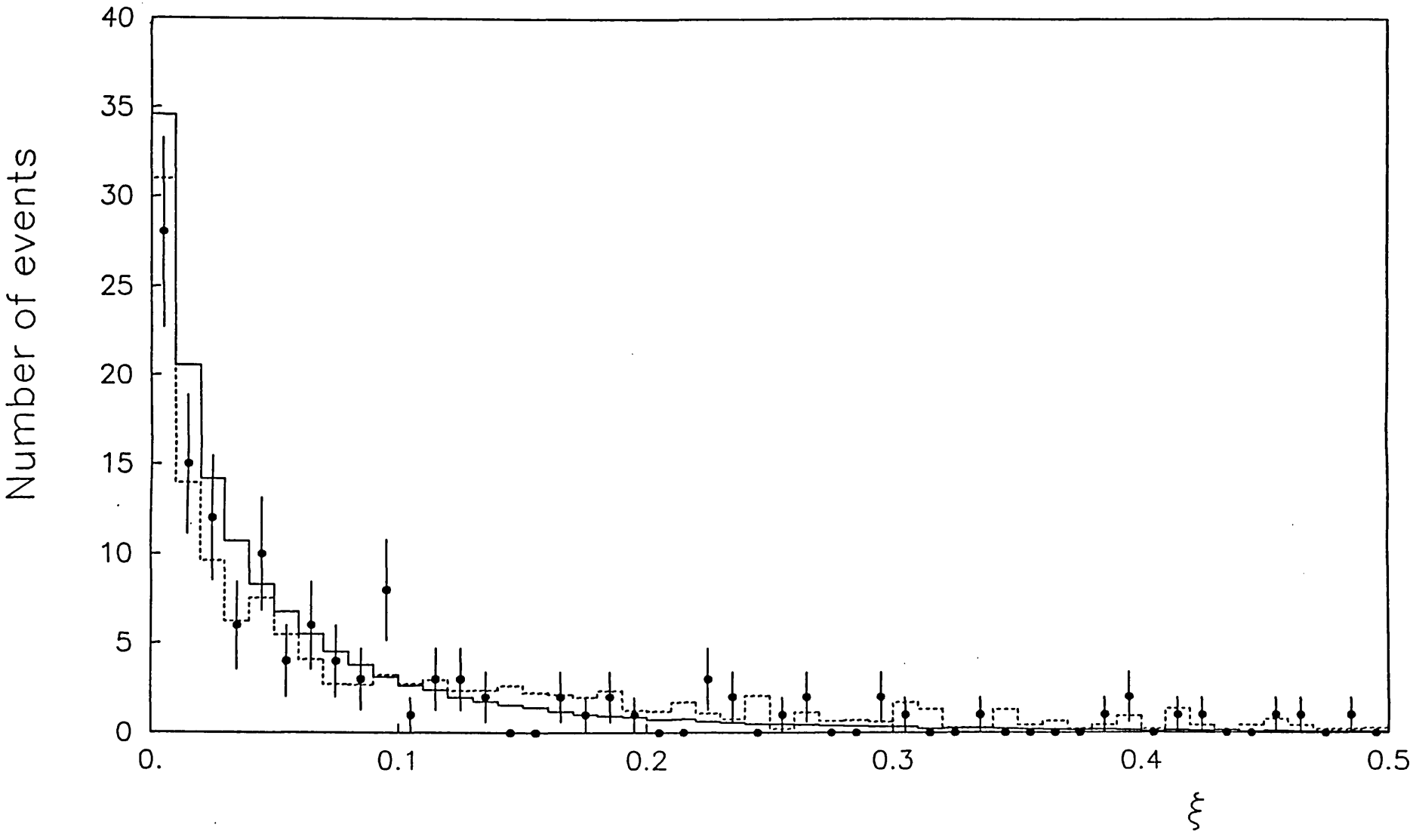



Figure 41: ξ distribution for NC candidates (data points), simulated tau decay events (full lines) and simulated background events (dashed lines).

same for electron and muon neutrinos. For hadron shower energies $E_H$ above 20 GeV, the apparent NC/CC ratio was measured to be 0.315±0.032±0.021 (table 39). The true NC/CC ratio expected for the mixture of $\nu$ and $\bar{\nu}$ CC events in these data is 0.312±0.008 (see subsection 7.3.1). The excess, 0.003±0.039, corresponds to events from both semileptonic and purely leptonic decays of the tau i.e.:

$$(NC)_O = (NC)_T + (NC)_\tau + N(\tau \rightarrow \nu_\tau + X) = (NC)_T + \Delta NC$$
$$(CC)_O = (CC)_T + N(\tau \rightarrow \ell + \nu_\ell + \nu_\tau) = (CC)_T + \Delta CC$$

where $(NC)_O$ and $(CC)_O$ are the observed number of NC and CC events which include conventional $(NC)_T$ and $(CC)_T$ plus contributions from tau. So the difference between the observed ratio $(NC/CC)_O$ and the expected conventional ratio $(NC/CC)_T$ becomes

$$\Delta = [(\ (NC)_T + \Delta NC\ )/(\ (CC)_T + \Delta CC\ )] - (\ (NC)_T/(CC)_T\ )$$

After a simple algebra the above equation reduces to:

$$\Delta = (\Delta NC - R_T \Delta CC) \ / \ (CC + \Delta CC) \qquad (8.41)$$

with $R_T$ being the true NC to CC ratio. The nominator on the right hand side of the above equation becomes

$$\Delta NC = (f_{NC}/f_{CC}) N_{\tau}^{CC} + (f_s/f_{CC}) N_{\tau}^{CC}$$

$$\Delta CC = (f_\ell/f_{CC}) N_{\tau}^{CC}$$

where $f_{NC}$, $f_s$ and $f_\ell$ refer to total weights from table 46 for $\nu_\tau$ NC interactions, $\nu_\tau$ CC interactions with subsequent semileptonic decays of the tau and $\nu_\tau$ CC interactions with subsequent purely leptonic decays of the tau respectively and $f_{CC} = f_s + f_\ell$. Using Eq. (8.41) and correcting for the number of $\nu_\tau$ CC events lost below 20 GeV $E_H$ cut we obtain

$$N_\tau^{CC} = 1.3 \pm 16 \qquad (8.42)$$

Thus all these methods are less sensitive than our kinematic method.

Combining results (8.37), (8.40) and (8.42) would give

$$N_\tau^{CC} = -6 \pm 10 < 14 \text{ at } 90\% \text{ c.l.} \qquad (8.43)$$

which is not significantly better than (8.37) alone.

## 8.10 ESTIMATE OF THE $D_S$ MESON PRODUCTION CROSS-SECTION

One can estimate the ratio of the $D_s$ to D meson production cross-sections from the ratio of $\nu_\tau$ events to prompt $\nu_\mu$ and $\nu_e$ events. To do this we assume the $D_s$ meson to be the only source of tau neutrinos (see sections 8.1) and the D meson to be the dominant source of prompt $\nu_\mu$ and $\nu_e$. We simulate the D meson production according to (8.7) with n = 5.7 (same as $D_s$ meson). The semileptonic decays of D was approximated by:

$$D \rightarrow K e \nu_e \qquad 50\% \qquad (8.44)$$

$$D \rightarrow K^{*} e \nu_e \qquad 50\% \qquad (8.45)$$

and the expected $\nu_e$ flux was simulated in a similar way to that of $\nu_\tau$ (see section 8.2). From table 26 our data contain 220±19 prompt $\nu_\mu$ and $\nu_e$ CC events with $E_\nu > 20$ GeV. Correcting Eq. (8.37) for the kinematic suppression of the charged current $\nu_\tau$ cross-section due to the large $\tau$ mass (using results (8.27) and (8.29) combined) we obtain a weighted number

$$N_{\tau}^{CC} = -25 \pm 21 < 29 \text{ at } 90\% \text{ c.l.} \qquad (8.46)$$

which can be compared directly with the number of $\nu_\mu$ and $\nu_e$ events. From the above results it can be seen than less than 13% of the integral energy-weighted prompt neutrino flux above 20 GeV through the detector is therefore due to $\nu_\tau$ or $\bar{\nu}_\tau$. Thus we can estimate an upper limit for $D_s$ meson production cross-section in hadron-hadron collisions, i.e.

$$N(\nu_\tau)/N(\nu_\mu,\nu_e) = [\sigma(pN \rightarrow D_s + X).BR(D_s \rightarrow \tau\nu_\tau).R(\nu_\tau)] \times [\sigma(pN \rightarrow D + X).BR(D \rightarrow \ell\nu_\ell + X).R(\nu_\mu,\nu_e)]^{-1} \qquad (8.47)$$

where the left hand side of the above equation is the ratio of the integral energy weighted prompt $\nu_\tau$ to prompt $\nu_\mu$ and $\nu_e$ fluxes. $R(\nu_\tau)$ and $R(\nu_\mu,\nu_e)$ are factors which take into account the acceptance of our bubble chamber to tau neutrino and prompt conventional neutrino fluxes and their interaction probabilities. These factors were obtained from the Monte Carlo simulations of $D_s$ and D mesons as described above. Using the results from the Monte Carlos we obtain for the ratio

$$R(\nu_\tau)/R(\nu_\mu,\nu_e) = 1.2 \qquad (8.48)$$

Assuming (a) a 3.9% branching ratio for $D_S \to \tau\nu_\tau$ (8.6) and (b) branching ratios for D into $\nu_\mu$ or $\nu_e$ of 12% each (about equal rate of charged and neutral D mesons), we obtain

$$\sigma(pN \to D_s + X)/\sigma(pN \to D + X) < 0.65 \text{ at } 90\% \text{ c.l.} \qquad (8.49)$$

For a $\bar{D}$ production cross-section of 17 μb per nucleon [1], for example, this gives a $\bar{D}_s$ production cross-section below 11 μb. These limits would increase (decrease) by about a factor 1.7 (1.4) for each unit of increase in the n value for $D_s$ (D) production as given in Eq. (8.7). They indicate only the degree to which this analysis is sensitive to the signal that might be expected.

## Chapter IX

## CONCLUSIONS

The previous CERN beam dump experiments proved the existence of a prompt neutrino signal. The 1982 CERN beam dump experiments were carried out in order to settle the question of whether there is a significant difference in fluxes of prompt electron and muon neutrinos. The resulting electron event sample is clean with the conventional background being small. The muon sample is more complicated because the expected conventional background is much larger than the electron sample. Given this there are two unexpected effects:

a) the first one is the low $\mu^-$ rate in the full density data, which differs appreciably from the rate expected from the 1979 experiments or from the other two experiments in the 1982 exposure. The ratio of the present $\mu^-$ rate to that of 1979 BEBC is $2.56 \pm 0.34$ while one expects $3.5 \pm 0.1$. This low ratio is remarkable, since the muon identification in the present experiment is superior because of the addition of the Internal Picket Fence, which was used, in conjunction with the EMI, to find muons lost in the normal scanning procedure. However, since the low $\mu^-$ rate in the full density data is also apparent when comparing with the

counter experiments, it is most likely due to a statistical fluctuation;

b) the second effect is the low ratio of $e^+$ to $e^-$ events. The prompt electron ratio accounted for $\bar{\nu}$ to $\nu$ cross-sections ratio is less than unity whereas the prompt muon ratio corrected similarly is compatible with 1.

However, it has been possible to improve the muon rates by using the large number of through-going muons from neutrino interactions upstream of BEBC. This enabled measurements of muon rates with similar precision to those of electrons.

From the prompt rates of electron and muon events above 20 GeV an asymmetry $A_{e\mu} = ( N_e - N_\mu ) / ( N_e + N_\mu ) = 0.07 \pm 0.08$ is derived in agreement with equal rates. The corresponding asymmetries for the different charges are: $A^+_{e\mu} = -0.28 \pm 0.14$ and $A^-_{e\mu} = 0.19 \pm 0.10$. The asymmetries between neutrino and antineutrino fluxes are $A_{\nu\bar{\nu}} = 0.15 \pm 0.08$ for electrons and muons combined. For muon neutrinos and electron neutrinos separately, the asymmetries are $A^\mu_{\nu\bar{\nu}} = -0.09 \pm 0.11$ and $A^e_{\nu\bar{\nu}} = 0.38 \pm 0.14$. The consequence of the above results is that, although the overall e,μ asymmetry is compatible with equal rates, the charge separated asymmetries are different by more than 2.7 standard deviations. Such a difference, if true, would require a radically different interpretation of the experimental situation, involving previously unknown physics. In view of these far-reaching consequences the interpretation in terms of statistical fluctuations appears more reasonable, albeit not wholly satisfactory.

The neutral current to charge current ratios obtained are compatible with those observed in normal neutrino experiments. From the observed NC to CC ratio and the known value for muon neutrinos the NC/CC ratio for electron neutrinos in the full density sample is found to be 0.312±0.154±0.121. The corresponding value for 1/3 density data is 0.380±0.257±0.140.

The excess of low energy neutral current events is -3±11 for hadron energies between 5 and 10 GeV (using both full and 1/3 density data) and 7.5±8 events for hadron energies between 10 and 20 GeV using full density data only. These values indicate that we are compatible with no excess of low energy NC events.

Despite a substantial increase in the statistics in this experiment compared to previous BEBC beam dump experiments, no $\nu_\tau$ interactions has been observed. Using a new kinematical method the number of $\nu_\tau$ CC interactions with $E_\nu > 20$ GeV in the full density data is estimated to be -14±12 events. This number is conservatively interpreted as an upper limit of 17 events at 90% confidence level. Other methods used before give weaker upper limits. Using this upper limit, the ratio of $D_s$ meson (previously called F meson) to D meson production cross-sections is estimated to be below 0.65 at 90% confidence level.

Still, the search for $\nu_\tau$ remains a gamble. By far the most promising development is the use of holography in the next generation of beam dump experiments such as the one proposed in Fermilab, if they ever materialise.

## REFERENCES


1. H. Grassler et al, Nucl. Phys. B273 (1986) 253.

2. B. Pontecorvo, Proc. XV:th Int. Conf. on High Energy Phys., Kiev, (1970) 643.
   B. Pontecorvo, Sov. Phys. JETP 42 (1975) 452.

3. H. Faissner et al., Phys. Lett. 60B (1976) 401.

4. P.C. Bosetti et al., Phys. Lett. 74B (1978) 143.

5. P. Alibran et al., Phys. Lett. 74B (1978) 134.

6. T. Hansl et al., Phys. Lett. 74B (1978) 139.

7. P. Fritze et al., Phys. Lett. 96B (1980) 427.

8. M. Jonker et al., Phys. Lett. 96B (1980) 435.

9. H. Abramowicz et al., Z. Phys. C13 (1982) 179.

10. H. Wachsmuth: Neutrino and Muon Fluxes in the CERN 400 GeV Proton beam dump experiment (CERN report EP/79-15,1979)

11. C. Brand et al., Nucl. Instr. Meth. 136 (1976) 485;
    R. Beuselink et al., Nucl. Instr. Meth. 154 (1978) 445

12. a) H. Foeth, Nucl. Inst. Meth. 176 (1980) 203.
    b) C. Brand et al. CERN report EF/81-13,1981.

13. P.O. Hulth, private communication.

14. THIRA and EMI pam files long write-up, Hydra Application Library, 1976 (CERN).

15. BD - Bank (CERN/EP/NBU 82-2)

16. H. Kreutzmann, Diploma thesis, University of Bonn 1985.

17. G. Gerbier et al., Z. Phys. 29C (1985) 15.

18. F. James and M. Roos, Minuit - A system for function minimization and analysis of the parameter errors and correlations, (Comp. Phys. Comm. 10, 434 (1975)).

19. M. Aguilar-Benitez et al. (Partcile Data Group), Phys. Lett. 170B, 1 (1986).

20. D.H. Perkins, (1975). Contemp. Phys. 16, 173.

21. P. Bosetti et al., Phys. Lett. 110B (1982) 167.

22. For example see F.E. Close, An introduction to quarks and partons, Academic press, London (1980) p239.

23. M. Aderholtz et al., submitted to Phys. Lett. B (1986)

24. H. Atherton et al., CERN experiment NA20: Measurements of particle production in 400 GeV/c proton copper collisions (1980), paper in preparation

25. G. Myatt, workshop on SPS Fixed-Target Physics in the years 1984-1989, CERN yellow report 83-02, Vol 2, 121.

26. E.L. Berger, L. Clavelli and N.R. Wright, Phys. Rev. D27, 1080 (1983)

27. For example see D. Bailin, Weak Interactions, Graduate student series in physics, second edition, Adam Hilger 1982, p99.

28. H. Wachsmuth, Report on the CERN 1982 beam dump experiments, Invited talk given at Telemark III Miniconference, October 1984, Telemark Lodge, Cable, Wisconsin, USA, CERN/EP 85-21.
P.O. Hulth, CERN beam dump results, 11th International Conference on Neutrino Physics and Astrophysics, Nordkirchen near Dortmund 1984, p512.

29. R.C. Ball et al., Phys. Rev. Lett. 51 (1983) 743;
M.E.Duffy et al. Phys. Rev. Lett. 52 (1984) 1865.

30. S. Weinberg, Phys. Rev. Lett. 19, 1264(1967);27,1688 (1972); Phys Rev. D 5, 1412 (1972);
A. Salam and J.C. Ward, Phys. Lett. 13, 168, (1964)

31. F. Hasert et al., Phys. Lett. 46B (1973) 138.

32. J. Blietschau et al., Phys. Lett. 88B (1979) 381.

33. H. Abramowicz et al., Z. Phys. C28 (1985) 51.

34. G.L. Fogli, Neutrino-induced deep inelastic scattering and the structure of the neutral current: a review and an updated analysis, La rivista del Nuovo Cimento, Vol. 9, No. 8, 1986.

35. M.L Perl et al, Phys. Rev. Lett. 35 (1975) 1489.
M.L Perl et al, Phys. Rev. Lett. 38 (1978) 117.

36. PLUTO coll. (J. Burmester et al.), Phys. Lett 68B (1977) 297.

37. DASP coll. (R. Brandelik et al.), Phys. Lett. 74B (1978) 109.

38. H.C. Ballagh et al., Phys. Rev. D30, 2271 (1984) and references there.

39. Review talk by M.G. Gilchriese at XXIII International Conference on High Energy Physics, Berkeley, California July 1986.

40. C.H. Albright, R. Schrock and J. Smith, Phys. Rev. D20 (1979) 2177.

41. Y.S. Tsai, Phys. Rev. D4, (1971) 2821.
Y.S. Tsai, Erratum, Phys. Rev. D13 (1976) 771.

42. J.E. Augustin, Proceedings of the LEP Summer Study, CERN Yellow Report 79-01, Vol 2, p499 (1979).

43. F. James, Multibody phase space generator 'GENBOD', CERN program library (1986).

44. W. Bacino et al., Phys. Rev. Lett. 43 (1979) 1073.

45. A. Ali and E. Pietraninen, Nucl. Phys. B154 (1979) 519.

46. C.H. Albright and C. Jarlskog, Nucl. Phys. B84, (1975) 467.

47. Jon Guy, private communication.

48. Wilbur Venus, private communication

49. Horst Wachsmuth, private communication

50. For example see M.G. Kendall and A. Stuart, The advanced theory of statistics, Hafner, New York.

51. M. Talebzadeh et al., CERN/EP 87-47, to be published in Nuclear Physics B (1987).

52. M. Poppe, Phys. Lett. 100B (1981) 84.

53. See review by J. Wotschack, Proc XIth Int. Conf. on Neutrino Physics and Astrophysics, Nordkirchen 1985, p117.